WIND-DRIVEN NEARSHORE DYNAMICS IN THE GULF OF MEXICO

A Dissertation

by

TARIQ I.S.I. ALRUSHAID

Submitted to the Office of Graduate and Professional Studies of
Texas A&M University
in partial fulfillment of the requirements for the degree of

DOCTOR OF PHILOSOPHY

Chair of Committee,	Timothy Dellapenna
Co-Chair of Committee,	Jens Figlus
Committee Members,	Ayal Anis
	Kyeong Park
Head of Department,	Shari Yvon-Lewis

May 2018

Major Subject: Oceanography

ABSTRACT

Coastlines around the Gulf of Mexico are dynamic, due to prevailing energetic wind systems such as frequent cold fronts and diurnal wind systems. In the last two decades, more research has focused on the surf zone's complex coupling effects between wind-driven waves and currents.. However, there is still a need for further field based experiment to elucidate, (1) how offshore cold fronts impact nearshore morphodynamics and sediment dynamics, when compared to onshore fronts, (2) what is the main physical forcing that controls the surf zone and the inner-shelf region current circulation during relatively intense onshore and offshore wind events, and (3) does the cumulative effect of sea breeze cycles result in more morphodynamic variation than cold fronts? Therefore, two field based studies were conducted in the Gulf of Mexico to advance our understanding of the complex coupling effects between wind-driven waves and currents, including turbulence quantities, sediment transport parameters, and morphodynamic processes. Both field experiments included time-series of highly resolved hydrodynamics and suspended sediment concentration obtained at different cross-shore locations across the surf zone.

The first field experiment was conducted at a sea breeze dominated beach on Sisal, Yucatán peninsula, México. Time-series observations suggest that the impact of sea breeze cycles on the nearshore hydrodynamics and morphodynamics is comparable to the effect of onshore-directed cold front, and cumulatively the sea breeze cycles will result in higher sediment loss. Regardless, it is also suggested that the cumulative accretional of the land breeze cycles can be sufficient to compensate for the loss of sediment by either the sea breeze cycles or the cold fronts. The second field experiment evaluated surf zone hydrodynamics and sediment dynamic processes within the upper Texas coast during three offshore cold front events and three onshore Gulf breeze events. Observations show en-

hanced eastward suspended sediment transport following the passage of cold fronts, while westward transport was experienced during the Gulf breeze events. The study suggests that during late fall and early spring seasons, Galveston Island will experience higher erosion rates in the eastside, while accretion of sediment on the west side will occur.

DEDICATION

I would like to dedicate this dissertations to my mother, father, my wife and the love of my life Norah, and the amazing Rusheed and Loura my kids.

ACKNOWLEDGMENTS

First, I thank god for giving me the chance to pursue my graduate studies, and providing me with guidance, strength, patient, and good company throughout my time here in Texas A&M.

I would like to also thank my faculty adviser, Dr. Timothy Dellapenna, for giving me the chance to be a part of his lab, and providing me with much help and advising throughout the past few years. Throughout the difficult times of my dissertation, his words boosted my self-confidence, and helped me to become a better scientist. I especially appreciate his dedication towards his students, as he always had his door open for anything that was needed. I am and I will always be grateful for my co-adviser and friend Dr. Jens Figlus. Dr, Figlus welcomed me to his lab, and trusted in me to conduct my own planned field experiment. His guidance and steadfast support within this work has been monumental in the success of my project. Particularly, during the field deployment, he always steered me towards the right path whenever we faced an issue. I remain continuously inspired by his dedication to his own work, including his ability to manage writing papers, leading field excursions, teaching courses, while remaining always available to mentor his students (even when visits to his office were unannounced, $\sim 90\%$ of the time).

I am also extremely thankful to Dr. Ayal Anis for being a member of my committee. Dr. Anis has been a mentor and a father figure to me. I had the opportunity to meet him before joining Texas A&M, while we were working on a field deployment in Kuwait. He was so humbled and inspiring! Throughout my time at Texas A&M, he always had his door open for me to discuss scientific matters or even personal matters. I remain so grateful for the time he has spent with me, including the many insightful comments he has provided for my work. Although I was 12,000 km away from my family in Kuwait, both Dr. Anis

and his wonderful wife, Mrs. Ruthy Anis have given me a home and made me feel like a member of their own family. I am also thankful to Dr. Kyeong Park for willingly being a member of my committee and allowing me to learn from his robust expertise on physical properties and coastal systems. I am grateful for the time he spent with me, regardless of his busy schedule, which allowed me to learn so much about this subject. I am also thankful to Dr. Alec Torres-Freyermuth for hosting me during my field excursion in Sisal, while giving me the opportunity to learn from his experience.

This dissertation would have been impossible without the help and support I had from my friends and Aggie family. Especially without my former OCSB 3^{rd} floor desk mates and soon to be faculty colleagues, Dr. Mohammad Al Mukaimi and Dr. Fahad Al Senafi. Throughout my entire Ph.D. (whether they were in Kuwait or in Galveston), they have provided me with countless hours of help, advice and support. I am grateful to Sergey Molodtsov for being my friend, and for providing his help during my field experiment, which was a time that I needed it most. Special thanks to my friends Dapeng Li and Andrew McGuffin for their support, and great sense of humor that kept my morale high! I would also thank my friend Anne Tamalavage for providing her help with my writing and for showing continuous support. I would also like to take this opportunity to thank William Prouse, Zachary Hinojosa, and Hunter Myres for helping me with my field components. I would like to also thank the department faculty and staff for making my time at Texas A&M University a great experience, especially Holly Richards, Nicole Kinslow, and Patricia Lambert from Texas A&M University at Galveston Research and Graduate Studies Office (RGSO) for all the unyielding help and support they have given me.

Thanks to Kuwait University for trusting in me, and providing a generous scholarship to pursue my Ph.D. degree. I am also very thankful to Ms. Karla Pettey, my academic adviser at the Kuwait embassy; she was continuously throughout my Ph.D. I am also thankful to Alrushaid Co. for providing me with funding for Sisal travel expenses.

I have a great family back home that have always provided me with love and support. Without them, this work would have not been possible. I would like to give my mother (Maha) and father (Abraham) my greatest gratitude, for their encouragement and their warm words that helped me during the tough times. I am so grateful that they are in my life, as they continue to provide me with guidance and point me to the direction of greatness. I sincerely hope that this work will make them proud. Also, I would like to thank my two brothers (Suliman and Ali), and my two sisters (May and Fay) for their encouraging words and their unconditional love.

Last but certainly not least, I would like to thank the most amazing and beautiful woman I ever met, my wife Norah, for her support and patience during all of these years. She has been the source of my strength and dedication, and it would absolutely not have been possible to achieve this without her. I am so motivated to repay her for all of the time I was away from her while working on this dissertation! I am also grateful to my son (Rusheed) and daughter (Laura) for their smiles and hugs that kept me going and filled me with energy. I apologize for not being around to watch you during your baskettball and football games, but I dedicate my whole future to both of you. I thank you all from the bottom of my heart.

CONTRIBUTORS AND FUNDING SOURCES

Contributors

This document was supervised by a dissertation committee made of Dr. Timothy Dellapenna [Chair], Dr. Jens Figlus [Co-Chair], Dr.Ayal Anis , and Dr. Kyeong Park.

Funding Sources

The field work presented in Section 2 was supported by the Institute of Engineering at the National Autonomous University of Mexico (UNAM) as part of the International Collaborative Research Project UNAM-UD "Nearshore Coastal Dynamics on a Sea-Breeze Dominated Micro-Tidal Beach" (CB-167692). The project PIs Dr. Alec Torres-Freyermuth (UNAM) and Dr. Jack Puleo (University of Delaware). Dr. Jens Figlus and Tariq Alrushaid were supported by Texas A&M University at Galveston.

The field work presented in Section 3 and Section 4 was supported in part by an Institutional Grant (NA14OAR4170102) to the Texas Sea Grant College Program from the National Sea Grant Office, National Oceanic and Atmospheric Administration, U.S. Department of Commerce and Texas A&M University. Furthermore, the field work received additional support from the NSF under Grant No. OISE-1545837.

All other work conducted for the dissertation was completed by the student independently.

Tariq Alrushaid graduate study was supported through a full scholarship provided by Kuwait University.

NOMENCLATURE

ADCP	Acoustic Doppler Current Profiler
AQUADOPP	Aquadopp Acoustic Doppler Profiler
ADCP-HR	High Resolution Acoustic Doppler Current Profiler
ADV	Acoustic Doppler Velocimeters
ADVP	Vectrino II Acoustic Doppler Profiling Velocimeters
AD2CP	Advanced-Five-Beam Current Profiling System
CA	Continental Arctic
CP	Continental Polar
DGPS	Differential Global Positioning Systems
DIWASP	DIrectional WAve SPectra Toolbox
EOF	Empirical Orthogonal Eigen Function
ENSO	El Niño-Southern Oscillation
GoM	Gulf of Mexico
GPS	Global Positioning System
UTC	Universal Time Coordinate
UNAM	Universidad Nacional Autónoma de México (National Autonomous University of Mexico)
E	East
W	West
N	North
S	South

LATEX	Texas and Louisiana Shelf
MSL	Mean sea level
NNM	Nivel Medio del Mar
MP	Maritime Polar
OBS	Optical Backscatter Sensor
PC	Principal Component
PCA	Principal Component Analysis
PUV	Pressure, cross-shore velocity, longshore velocity method
PT	Pressure Transducer
PSD	Power Spectral Density
RSSI	Received Signal strength Indicator
RTK	Real Time Kinematic
SSC	Suspended sediment concentration
SSC_{ADV}	Suspended sediment concentration measured by the ADV
SST	Sea-surface temperature
TKE	Turbulent Kinetic Energy
U/U_{10}	Wind speed at 10 m height above mean sea level
u	Cross-shore velocity
u_*	Frictional velocity
v	Longshore velocity
w	Vertical velocity
q_u	Cross-shore suspended sediment flux
q_v	Longshore suspended sediment flux

Q_v	Longshore total suspended mass
Q_u	Cross-shore total suspended mass
E_i	Echo intensity
E_r	Echo strength
ρ_a	Air density
ρ_w	Water density
c	Phase velocity
C	Calibration constant
C_D	Drag coefficient
H_s	Significant wave height
H_b	Breaking wave height
m_0	Wave elevation variance
T_s	Significant wave period
T_p	Wave peak period
f_p	Peak frequency
τ_b	Near bed shear stress
τ_w	Wind shear stress
ε	Turbulent Kinetic Energy dissipation rate
k	Wavenumber
α	Empirical Kolmogorov constant
κ	Emprical von Kármán constant
S_{xy}	Alongshore component of the wave radiation stress
θ_b	Breaking wave angle
γ	Breaking wave index

c_g	Group velocity
η	Water level
Φ_{pv}	Longshore velocity cross spectra
Φ_{pu}	Cross-shore velocity cross spectra
V	Current magnitude
σ	Variance of the wave induced horizontal velocity
θ	Angle
S_v	Volume backscatter strength
R	Slant range
L_{DBM}	Transmitted pulse length
P_{DBW}	Transmitted power
α_{ab}	Absorption coefficient
K_c	Scale factor
z	Targeted measurement height above the seabed

TABLE OF CONTENTS

Page

LIST OF FIGURES

FIGURE Page

LIST OF TABLES

TABLE Page

1. INTRODUCTION

Throughout history, civilizations have congregated around coastal areas. This increase in population densities at the coastal areas is because of access to open-sea providing sustenance and rapid growth in economic development. However, along the coasts of the Gulf of Mexico (GoM), beaches are under ever increasing pressure due to geophysical processes like tropical storms and erosion. As a result, infrastructures and populations are under threat.

The nearshore region (Figure 1.1) is the most complex part of the coastal system that contains three dynamic zones. Waves coming from offshore will become unstable and start to break at the breaker zone and most of the wave energy will dissipate in the surf zone. Sandbars can be found in the surf zone and they provide protection for the beach from high waves attack. The variation of sandbar height and position will affect nearshore waves and currents (Lippmann & Holman, 1990), ultimately affecting the sediment transport and morphological features of the beach profile. The swash zone is characterized by an inundation phase during the run-up and an exposure phase during the backwash. The nearshore wave field is strongly influenced by meteorological forcing. Meteorological forcing can be syntopic scale (e.g. hurricanes and cold fronts) and mesoscale (e.g. sea and land breezes). Wind events associated with both syntopic and mesoscale scale have been topics of substantial research effort in the last few years, especially investigating their role rapid changes of nearshore morophodynamics .

P. Wang and Oey (2008) investigated the affect of hurricanes on hydrodynamics using offshore buoys, while Vatvani et al. (2012) investigated hurricane surge level using on-land surge gauges. Additionally, studies relating to the hydrodynamic response of hurricanes to land loss were carried out using Light Detection and Ranging (LIDAR) and/or manual

beach profiling survey of pre and post hurricanes (Edmiston et al., 2008; Otvos, 2004). However, the documented results regarding the cold fronts suggests that due to their frequent occurrence they can have a greater impact on the nearshore region dynamics than hurricanes (Carlin et al., 2016a; Pepper et al., 1999; Moeller et al., 1993). Literature has shown that cold fronts result in a significant decrease in Sea Surface Temperature (SST) and increased in turbidity (Moeller et al., 1993), beach erosion and overwash events (Keen, 2002; Dingler & Reiss, 1990), and significant increase in wave height, period, and current speed (Keen, 2002). Additionally, the significant impact of onshore syntopic storms to sandbar migration have been noted in several studies (e.g. Elgar et al., 2001; Thornton et al., 1996; Lippmann & Holman, 1990).

Beaches in the north central GoM have a high erosion rate; beaches around barrier islands such as Galveston have an average erosion rate of 3.5 m/yr (Paine et al., 2012), while beaches around Isles Dernieres that has an average erosion rate of 10 m/yr (Dingler et al., 1993). Observations from Dingler and Reiss (1990) suggest that high erosion rates in the Louisiana barrier island arc was partially a result of the cumulative effect of cold fronts. However, Kineke et al. (2006) suggest that cold fronts result in accretion of sediment along the Louisiana's Chenier-plain coast. Similarly, in the southern part of the GoM (e.g. Yucatán peninsula), beaches are under threat from erosion by seasonal cold fronts and a strong sea breeze system (Mendoza et al., 2013). In the northern part of Yucatán peninsula the sea breeze system can result in wind velocity up to 13 ms^{-1}. Nevertheless, the influence of how cold fronts approach the coast and impact nearshore hydrodynamics, bottom boundary layer characteristics, morphodynamics and sediment transport in the GoM is poorly documented. Additionally, to the author's knowledge there is no current literature available that compares the impact of onshore and offshore cold fronts to the nearshore region.

Sea and land breezes are very well documented in atmospheric science. Several stud-

ies have covered the subject of its circulation dynamics (Miller et al., 2003; Sonu et al., 1973), pollution transport (Buckley & Kurzeja, 1997), and atmospheric turbulent characteristics in the lower surface layer (Chiba, 1993). Additionally, this topic has gained the interest of oceanographers and coastal engineers within the last few decades. Previous research efforts investigating nearshore dynamics during sea breezes events focused on sediment suspension (Miller et al., 2003; Sonu et al., 1973), surface currents (Sonu et al., 1973), surf zone sediment transport and morphodynamics (Masselink & Pattiaratchi, 1998; Pattiaratchi et al., 1997). The stability of the sea breeze has noticeable impact on nearshore processes, particularly on wave climate, nearshore currents, and morphodynamics (Pattiaratchi et al., 1997; Abbs & Physick, 1992; Sonu et al., 1973). However, despite the work that has been done on studying the sea breezes impact on nearshore hydrodynamics, morphodynamics, and sediment dynamics, there has been no work devoted to study the effect of sea breezes on nearshore processes in the GoM. Additionally, the cumulative effect of sea breezes to cold front events has not been documented nor covered in GoM studies.

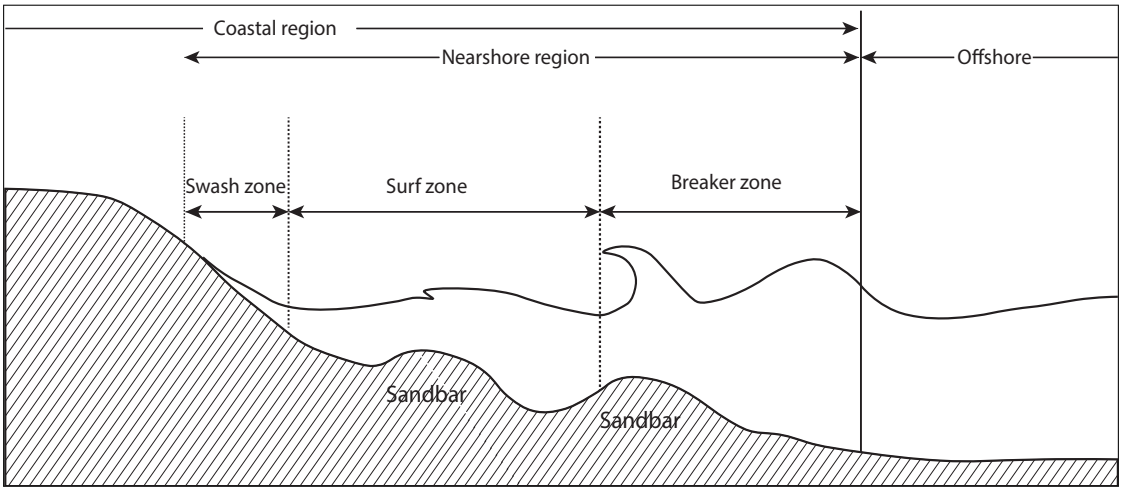

Figure 1.1. Schematic of cross-shore beach profile showing coastal region zones.

From an oceanographer's standpoint, understanding the effect of sea breezes and cold fronts on different coastal environments is fundamental. Intense wind events can induce sediment resuspension (Booth et al., 2000). This may have direct impact on coastal ecosystems by transporting organic matter and nutrients (Booth et al., 2000; Madden et al., 1988), re-exposing some of the oil residues (Michel et al., 2013), or by despersion of oil spills from the beach to ocean (Balseiro et al., 2003). Thus, more scientific investigation and quantification of cold fronts and sea breezes influence on nearshore processes needs to be better understood (e.g. waves, current, turbulence quantities, sediment transport). More importantly, how would the onshore and offshore cold fronts affect nearshore current circulation and sediment transport.

By understanding the physical processes that occur during sea breeze cycles and cold front events will help having:(1) a better approach for beach management (e.g. beach nourishment and defining the vulnerable areas of the beach), (2) an effective functionality of nearshore processes predication in numerical models regarding different wind forcing and the resulting changes in morphodynamics. Therefore, the primary aims of the present study are:

I. To best understand and describe the response of nearshore hydrodynamics (e.g. currents and waves), morphodynamics, and sediment processes under different wind forcing conditions.

II. Design a conceptual model for the effect of onshore vs. offshore wind on nearshore current circulation and changes in the beach morphology.

1.1 Cold front characteristics and nearshore processes

Cold fronts are synoptic scale atmospheric phenomena associated with intense wind events. They are characterized by a cold air mass advancing under warmer air mass (Figure

1.2). The direction of the front can be either directed offshore (Figure 1.2a) or onshore (Figure 1.2b). In the GoM, a cold front can exist any time of the year, but they are more frequent and active during the winter season. There are approximately 30-40 cold fronts crossing the GoM in a year (Stone et al., 2004; Keen et al., 2003; Huh et al., 2001). Wind velocities during these events range between 4 ms^{-1} and 18 ms^{-1}. The average duration of cold fronts is one to two days, but can last longer during winter months (Henry, 1979).

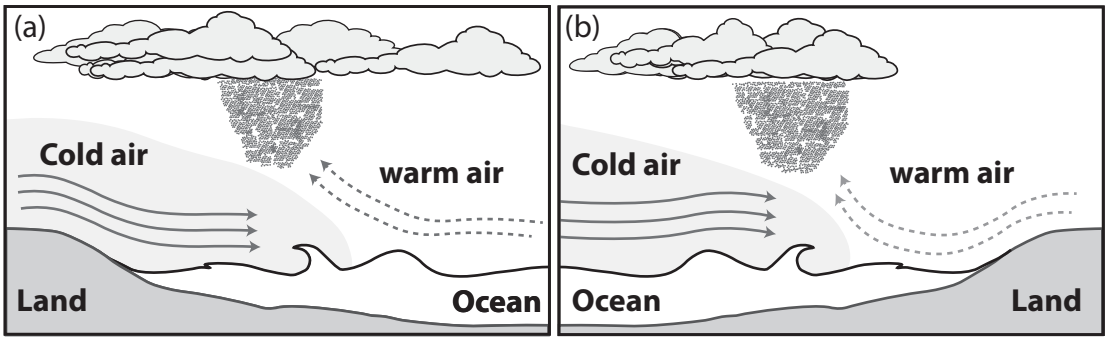

Figure 1.2. Schematic showing: (a) offshore-directed cold front (b) onshore-directed cold front.

According to Henry (1979) cold fronts entering the GoM can come from the north (Continental Polar-CP, and Continental Arctic-CA) or come from the Pacific Ocean (Maritime Polar-MP). Observations from Henry (1979) reveals that MP cold fronts are the most frequent fronts entering the GoM throughout the year, except in summer months (Figure 1.3). Occasionally MP cold fronts enters between Galveston Island and Corpus Christi (Henry, 1979).

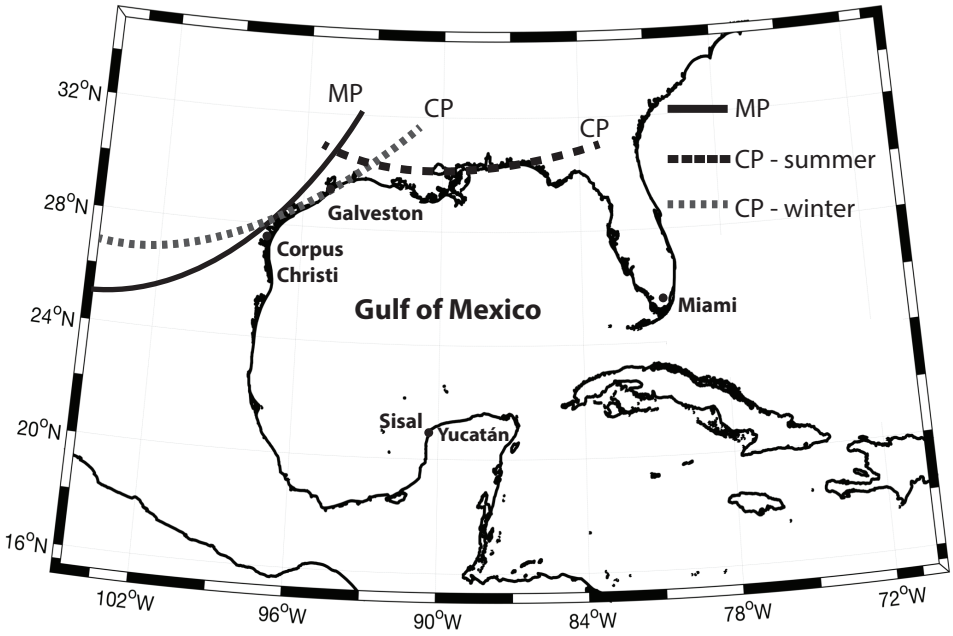

Figure 1.3. Schematic of GoM cold fronts entry locations and the seasonal changes of CP and MP fronts, modified from Henry (1979). Reprinted with permission from ©American Meteorological Society. Used with permission.

Atmospheric disturbance resulting from cold fronts leads to high wind stress amplitudes and an increase in nearshore turbulent kinetic energy (Stech & Lorenzzetti, 1992). This can mobilize large volumes of sediment. For instance, during the passage of offshore-directed cold front over the inner-shelf of Louisiana Pepper and Stone (2004) noted an increase of the cross-shore sediment transport that was five times higher than normal conditions, approximately from 0.1 $\mathrm{gcm^{-1}s^{-1}}$ to 6 $\mathrm{gcm^{-1}s^{-1}}$, respectively. During this process, the direction of the transport was shifted towards offshore. In most cases the suspended sediment transport rate is less than bed-load transport. However, Keen et al. (2003) suggested that during the passage of cold fronts the suspended sediment transport rate can be an order of magnitude higher than bed-load transport rate.

1.2 Sea and land breeze cycle characteristics and nearshore processes

The atmospheric phenomena of sea and land breezes are caused by thermal temperature variation between land and ocean. At night, the ocean is warmer than land causing the wind to flow from the land to the ocean (Figure 1.3a). During the day, the wind flow is reversed due to heating of the land (Figure 1.4b). The circulation strength of the sea breeze cycle is mainly a function of the difference of the air temperature between the land and the ocean (Hsu, 1988). Thus, higher temperatures will result in intense sea breeze wind events (Federico et al., 2010). Impact on the nearshore wave field and surface currents can significantly increase during hot summer days (Masselink & Pattiaratchi, 1998). It has been noted that sea breeze dominated areas are found in tropical and subtropical regions (i.e. between 35^{o}S and 35^{o}N). However, the investigation of global sea and land breezes variation by Gille et al. (2003) suggests that the most intense sea breeze system in the GoM is located around the north part of Yucatán peninsula.

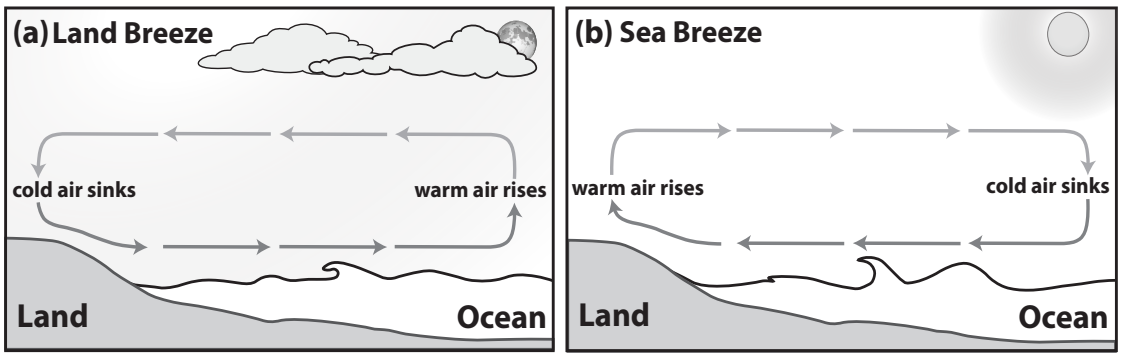

Figure 1.4. Schematic showing: (a) land breeze cycle (b) sea breeze cycle.

Previous studies on sea breeze cycles have shown that wave induced currents, high wave energy, and suspended sediment fluxes were substantially increased following the onset of the sea breeze cycles resulting in rapid morphological changes within the surf zone

(e.g. Gallop et al., 2011; Masselink & Pattiaratchi, 1998; Pattiaratchi et al., 1997; Sonu et al., 1973). Pattiaratchi et al. (1997) observed an increase in longshore currents from 0.05 ms^{-1} to 1 ms^{-1} three hours following the onset of the sea breeze cycle. According to Masselink and Pattiaratchi (1998), one cycle of sea breeze resulted in inducing longshore and cross-shore suspended sediment transport rate approximately by a factor of 90 and 40, respectively, leading to an erosion of the beachface and deposition of sediment within the surf zone.

1.3 Field experiments obstacles in the nearshore

Both in oceanography and coastal engineer studies, the nearshore region has been and still is difficult to study and obtain reliable data from. This is because of the complexity and the very dynamic processes that occur in the nearshore region (i.e. high spatial variability of hydrodynamics and sediment dynamics over a very short distance, $\approx$ 250 m). When using acoustic instruments for measuring currents in any zones of the nearshore region, high noise level impacts the data quality, making data post-processing difficult. Exploring this region, the acoustic instruments requires regular maintenance almost twice a day or more. The maintenance includes checking if the instrument is operational and removing anything that might get caught on the instruments transducer or receiver.

Some of the nearshore regions are very active, where erosion and deposition occurs simultaneously (e.g. surf zone, and swash zone). Therefore, instruments needs to be vertically adjusted to targeted depths. Sometimes during the passage of an offshore or onshore-directed cold front events or strong onshore winds, instruments can be buried overnight from intense deposition. In addition, instruments can also be buried under sandbars during sandbar migration. Nevertheless, these kind of field experiments requires comprehensive planning and testing before deployment, in addition to the manpower required to make it possible. This can be done by studying the regional wind pattern, tide, wave climate,

currents, and calibrating and testing the functionality of the instruments.

1.4 GoM summer vs. winter wind and selection of study sites

Seasonal surface (10 m above sea level) meteorological observations reveals a distinct variation in wind pattern and magnitude between summer and winter seasons. Strong wind dominates the Yucatán peninsula during both winter and summer seasons, while in the northwest GoM winds are found to be more intense during the summer (Figure 1.5).

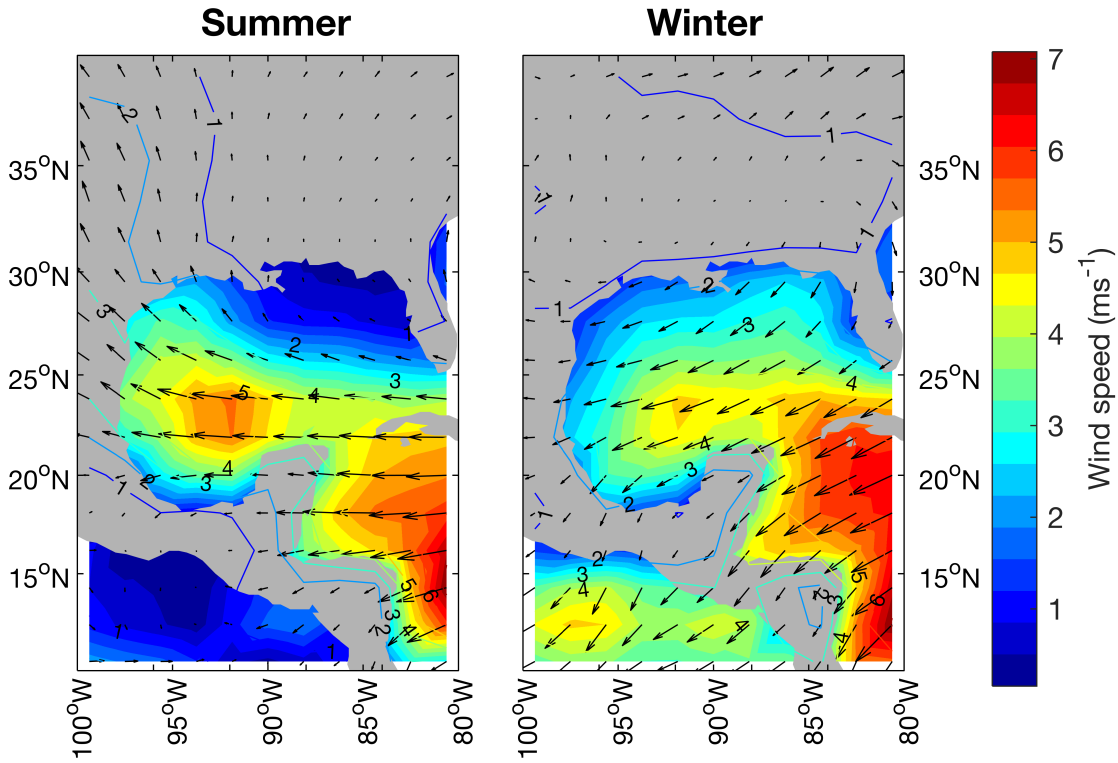

Figure 1.5. GoM summer and winter months wind variation (averaged from years 2000 to 2016) wind variation. Wind data presented in this figure were obtained from Kalnay et al. (1996).

Galveston Island (Texas, US) and Sisal (Yucatán, Mexico) were the perfect candidates for studying different weather forcing conditions and the subsequent impact on the surrounding coastal region. These locations were selected as both are sandy, microtidal, and low wave energy beaches. Additionally, both locations are mainly influenced by wind, as Sisal is a sea breeze dominated beach, while Galveston is influenced by the strong southerly wind. The selected sites will make it possible to compare the offshore-directed cold fronts exiting Galveston Island and the onshore-directed cold fronts reaching Sisal, in terms of their influence on nearshore hydrodynamics, sediment dynamics, and morphodynamics.

1.5 Dissertation structure, description, and research questions

This dissertation describes field based observations conducted on sandy microtidal beaches in the GoM to investigate the different wind system impact on the nearshore region hydrodynamics, morphodynamics, and sediment dynamics. This was done by comparing the onshore and offshore-directed cold fronts, sea and land breeze cycles, and Gulf breeze wind with the resultant characteristics of current circulation, energy levels, beach morphology, and suspended sediment flux within the surf zone. To achieve the goal of this dissertation, several questions were addressed:

I. What is the effect of onshore and offshore wind events on nearshore currents?. *I hypothesize that strong onshore wind events induce undertow currents, while strong offshore wind events induce onshore currents*.

II. Does cold front approach directly effect the nearshore sediment in terms of accretion and erosion?. *I hypothesize that offshore-directed cold fronts will lead to erosion around sandbars and the foreshore and an accretion of sediment within the trough (between sandbars), while an onshore-directed cold fronts result in higher erosion rate within the entire surf zone*.

Section 1 describes the motivations behind this work. This section also provides a detailed description of both cold fronts and sea breeze dynamics characteristics. Additionally, it includes a review of the most outstanding field studies that have been undertaken within the nearshore region and addressing impact of offshore-directed cold fronts and the diurnal sea and land breeze system on surf zone hydrodynamics and sediment dynamics. Moreover, it also provides a sense of how difficult it is to have a field experiment within the surf zone (see section1.3).

The second portion of this dissertation (Section 2) uses in-situ observations of nearshore hydrodynamics and morphodynamics on a microtidal, sandy, sea breeze dominated beach in Sisal, Yucatán, México. The study investigated wind-driven waves and currents, with the resulting energy levels, sediment transport, and morphodynamic processes. The study scope was to understand the cumulative impact of a sea breeze system when compared to intense wind event such as a cold front, in terms of erosion and accretion. As previously mentioned the surf zone hydrodynamics and sediment transport parameters were found to be intensified during both sea breeze and cold fronts (see section1.1 and section1.2). However, to the author's knowledge, no study has been found to compare the cumulative effect of both the sea breeze system to cold fronts, in terms of surf zone energy levels, and sediment transport and morphodynamics. Therefore, the goal of this study was to answer the following questions:

I. Does the cumulative effect of sea breeze events result in more morphodynamic variation than cold fronts?. *I hypothesize that sea breezes have more impact on the nearshore sediment flux than cold fronts due to the stability and the diurnal cycle of the system.*

II. During the period of increased wind and longer land breeze cycle, what is the morphological response of the surf zone?. *I hypothesize that during longer than average*

land breeze cycle, the available energy within the surf zone will be low, leading to low sediment suspension; therefore, resulting in a significant sediment deposition.

Section 3 examines the nearshore circulations following three offshore-directed cold front and three Gulf breeze events using field based data of highly resolved hydrodynamics collected within the surf zone and the inner-shelf region. The study discusses the role of different oceanographic and atmospheric forcing in driving nearshore current circulation, under fluctuating wind events. Recent study by Torres-Freyermuth et al. (2017), suggests that during the period of onshore-directed cold fronts, the Yucatán current controls the circulation within the inner-shelf, while waves control the circulation within the surf zone. However, there has been no work devoted to study the impact of offshore-directed cold fronts on the nearshore circulation. This study aims to better understand the role of the resultant oceanographic and atmospheric forcing on the nearshore circulation from offshore-directed cold fronts. This study was designed to answer the following questions:

I. What are the main physical forces that controls the surf zone and the inner-shelf region current circulation during the periods of offshore-directed cold fronts?. *I hypothesize that during the period of cold fronts, waves breaks and drive an eastward current within the surf zone, while the shelf currents control the circulation with in the inner-shelf region*.

II. What are the main physical forces that controls the surf zone and the inner-shelf region current circulation during the periods of onshore winds?. *I hypothesize that during the period of Gulf breeze events, southeasterly waves break driving a westward current flow, while wind shear stress and shelf currents control the circulation with in the inner-shelf region.*

Section 4 uses field based data of highly resolved hydrodynamics and suspended sediment concentration within the surf zone of the upper Texas coast. Little is understood

regarding the impact of offshore-directed cold fronts compared to regular onshore Gulf breeze winds on the surf zone dynamics within the northern GoM; therefore, this study focused on addressing the impact of fluctuating onshore and offshore winds on the surf zone sediment transport, current characteristics, energy levels, morphodynamics processes. This study aimed to answer the following questions:

I. How does the turbulence quantities differ during the offshore-directed cold front events compared to the Gulf breeze events?. *I hypothesize that during the period gulf turbulence quantities will be higher due to the increase in wave energy*.

II. Do offshore-directed cold fronts result in onshore suspended sediment flux? and how much sediment is gained or lost within the surf zone when compared to Gulf breeze events. *I hypothesize that during the period of cold fronts, suspended sediment concentration is low and the cross-shore velocity will be onshore, thus cold fronts will result in onshore sediment flux. However, the cumulative sum of Gulf breeze will result in high suspension of sediment and will transport it seaward*.

Section 5 provides a discussion and a comparison of the findings between Section 2 to Section 4. The comparison includes the impact of different wind forcing on waves, currents, turbulence quantities, suspended sediment fluxes, and beach morphology. Finally, Section 6 provides a conclusion and a brief summary of the mean findings of this dissertation.

2. NEARSHORE HYDRODYNAMICS AND MORPHODYNAMICS OF A MICROTIDAL, SANDY BEACH: ONSHORE COLD FRONT, LAND AND SEA BREEZE EFFECTS

2.1 Introduction

Beach erosion is a threat many coasts are facing and beaches along the Yucatán peninsula are no exception. Over the last decades, the Yucatán peninsula has experienced episodic coastal erosion problems (Meyer-Arendt, 1991). This has resulted in extensive loss of property and land (Mendoza et al., 2013; Salles et al., 2013). Investigations of erosion events along various stretches of the Yucatán coast by Cuevas Jiménez et al. (2016) and Meyer-Arendt (1993) suggest that beach loss can be attributed to natural forcing from cold fronts and hurricanes as well as anthropogenic alterations of the coastline in the form of piers, jetties, and seawalls. Wave-induced erosion is considered to be a significant contributor to overall erosion trends along the Yucatán coasts despite the relatively low-energy normal wave conditions in the Gulf of Mexico (Appendini et al., 2012). Several engineering projects attempted to mitigate effects of erosion, yet most were unsuccessful (Meyer-Arendt, 1991). This failure could be due to the lack of understanding of the complex interactions between varying wind forcing, coupled nearshore hydrodynamics, and morphological changes resulting from sediment transport processes. Apart from infrequent hurricanes, the Yucatán coast experiences meteorological forcing conditions related to local land and sea breeze wind cycles as well as synoptic cold front systems (refer to as Nortes) with potentially significant effects on nearshore currents, waves, and sediment dynamics. The work presented herein sheds some light on the nearshore hydrodynamics and associated beach morphology changes due to meteorological forcing conditions created by land and sea breeze cycles as well as a Norte event. A better understanding of the

complex feedback mechanisms involved can inform more effective coastal management practices.

The nearshore region is mainly influenced by wind driven waves. During intense wind events wave height increases resulting in wave-induced nearshore currents (Matsunaga et al., 1997), which in turn will result in truculent flow that can cause resuspension and transport of sediment leading to morphological changes across the entire surf zone. For example an important morphological feature of a sandy beach such sandbars are significantly affected by the complex response to storms and non-storms hydrodynamic forcing (Gallagher et al., 1998; Houser & Greenwood, 2007). During the high energetic conditions such as storms sandbars tend to migrate seaward due to the increase of offshore current induced by the incident waves breaking on the sandbar crest. Meanwhile, low energetic conditions result in slow landward migration (Wijnberg & Kroon, 2002; Elgar et al., 2001). Sandbars can contain a large volume of sand, therefore accounts as major part of the surf zone sediment budget (Lippmann et al., 1993).

During the summer months the Yucatán peninsula is subject to tropical and extratropical storms. On the other hand, Nortes can occur throughout the year with most frequent appearances during the winter season (Torres-Freyermuth et al., 2017; Figueroa-Espinoza et al., 2014). In the northern Gulf of Mexico (GoM) cold fronts (which may become Nortes as they progress south across the GoM) have a significant impact on the coastal environment, due to their frequent occurrence (e.g. Carlin et al., 2016a; Stone et al., 2004; Moeller et al., 1993; Roberts et al., 1989). Previous studies revealed that cold fronts can result in a significant decrease in Sea-surface temperature (SST), increase turbidity (Moeller et al., 1993), cause beach erosion and even overwash events (Keen, 2002; Dingler & Reiss, 1990), increased longshore sediment transport (Kineke et al., 2006), as well as increase wave height and current speed (Torres-Freyermuth et al., 2017; Keen, 2002). Appendini et al. (2018) classified Norte events into five categories based on the derived wave power.

The study suggested that within a year on average the Yucatán peninsula experienced a 24 intense Norte event with a mean duration of 44 hours. However, based on the future Representative Concentration Pathways (RCP) 8.5 emission scenario Appendini et al. (2018) suggests that the number of intense Norte events will decrease and the Yucatán peninsula will have more frequent mild Norte events.

The sea breeze and land breeze cycles are common local atmospheric systems existing in several parts of the world. However, sea breeze cycles have been found to be more stable and intense in tropical and sub-tropical regions due to weaker trade wind systems (Inman & Filloux, 1960). Results from Gille et al. (2003) on global land and sea breezes based on QuikSCAT wind analysis, suggested that the northern coast of the Yucatán peninsula is subject to relatively strong sea breeze cycles. The actual sea breeze cycle can extend from north of the Yucatán peninsula across almost the entire GoM (Gille et al., 2003). The strength of the sea breeze cycle is a function of temperature between land and sea (Hsu, 1988). This temperature difference is more pronounced during the summer season, leading to increased peak intensity of sea breeze cycles (Masselink & Pattiaratchi, 1998).

Studies have shown that sea breeze cycles induce wind that results in increased Suspended Sediment Concentration (SSC) and sediment transport rate (Pattiaratchi et al., 1997), increased offshore currents (Masselink & Pattiaratchi, 1998; Pattiaratchi et al., 1997), increase wave height (Masselink & Pattiaratchi, 1998) and change in wave angle (Sonu et al., 1973), all of which can that significantly affect beach morphology (Pattiaratchi et al., 1997; Inman & Filloux, 1960). In contrast, land breeze cycles are found to be associated with weaker wind due to the increased topography roughness over land and the lack of air convection (Sonu et al., 1973), resulting in low wave energy. For example, observations from Masselink and Pattiaratchi (1998) and Pattiaratchi et al. (1997) showed that longshore currents, wave height, and SSC were a factor of 20, 3, and 6 lower during the land breeze compered to the sea breeze cycle observations.

Several studies have been conducted in the northern part of the Yucatán peninsula investigating longshore sediment transport (e.g. Appendini et al., 2012), heat fluxes (e.g. Zavala-Hidalgo et al., 2014), and wind shear stress (e.g. Figueroa-Espinoza et al., 2014; de Velasco & Winant, 1996). However, to our current knowledge, there has not been a study in this area addressing the influence of land and sea breeze cycles as well as cold fronts (Nortes) on the nearshore hydrodynamics and sediment dynamics, except Torres-Freyermuth et al. (2017), which is based on the same field experiment focusing primarily on explanation of the field campaign and nearshore current circulation. Additionally, to the authors knowledge, there has not been a field study conducted to assess the relative importance of sea breeze cycles and cold fronts (Nortes) in light of nearshore morphodynamics. The work presented herein focuses on understanding the effect of mesoscale (i.e. land and sea breeze cycles), as well as synoptic scale (i.e. cold fronts) meteorological systems on nearshore hydrodynamics (e.g. waves, currents, turbulent kinetic energy, turbulent kinetic energy dissipation rate, bed shear stress) and the coupled morphodynamics (beach erosion and accretion, and sandbar migration, sediment fluxes in the cross and longshore direction).

2.2 Field experiment location

The study area is located in Sisal ($21°9'58.40''$N $90°2'11.00''$W) along the northern coast of the Yucatán peninsula (Figure 2.1). The Yucatán coast is characterized by a 245 km wide continental shelf and a 1:1000 slope (Mendoza et al., 2013; Appendini et al., 2012; Enriquez et al., 2010). Analysis of sediment samples indicates sandy material with a mean grain size of 0.5 mm in the swash zone and 0.3 mm in 1 m depth. Carbonate sediment is dominant in the region, where calcareous beach sediment is primarily derived from biogenic processes (Jiménez & Ávila, 2009). Shell fragments were found in the swash zone at the study site. The net longshore sediment transport in the region is over

48,000 m^3yr^{-1} to the west (Reyes et al., 2015). The beach width is 30 m and has a mean slope of 3.5^o with a 0.5 m dune. Additionally, two subtidal sandbars were observed at the study area that were 60 m apart and parallel to the shore. The study site also known for its economic importance where tourism and local fishing villages have been growing (Morales-Vela et al., 2003; Meyer-Arendt, 1991).

The region has a mixed tidal cycle with a tidal range of 0.1 m during neaps and 0.8 m during spring tides (Mendoza et al., 2013; Salles et al., 2013; Appendini et al., 2012). The wave field is influenced by the continental shelf of the Yucatán peninsula with slightly higher levels of wave energy reaching the eastern beaches compared to the western ones (Appendini et al., 2012). The surf zone can experience maximum current velocities upto 0.4 ms^{-1} during storms and significant wave heights ranging from 0.75 m to 1 m primarily arriving from northeast and east-northeast (Brinkkemper et al., 2013; Salles et al., 2013; Appendini et al., 2012). Recent findings by Torres-Freyermuth et al. (2017) suggest that within the surf zone currents are mainly controlled by wind during more intense events like sea breeze cycles and Nortes.

The north coast of the Yucatán peninsula is exposed to atmospheric circulations including: tropical cyclones, anticyclones, Nortes and a strong sea breeze systems (Figueroa-Espinoza et al., 2014; Mendoza et al., 2013; Meyer-Arendt, 1991). The wind climate in Sisal shows wind velocity values 50% stronger than other locations within a 50 km radius (Figueroa-Espinoza et al., 2014).Wind analyses by Figueroa-Espinoza et al. (2014) and Torres-Freyermuth et al. (2017) suggest a semi-consistent intense northeasterly (sea breeze cycles) and moderate southeasterly (land breeze cycles) wind. This consistency in winds pattern explains why Sisal has stronger winds compared to other nearby locations. The study location was selected to be near the Universidad Nacional Autónoma de México (UNAM) campus along the beach between Sisal port and an east pier due to the prevailing sea breeze winds and the availability to use existing instruments operated by UNAM.

The instruments operated by UNAM included multiple cameras covering the area between Sisal port and the pier, in addition to three anemometers located at different heights.

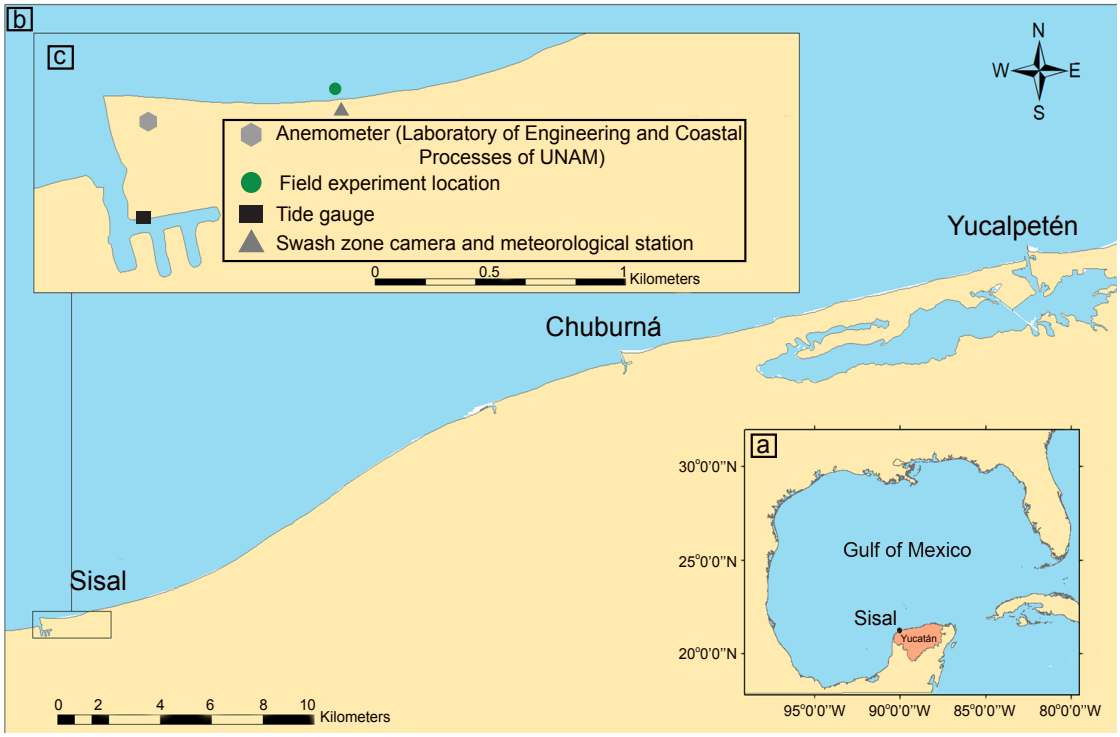

Figure 2.1. Map of the study area showing: (a) location of Sisal on the Yucatán peninsula, (b) a part of the northwest coast of the Yucatán peninsula, and (c) the study site and existing instrument locations.

2.3 Methodology

2.3.1 Field experiment

Data from this field experiment were acquired on Sisal beach from March 30 to April 12, 2014. The data were collected by more than 50 instruments, mostly along three cross-shore transects (West (W), Middle (M), and East (E), Figure 2.2). However, the present study will be focusing on the periods between April 1 and April 10, 2014, and limited to

some of the deployed instruments as detailed in Table 2.1. The instruments were deployed in the swash zone, surf zone, and inner shelf region. Two land-based meteorological stations were used to obtain wind, temperature, and atmospheric pressure measurements. The first meteorological station was located on the UNAM campus (approximately 0.6 km west of the study location). The station consisted of 3 ultrasonic anemometers sampling at 10 Hz positioned at 3, 6, and 24 m elevation, respectively. The second meteorological station (referred to as VISULA) was located on the dry beach near the middle transect. VISULA was set to collect mean values of wind speed and direction at 3 m elevation, temperature, and atmospheric pressure every 10 minutes. All data presented in this study are referenced to Universal Time Coordinate (UTC).

Instruments in the swash zone/inner surf were deployed along three cross-shore transects with a longshore spacing of 40 m. Sets of goalpost frames were made of galvanized steel pipes (dimensions of 2.5 m x 2.5 m x 12.5 m). Each transact had three stations (W1–W3: M1–M3:E1–E3) spaced 2.6 m (station 1 – station 2) and 4.9 m (station 2 – station 3) apart, respectively. Here, only the data from swash/inner surf zone stations W3, M3, and E3 are used. Each station held a Nortek Vectrino II acoustic Doppler velocimeter profiler (ADVP) measuring 3D current velocity profiles over a vertical range of up to 30 mm with an accuracy of 0.001 ms^{-1}. For the purpose of this paper only the top bin approximately 0.04 m above the local bed was used. The ADVPs were setup to sample continuously at 100 Hz. The ADVPs were wired to computers in a control trailer (Figure 2.2), for instant data display and storage. All computers were time-synchronized every second via satellite signal provided by a Trimble GPS antenna.

Water free-surface elevation was obtained using Druck pressure transducers (PT) sampling at 16 Hz with an accuracy of $\pm$ 0.10% of full scale. Data obtained from the PTs were stored using a data logger. All of the instruments deployed within the outer swash/inner surf zone were vertically adjustable. During the field campaign, sensors were adjusted

almost every 2 hours depending on the tide level, wave condition, and local bed level ensuring that instruments measured at the targeted depth.

Nortek Acoustic Doppler velocimeters (ADV) were used to obtain velocity point measurements in the surf zone that has an accuracy of $\pm$ 0.001 ms^{-1}. These ADV also feature a built-in PT to measure water free-surface elevation. Campbell Scientific optical backscatter sensors (OBS) were connected to the ADV internal logging system and were used to infer SSC from backscatter light amplitude. The ADVs were mounted to galvanized steel pipe goalpost frames looking downward, set to measure continuously at 16 Hz. In total, there were 5 ADVs and OBSs deployed in the surf zone, 3 located on the inner sandbar (E4, M4, and W4), one within the trough (M5), and one on the outer sandbar (M7). The ADVs were set to record velocities using the XYZ coordinate system, corresponding to cross-shore, longshore, and upward velocity respectively. A 2-MHz Nortek Aquadopp acoustic Doppler current profile (ADCP) was deployed in 4 m water depth (station M8) and set to measure the mean current velocity profile over 120 s intervals every 60 s and has an accuracy of $\pm$ 0.005 ms^{-1} (vertical bin size = 0.14 m).

Beach topography and wading depth surveys were conducted daily (except on April 5, 6, and 8) using a real time kinematic (RTK) differential global positioning systems (DGPS) consisting of a land-based base station and a pole-mounted rover antenna. The surveys were carried out along a number of cross-shore lines between the three transects with an accuracy of 0.01 m in the horizontal and 0.02 m in the vertical. The same system was used to record sensor locations in Universal Transverse Mercator (UTM – Zone 15).

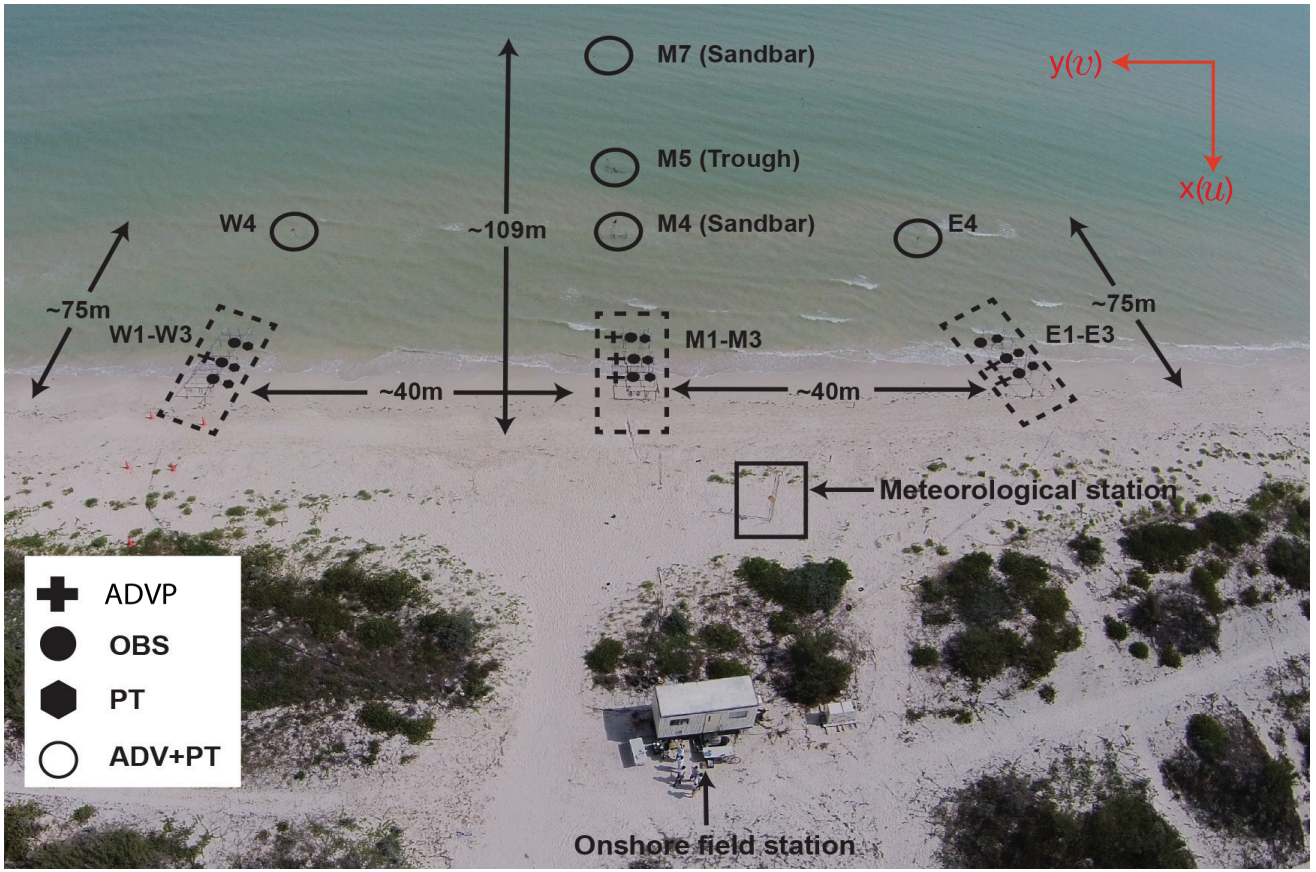

Figure 2.2. Aerial image of the study site showing the West, Middle, and East transects, VISULA, and the field trailer.

Table 2.1. Summary of the instruments used in this analysis.

Instrument	Position	Sampling	Sensor elevation above local bed and orientation	Measurment
Acoustic Doppler Velocimeter Profiler (ADVP)	W3 M3 E3	100 Hz continuous	0.04 m / down	current velocity
Pressure Transducer (PT)	W3 M3 E3	16 Hz continuous	0.0 m / down	pressure / water free-surface elevation
Acoustic Doppler velocimeter (ADV)	W4-W5 M4-M7 E4-E5	16 Hz continuous	0.15 m / down	current velocity, water free-surface elevation
Acoustic Doppler Current Profiler (ADCP)	M8	2 Hz every 120 s over 60 s intervals	0.4 m / up	current velocity, water free-surface elevation
Optical Backscatter Sensor (OBS)	W4 M3-M7 E4	16 Hz continuous	collocated with acoustic instruments / sideways	scattered infra-red radiation / turbidity
Meteorological station (MET)	on land	1 Hz continuous	-	temperature, relative humidity, atmospheric pressure, wind speed and direction

2.3.2 Data processing

The ADV and ADVP recorded the velocity in the XYZ coordinate system, corresponding to cross-shore (u), longshore (v), and upward (w) velocity respectively. Meanwhile the ADCP was set to record velocity in the ENU coordinate system. Prior to data analysis quality control was performed on both the recorded atmospheric and oceanographic data. Commonly acoustic velocity meters were used in deeper waters and usually velocities with correlation less than 70% were filtered out, but due to the natural environment of the surf zone high correlation is hard to obtain, thus measured velocities with correlation less than 55% were filtered out. Later, velocity and water free-surface elevation were block-averaged every two minutes and smoothed using a low pass filter over a ten minutes window.

Ten minutes mean wind stress (τ_w) was computed using wind speed observations from VISULA in the following way:

$$\tau_w = \rho_a \, C_D \, U_{10}^2 \tag{2.1}$$

where ρ_a is air density (assumed to be constant at 1.2 kgm^3), U_{10} is wind speed (ms^{-1}) at 10 m elevation above ground, and C_D is the drag coefficient estimated following the method by S. D. Smith (1988). Local wave parameters were computed using the data recorded by the pressure sensors. Prior to analysis, the data obtained by the pressure sensor were adjusted to account for depth attenuation using Fast Fourier transform and applying the pressure response factor (K_p). Significant wave height (H_s) was computed using the water free-surface elevation variance m_0 (zero$^{\text{th}}$ moment of the wave energy density spectrum using PWELCH spectrum), while the peak period (T_p) as computed using

the definition:

$$H_s = 4\sqrt{m_0} \tag{2.2}$$

$$T_p = \frac{1}{f_p} \tag{2.3}$$

where f_p represents the peak frequency of the wave energy density spectrum. Additionally, a zero-upcrossing method was used to obtain $H_{\frac{1}{3}}$ and significant wave period T_s to compare methods but the result is not discussed in this paper (Pierson, 1954). A common approach to estimate the cross-shore bed shear stress (τ_b) is the covariance method (e.g. Pope et al., 2006; Biron et al., 2004; Babaeyan-Koopaei et al., 2002; Kim et al., 2000) based on mean cross-shore and vertical velocity fluctuations ($\overline{u'w'}$) :

$$\tau = \rho_w \overline{u'w'} \tag{2.4}$$

where ρ_w is the density of salt water (assumed to be constant $\approx$ 1025 kgL^{-1}). Additionally, turbulent kinetic energy (TKE), and TKE dissipation rate (ε) were computed using the measured vertical velocities at each location, to minimize the effect of instrument noise (for details see Rusello, 2009). Two methods were used to estimate ε to provide redundancy and comparison between differing approaches. The first method includes fitting the Kolmogorov -5/3 slope within the inertial subrange of the Welch (1967) power spectral density (PSD) plot of turbulent velocity fluctuations (Kolmogorov, 1941) and assumes turbulence to be homogeneous and isotropic. Then ε can be estimated from:

$$E(k) = \alpha \varepsilon^{2/3} k^{-5/3} \tag{2.5}$$

where $E(k)$ is the energy spectra, k is the wavenumber, and α is the empirical Kolmogorov

constant for the vertical velocity component ≈ 0.71 (Lien & D'Asaro, 2006). The second method uses the bed friction velocity u_* assuming the wall logarithmic velocity profile shape is valid:

$$\varepsilon = \frac{u_*^3}{\kappa z} \tag{2.6}$$

where κ is the empirical von Kármán constant (≈ 0.4) and z is the height of measurement above the bed. These methods have been commonly used within surf zone field studies (e.g. Feddersen, 2012, 2007). However, Eq.2.5 and Eq.2.6 are difficult to estimate especially within the nearshore region where noise can interfere with the measurements leading to errors in the estimated ε values. Nevertheless, using the vertical velocity component in Eq.2.5 provides lower noise level compared to the horizontal velocity in terms of waves motion effect on the energy signature (Al Senafi, 2015; Thorpe, 2007; Gordon et al., 1999). TKE is estimated as:

$$\text{TKE} = \frac{1}{2}\left(\overline{u'^2} + \overline{v'^2} + \overline{w'^2}\right) \tag{2.7}$$

where $\overline{u'^2}$, $\overline{v'^2}$, and $\overline{w'^2}$ are the cross-shore, longshore, and vertical mean velocity variances, respectively.

OBS calibration to estimate SSC followed the method by Pratt (1990). The calibration procedure includes placing the OBS in a container filled with a known quantity of water and equipped with a stirring device that produces homogeneous turbulence throughout the calibration chamber. Known amounts (by weight) of dried sediment collected from the instrument site are added to the calibration chamber incrementally until the entire desired range of SSC is covered. The corresponding voltage readings are noted at each incremental step until the maximum voltage (5 V) is reached. SSC is then estimated by linear regression analysis of the calibration data creating a best-fit calibration curve to

convert OBS voltage to gl^{-1} concentration values.

A running average of longshore suspended sediment flux (q_v) and cross-shore suspended sediment flux (q_u), were obtained using the time averaged values of the instantaneous current velocity and SSC, following Jaffe et al. (1984):

$$q_v = \frac{1}{N}\sum_{i=0}^{i=n} v_{in}(SSC)_{in} \tag{2.8}$$

$$q_u = \frac{1}{N}\sum_{i=0}^{i=n} u_{in}(SSC)_{in} \tag{2.9}$$

where N is the number of data point in the sample, u_{in} is instantaneous cross-shore velocity, which is the sum of both the time averaged component ($\bar{u}$) and the fluctuation component (u'). The previous definition is also applied to SSC_{in}, and v_{in} in Eq.2.8 and Eq.2.9. A total suspended transport was also computed by integrating the suspended sediment flux obtained from Eq.2.8 and Eq.2.9 over each wind event period using the following definition:

$$Q_v = \sum_{i=0}^{i=n}\int_{t_1(i)}^{t_2(i)} q_v(t)dt \tag{2.10}$$

$$Q_u = \sum_{i=0}^{i=n}\int_{t_1(i)}^{t_2(i)} q_u(t)dt \tag{2.11}$$

where Q_v is the total suspended transport in the longshore direction, Q_u is the total suspended transport in the cross-shore direction, i is the number of events, t_1 and t_2 represent the start and end time of the event, respectively, and t is the time.

2.4 Results

2.4.1 Environmental forcing conditions

The time series measurements of wind speed and direction in Figure 2.3a display a typical sea and land breeze cycle with a weak offshore wind in the morning and strong onshore wind in the afternoon during the local time of Sisal. Over the 11-day duration of the study, the site experienced 9 sea breeze cycles, 8 land breeze cycles, and one Norte event. The wind events were categorized based on wind speed and direction, except for the first two sea breeze cycles they were categorized in terms of the wave energy level. On average, the duration of the land breeze cycle (12.6 hr) was three hours longer than the duration of the sea breeze cycle (9.6 hr). Sea breeze cycles were associated with intense bursts of wind with speeds ranging from 5 ms^{-1} to 12 ms^{-1}, blowing from a northeasterly to easterly direction (Figure 2.3a, light gray shaded areas). Land breeze cycles were found to be characterized by weaker and sustained winds (less than 6 ms^{-1}), primarily blowing from the southeast and south, except on April 7, 2014 (6 $ms^{-1} < U_{10} < 8$ ms^{-1}). The Norte event dominated the picture from April 8 to April 9, 2014 and was accompanied by a dramatic change in wind direction, rapidly increasing wind stress (up to 0.55 Nm^{-2} , Figure 2.4b) and wind speeds up to 15 ms^{-1} blowing from the north.

Measured water free-surface elevation (η) was recorded every one minute using a tidal gauge located in Sisal port and compared to the one hour predicted water free-surface elevation (Figure 2.3c). During the sea and land breeze cycles a deviation of $\pm$ 0.1 m between predicted and measured water free-surface elevation (η) was notable. In Figure 2.3c η is referenced to Mean Sea Level (MSL). During the Norte event, measured water free-surface elevation exceeded the predicted values by approximately 0.36 m due to the prevailing intense and sustained onshore wind. The variation of wind measurements is reflected in the inner shelf wave climate (i.e. H_s, T_p, and wave direction) and can be

related to the fluctuation of wind stress (Figure 2.3a, b, and d). During land breeze cycle offshore significant wave height was found to be with values between 0.1 and 0.32 m arriving mainly from the north and northeast. The onset of sea breeze events resulted in immediate increase in significant wave height (0.41 – 0.65 m) and period (4 – 5 s). The most discernible changes in wave climate occurred during the Norte with maximum wave height and period up to 1.3 m and 10 s, respectively, arriving from the north and northwest. This increase in wave energy levels can be linked to the increase in wind shear stress.

Measurements of mean offshore current (V_c) indicate a consistent direction towards the west during sea breeze cycles. Current velocities associated with these events ranged from 0.1 to 0.2 ms^{-1} (Figure 2.3-e). In contrast, currents during land breeze cycles were directed towards the west, except for April 7, 2014 when the current direction shifted towards the southeast with reduced magnitude (≈ 0.12 ms^{-1}). Currents during the Norte behaved similarly to those during the sea breeze cycles but velocities were sustained for a longer period of time.

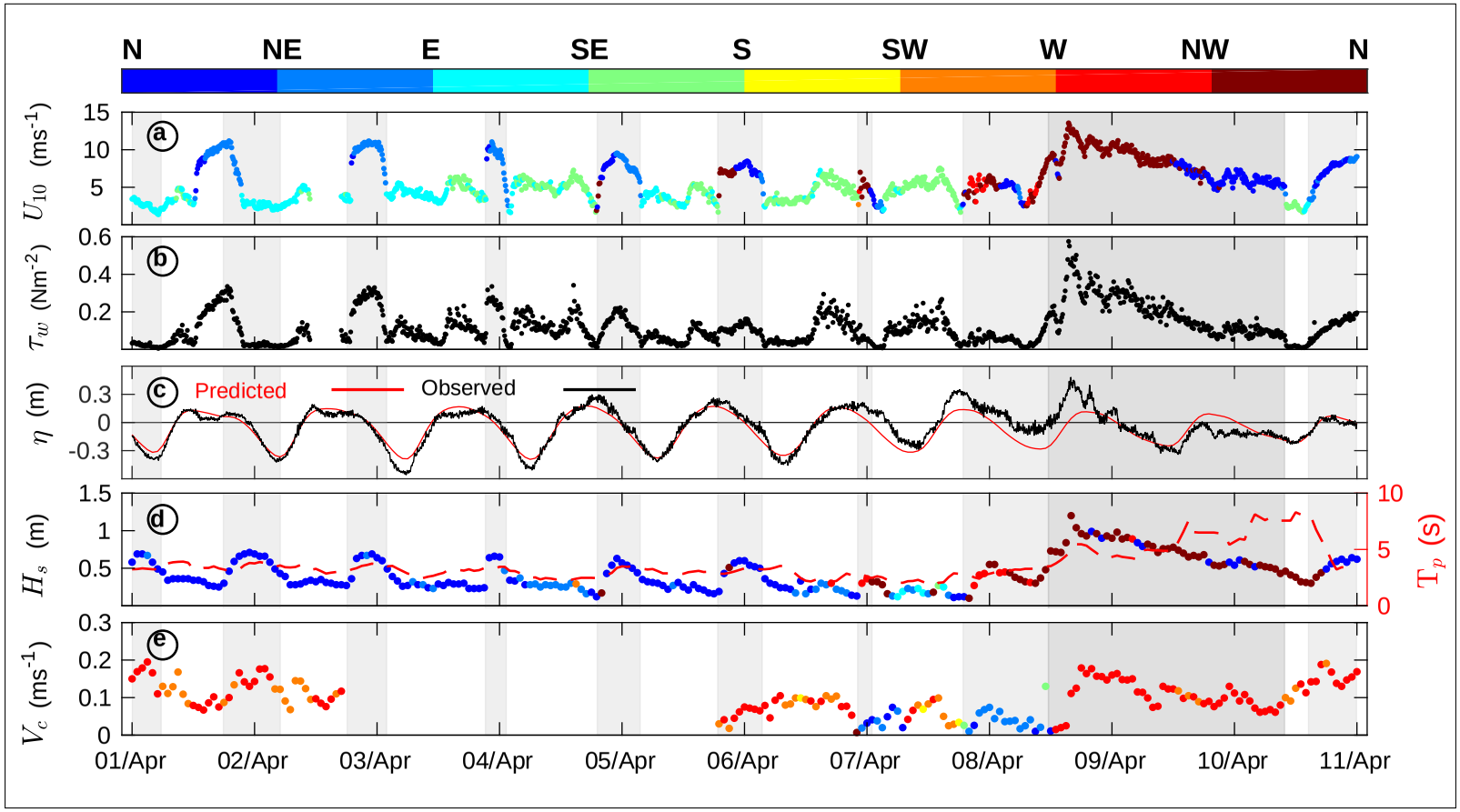

Figure 2.3. Meteorological observations and offshore hydrodynamics: (a) wind speed and direction, (b) wind shear stress, (c) comparison between observed and predicted water free-surface elevation with respect to NMM, (d) offshore significant wave height and peak wave period (station M8), (e) mean current velocity and direction (station M8). The light gray shaded areas represent sea breeze cycles, white areas refer to land breeze cycles and the dark gray shaded area indicates the Norte event. The color-bar indicates wind and waves coming from direction.

2.4.2 Nearshore hydrodynamics and suspended sediment concentration

Stations M7, M5, and W4 were selected to represent the wave climate within the surf zone, and M3 to represent the outer swash/inner-surf zone (see Figure 2.4). Gaps in the wave data record are due to exposure of pressure sensors to the atmosphere for short periods of time during the field experiment when water levels were low. Waves in the surf and the outer swash/inner-surf zone were generally weaker during the land breeze cycle (Figure 2.4a) and more intense during the sea breeze cycle with significant wave heights ranging from 0.2 m to 0.4 m (almost 50% lower than offshore wave conditions).

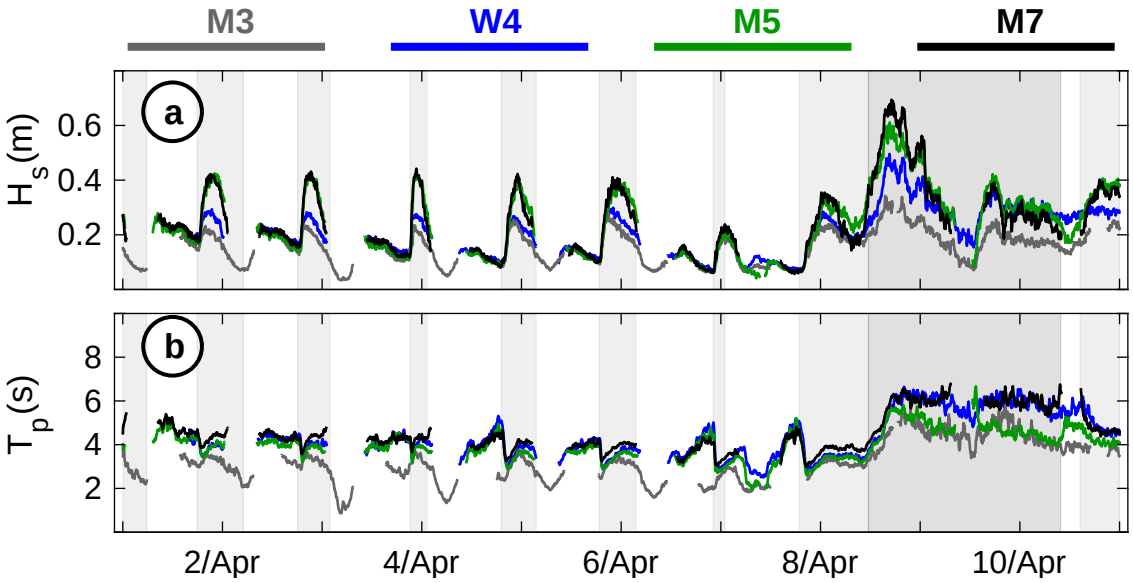

Figure 2.4. Measured time series of: (a) significant wave height and (b) peak wave period. The light gray shaded areas represent sea breeze cycles, white areas refer to land breeze cycles and the dark gray shaded area indicates the Norte event.

The overall characteristics of the cross-shore currents for the surf zone and the outer swash/inner-surf zone are shown in Figures 2.5a and 2.5b, respectively, where positive values indicate onshore currents and negative values indicate offshore currents. In comparison, the surf zone cross-shore velocities (0.06 to -0.24 ms^{-1}) are found to be higher than those in the outer swash/inner-surf zone (0.03 to -0.12 ms^{-1}). These differences count for approximately 50% in current velocities between the surf zone and the outer swash/inner-surf zone and can be due to the difference in wave energy levels between the zones as mentioned previously. During the sea breeze cycle the currents were mainly directed offshore and found to be more intense at stations W4, E4, M4, and M7. Station M5 showed a different current flow pattern than the other surf zone stations. During the sea breeze cycles velocities were primarily onshore-directed as opposed to offshore at the other stations. This may point to a complex three-dimensional circulation phenomenon related to the bar-trough morphology at the site. During the Norte, offshore flow was sustained at all stations with a mean velocity of -0.12 ms^{-1} in the surf zone and -0.06 ms^{-1} in the outer swash/inner-surf zone indicating erosive conditions. Stations located on the inner sandbar (W4, E4, and M4) experienced intense westward longshore currents with magnitudes between 0.05 ms^{-1} and 0.44 ms^{-1} during sea breeze cycles (Figure 2.5c). These shifted towards the east during the Norte with velocity magnitudes of up to -0.42 ms^{-1}. Similar longshore currents direction can be seen at the outer swash/inner-surf zone stations (W3, E3, and M3) as shown in Figure 2.5d during both the sea breeze cycles and Norte. However, current velocities were 60% lower than observed velocities within the surf zone.

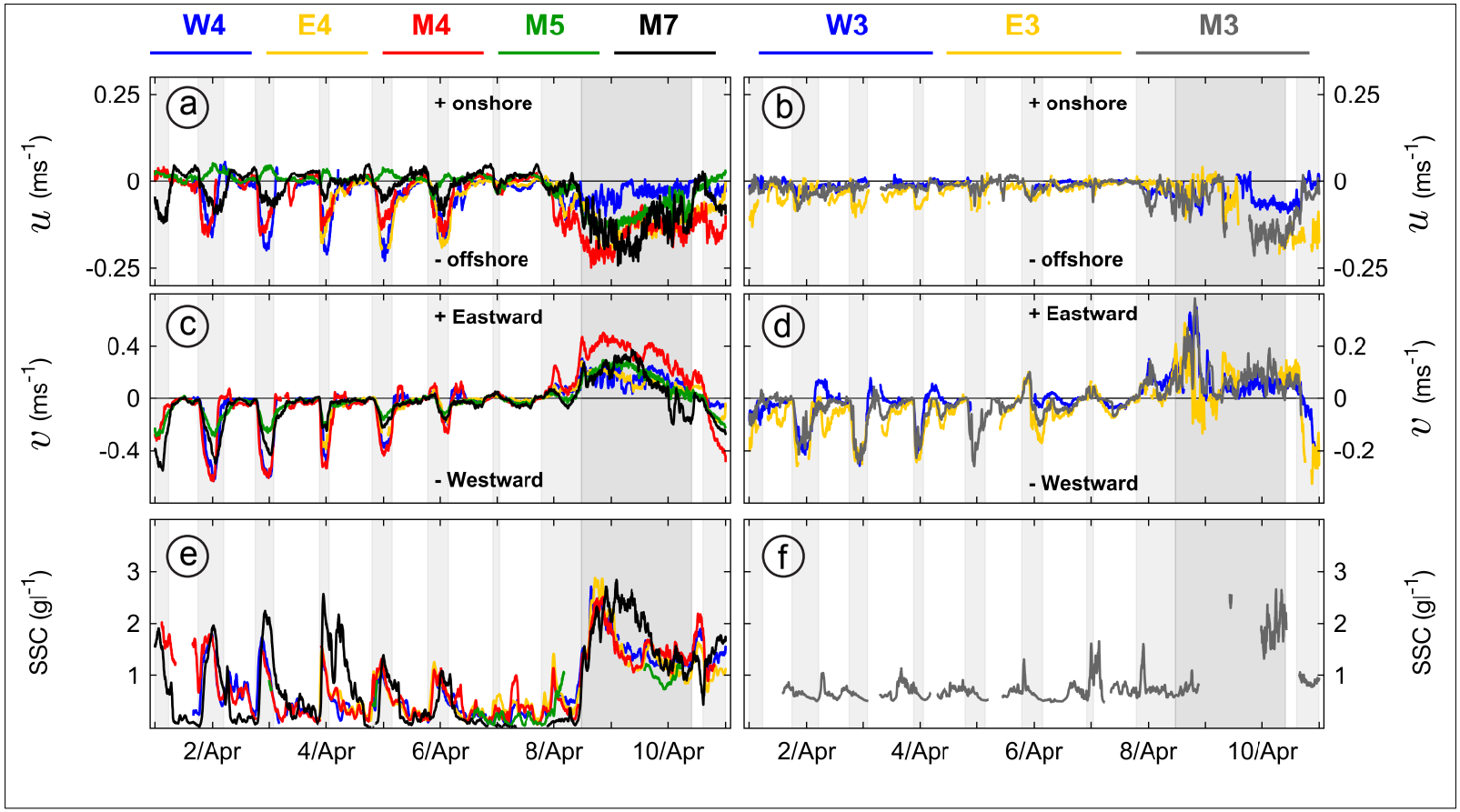

Figure 2.5. Measured time series of: (a) surf zone cross-shore currents, (b) outer swash/inner-surf zone cross-shore currents, (c) surf zone longshore currents, (d) outer swash/inner-surf zone longshore currents, (e) surf zone suspended sediment concentration , (f) outer swash/inner-surf zone suspended sediment concentration. The light gray shaded areas represent sea breeze cycles, white areas refer to land breeze cycles and the dark gray shaded area indicates the Norte event.

Suspended sediment concentrations (Figure 2.5e–f) experienced an immediate jump during the onset of the sea breeze cycles as nearshore energy levels increased. At the surf zone stations the mean suspended sediment concentration increased from 0.5 gl^{-1} during land breeze cycles to 1.1 gl^{-1} during the sea breeze cycles. This increase was also observed during the Norte, however, sediment suspension was sustained almost continuously at levels around 1.5 gl^{-1}. Additionally, the outer swash/inner-surf zone station (M3) experienced lower suspension values compared to the surf zone measurements during sea breeze cycles with a mean of 0.7 gl^{-1}. The outer swash/inner-surf zone station recorded lower velocities and contained coarser sediment grains than the surf zone stations, which may explain the lower SSC values.

2.4.3 Turbulence and near bed shear stress

The energy levels experienced within the nearshore regions vary and mostly depend on the beach energy levels that is primarily linked to the beach slope. For example a beach with a plunging breakers waves will have a higher TKE and turbulent kinetic energy dissipation rate levels higher than a beach with a spilling breaker. The reported values of TKE levels within the nearshore region ranged from 10^{-5} m^2s^{-2} to 10^{-2} m^2s^{-2} and with turbulent kinetic energy dissipation rate up to 10^{-2} m^2s^{-3} (e.g. Brinkkemper et al., 2017; Feddersen, 2012; Ruessink, 2010; Feddersen et al., 2007). The turbulent kinetic energy dissipation rate is estimated using Eq.2.5 and Eq.2.6 with results shown in Figure 2.6a–b and Figure 2.6c–d, respectively, for the two different approaches. Both methods display a similar pattern, but with higher estimated values of ε with Eq.2.5, especially within the outer swash/inner-surf zone. ε values estimated using Eq.2.6 show less fluctuation and more pronounced influence of the effect of wind events. Results from Eq.2.6 take into account the frictional velocity, unlike Eq.2.5 that only depends on the vertical velocity. Therefore Figure 2.6c–d display a similar pattern to the cross-shore velocity and wind pat-

tern. During the land breeze cycles the maximum ε recorded across all surf zone stations was 3.5×10^{-4} m^2s^{-3}. Higher ε values were observed over the inner sandbar stations, with magnitudes between 3×10^{-4} m^2s^{-3} and 2.5×10^{-3} m^2s^{-3} using Eq.2.5 and magnitudes between 4×10^{-4} m^2s^{-3} and 1.4×10^{-3} m^2s^{-3} using Eq.2.6. The increase in ε values especially over the sandbars can be a result from wave breaking. Norte values of ε were higher and gradually increased during the first 12 hours ranging from 1.9×10^{-4} m^2s^{-3} to 3.5×10^{-3} m^2s^{-3} (Figure 2.6a). After that ε values decreased as wind intensity began to subside. During the land breeze cycles, the outer swash/inner-surf zone was characterized by low ε values ranging from 2×10^{-4} to 1×10^{-3} m^2s^{-3} (Figure 2.6d). Meanwhile, higher values of ε was experienced during the sea breeze cycles with values ranging from3×10^{-4} to 2×10^{-3} m^2s^{-3} (Figure 2.6d). During the Norte event, the estimated ε values in the outer swash/inner-surf zone were higher than values observed by the surf zone stations with a maximum value of 5×10^{-3} m^2s^{-3}.

The estimated TKE values (Figure 2.6e–f) behaved similarly to ε, with lower TKE values during land breeze cycles exhibiting a mean of 7.4×10^{-4} m^2s^{-2} $\pm$ 3×10^{-4} in the surf zone and 2.9×10^{-3} m^2s^{-3} $\pm$ 1.6×10^{-3} in outer swash/inner-surf zone. Higher TKE values were observed during the sea breeze cycle with a mean of 1×10^{-3} m^2s^{-2} $\pm$ 4×10^{-4} in the surf zone and 5.6×10^{-3} m^2s^{-2} $\pm$ 2.6×10^{-3} in outer swash/inner-surf zone. TKE values during the Norte, were higher than those during the diurnal wind cycle for all stations and were almost constant for the surf zone stations with a mean of 3.7×10^{-3} m^2s^{-2}. Meanwhile, at the outer swash/inner-surf zone stations the mean Norte TKE value was 1×10^{-2} m^2s^{-2}.

Measurements of shear stress are essential components of almost all sediment transport models and specifically are of interest in terms of motion thresholds for sediment movement. Thus, it is important to investigate the spatial and temporal changes in near-bed shear stresses within the nearshore region to better estimate conditions where large

amount of sediment can be mobilized. The near-bed shear stress at the surf zone stations during the field experiment ranged from 1 Nm^{-2} to 21 Nm^{-2} (Figure 2.7a). During the land breeze cycles values were relatively low with an average of 2.7 Nm^{-2}. An abrupt increase in τ was observed with the onset of each sea breeze cycle exhibiting a mean of 5.5 $Nm^{-2} \pm 1.5$ and a maximum value up to 11 Nm^{-2}. The peak values of τ were significantly higher during the Norte period with the highest at the outer sandbar station (M7) with a mean maximum shear stress value of 14 Nm^{-2} and lowest within the trough station (M5) with a mean maximum shear stress value of 10 Nm^{-2}. The overall surf zone shear stress during the Norte event ranged from 8 Nm^{-2} to 21 Nm^{-2}. Similar observations were made in the outer swash/inner-surf zone (Figure 2.7b). However, values of τ in theouter swash/inner-surf zone were higher than those in the surf zone. Mean shear stress magnitudes during land breeze cycles, sea breeze cycles, and the Norte event were 7.4, 9.2, and 36.3 Nm^{-2}, respectively. However, stations at outer swash/inner-surf zone had a significant portion of data gaps in the beginning of the Norte event and certainly affected the statistical analysis of computed mean and max values that could have been higher based on τ values of stations located in the surf zone.

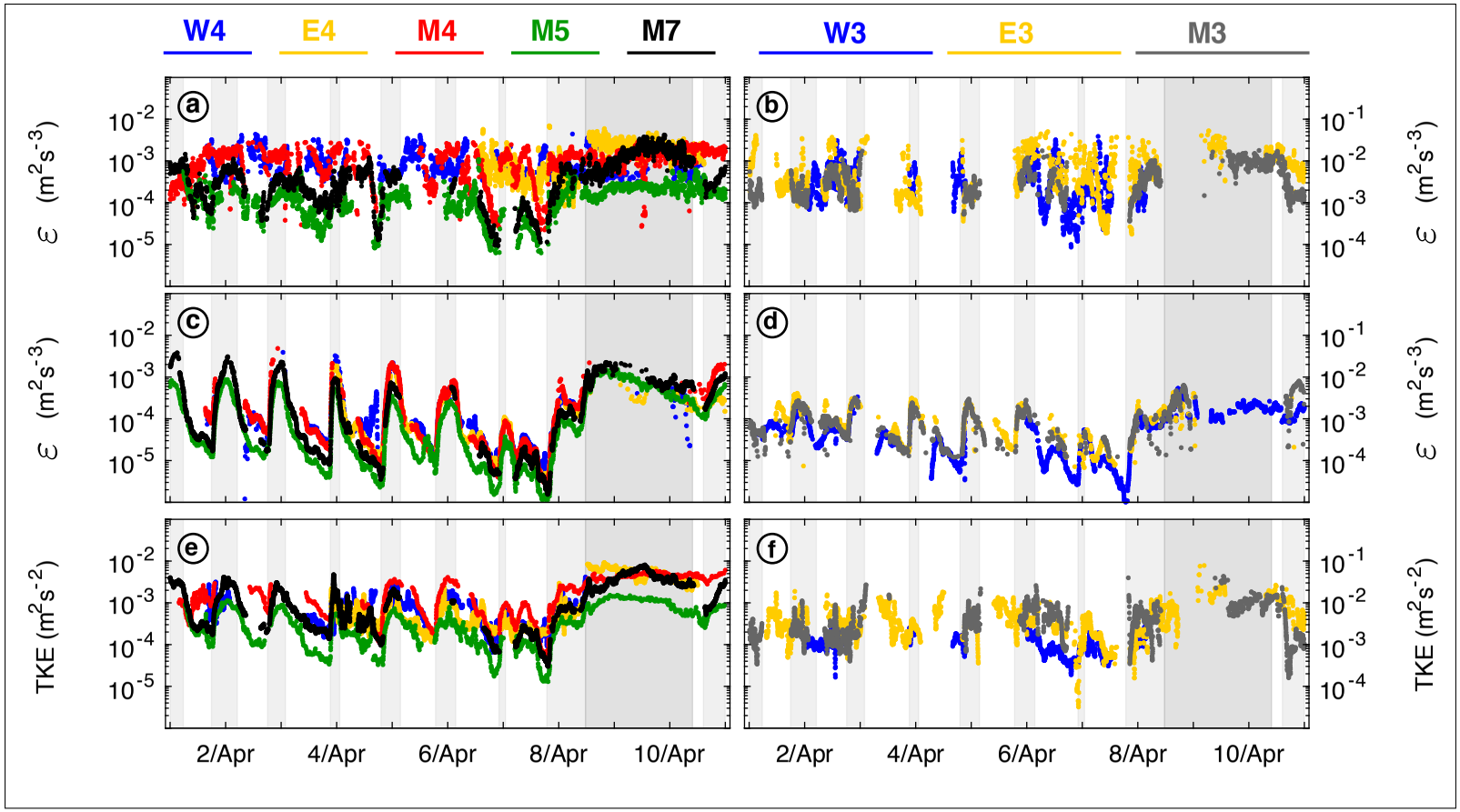

Figure 2.6. Measured time series of: (a) surf zone ε computed using Eq.2.5 , (b) outer swash/inner-surf zone ε computed using Eq.2.5, (c) surf zone ε computed using Eq.2.6, (d) outer swash/inner-surf zone ε computed using Eq.2.6, (e) surf zone TKE, (f) outer swash/inner-surf zone TKE. The light gray shaded areas represent sea breeze cycles, white areas refer to land breeze cycles and the dark gray shaded area indicates the Norte event.

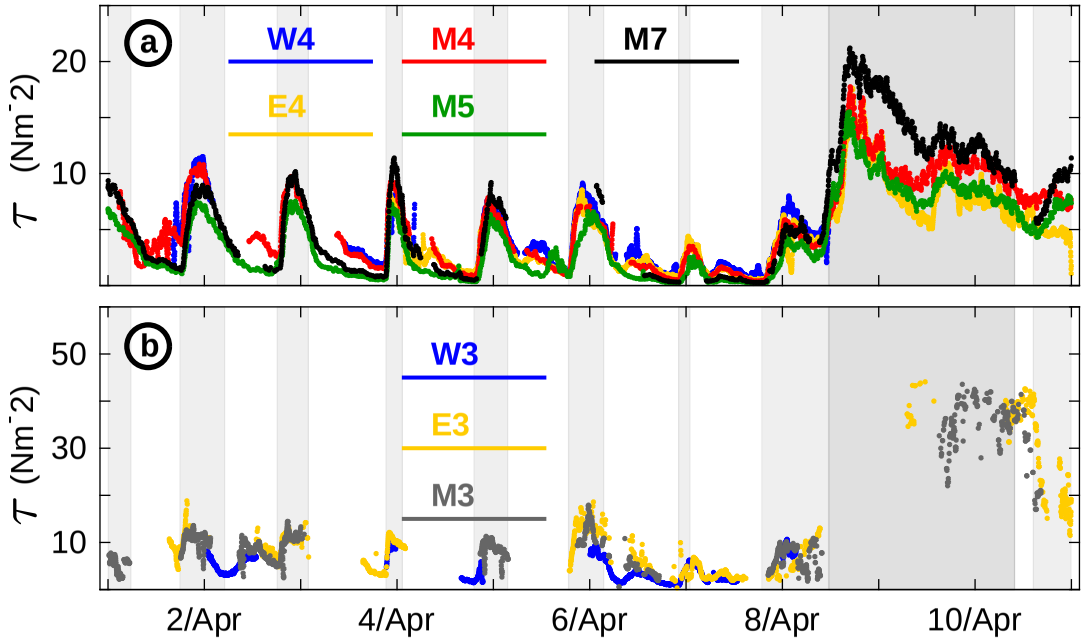

Figure 2.7. Estimated bed shear stress at: (a) surf zone stations, (b) outer swash/inner-surf zone stations. The light gray shaded areas represent sea breeze cycles, white areas refer to land breeze cycles and the dark gray shaded area indicates the Norte event.

2.4.4 Beach morphology

Despite the study site location taking a place between the Sisal port and the Sisal pier, this section of the cost can be described as fairly uniform in the longshore direction. The bathymetry survey boundaries covered a longshore distance of 120 m and 140 m in the cross-shore. In total 24 bathymetry surveys were made with a spacing ranging between 4 m and 6 m. Snapshots of the nearshore bathymetry at three different instances in time are displayed in Figure 2.8a–c. The given bathymetric measurements represent sample bed elevation data collected during/after a sea breeze cycle (Figure 2.8a), a land breeze cycle (Figure 2.8b), and the Norte event (Figure 2.8c). All bed level data were obtained via real-time kinematic (RTK) global positioning system (GPS) wading depth surveys and revealed two nearshore sandbars. The inner bar was located between 90 m and 110 m and characterized by a height of 1.1 m and a slope of 2.1°, while the outer bar was located between 150 m and 170 m and characterized by a height of 1.85 m and a mean slope of 1.7°. The bars were separated by a trough (located between 110 and 150 m). The beach included a step that migrates between 58 m and 62 m and the overall mean slope of the beach profile was 1.3° (Figure 2.9a)

Comparing observations from Figure 2.8a and Figure 2.8b it can be seen that after the sea breeze cycle on April 3 sandbars are more pronounced than those seen after the land breeze cycle on April 7. Additionally, after the land breeze cycle on April 7 the outer sandbar width increased by 8 m. On the other hand, the Norte resulted in wider sandbars, specifically the outer sandbar experienced a 12 m increase in width and became more flattened and resulted in a deeper trough (Figure 2.8c). Bed level changes between selected measured profiles are presented in Figure 2.8d–f to assess areas of erosion and accretion related to different forcing conditions. Sea breeze, land breeze, and Norte conditions influence the nearshore bathymetry in different ways (Figure 2.8d–f). Bed level changes

after the sea breeze cycle on April 4 indicate that accretion took place over both sandbars ranging from 0.05 m to 0.21 m, while erosion occurred in the trough and the inner surf zone ranging from 0.05 m to 0.34 m (Figure 2.8d). In contrast, bed level changes resulting from the land breeze cycle on April 7 indicate a mean of 0.15 m accretion over the surf zone and 0.05 m erosion in the outer outer swash/inner-surf zone (Figure 2.8e). Increased erosion rates over the entire study site occurred during the Norte event with the exception of the outer swash/inner-surf zone, where significant accretion up to 0.28 m was recorded (Figure 2.8f). For the selected events (Figure 2.8d–f) a summary of total volume losses and gains normalized over the longshore distance (140 m) is given in Table 2.2. Result from Table 2.2 indicates that accretion volume that is associated with the land breeze cycle was 7 times higher than the volume loss. The sea breeze cycle resulted in erosion mainly around the trough region and the inner sandbar with an increase of 350% of volume loss compared to the extended land breeze cycle. The most significant volume loss was observed during the Norte event with an increase of 129% higher compared to the sea breeze cycle.

Table 2.2. Comparison of volume losses and gains from selected events.

Event	Volume loss (m^3m^{-1})	Volume gained (m^3m^{-1})
Post sea breeze (April/3 – 4)	7	3
Post land breeze (April/4 – 7)	1.8	13
During Norte (April/9)	16	4

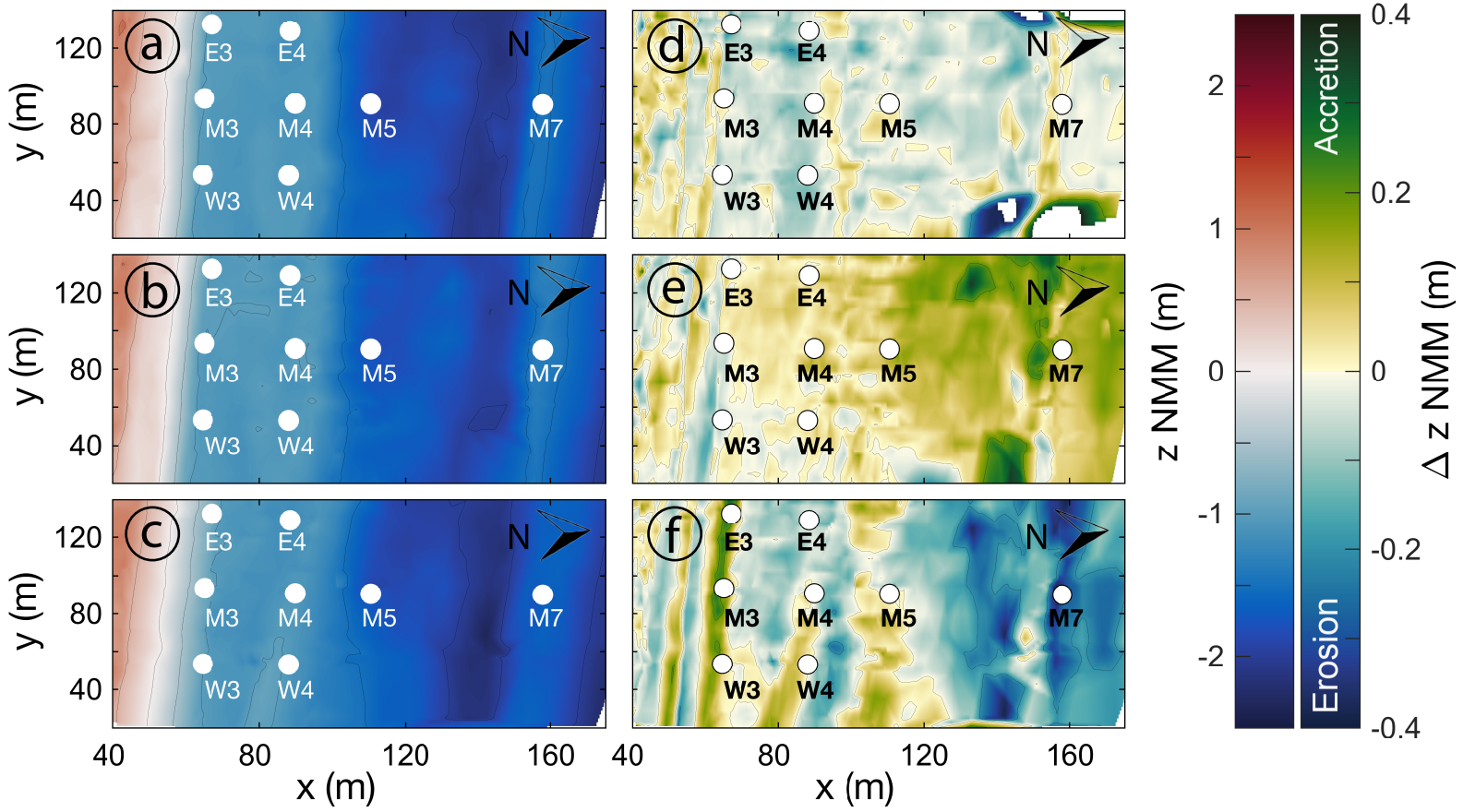

Figure 2.8. Plan view of nearshore bathymetry measured: (a) during the sea breeze cycle on April/3, (b) during the land breeze cycle on April/7, (c) and during the Norte event on April/9. Measured bed changes between (d) April/3 – 4 (post sea breeze), (e) April/4 – 7 (post land breeze), and (f) on April/9 (during Norte).

Further insight into nearshore morphodynamics over the duration of the field study is provided by examining measured beach profiles along the middle transect (Figure 2.9). Elevation changes in response to five sea breeze events (April 1 – 4, and 10), a strong land breeze event on April 6 – 7, and the Norte event on April 9 are captured. During the sea breeze events, the beach profile elevations encountered significant variation. Most of these changes were observed between M3 and M7, specifically between the two sandbars, while the foreshore remained almost unchanged with low vertical variation on the order of $\pm$ 0.05 m. Energetic conditions during the selected sea breeze cycles resulted in mean erosion of the inner and outer sandbars of 0.15 m and 0.13 m, respectively (Figure 2.9b, and c).

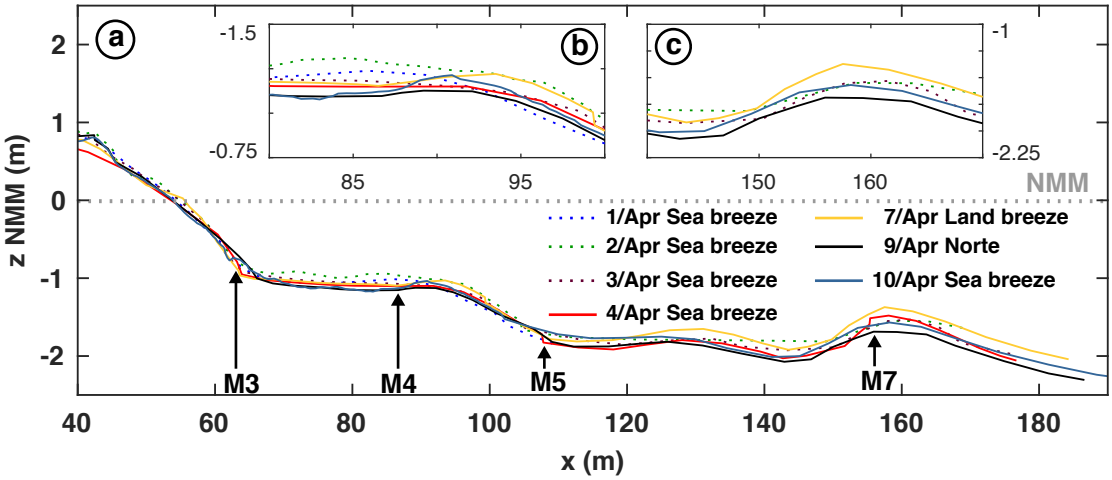

Figure 2.9. Measured beach profiles along the middle transect. The vertical axis represent elevation above Nivel Medio del Mar (NMM, i.e. mean tidal level), while horizontal axis represents cross-shore distance. Inset panels (b) and (c) provide a zoomed-in view of the profile evolution around the inner and outer sandbar, respectively.

During sea breeze cycles, the outer sandbar became more skewed toward the land and increased in steepness and height. During the strong land breeze event on April 6 – 7, pro-

file elevation increased and both sandbars migrated onshore by 2 – 3 m. The most abrupt morphological change occurred during the onset of the Norte event, resulting in a steeper foreshore by 1.5° than others observed during the sea breeze cycle with approximately 0.2 m of sediment accumulation at M3 (beach step). Additionally, during the Norte event sandbars eroded by 0.25 m at M4 and 0.5 m at M7, respectively, and migrated approximately 2 m seaward. During the Norte event the inner sandbar increased in steepness by 1°, while a decrease of 0.4° was recorded at the outer sandbar slope. These changes in the morphodynamics are mainly linked to bed-load transport due to the increase in near bed shear stress.

2.4.5 Longshore and cross-shore suspended sediment flux

Suspended sediment flux was estimated using Eq.2.8 and Eq.2.9 as introduced in Section 2.3.2. Figure 2.10 displays time series of suspended sediment flux at M3, W4, E4, M4, M5, and M7 separated into the cross-shore (Panel a) and longshore (Panel b) component. Cross-shore values are positive for onshore-directed transport and negative for offshore-directed transport. Longshore values are positive toward the East (downdrift) and negative toward the West (updrift). Maximum values of cross-shore suspended sediment flux (Figure 2.10a) were generally one order of magnitude higher during sea breeze cycles (0.3 $kgm^{-2}s^{-1}$, directed offshore) compared to land breeze cycles (0.03 $kgm^{-2}s^{-1}$, directed onshore). Stations located on the inner sandbar (W4, E4, M4) registered the largest magnitudes of cross-shore suspended sediment flux. During the extended land breeze event on April 6 – 7, the suspended sediment flux was almost constant with very little fluctuation across all stations (between -0.002 $kgm^{-2}s^{-1}$ and 0.01 $kgm^{-2}s^{-1}$).

The transition from pre-frontal to frontal phase at the onset of the Norte was marked by an abrupt increase in offshore-directed suspended sediment flux with a mean of 0.2 $kgm^{-2}s^{-1} \pm 0.9$. The longshore suspended sediment flux component (Figure 2.10b) dis-

played similar characteristics to its cross-shore counterpart but larger magnitudes up to 1 $kgm^{-2}s^{-1}$ during sea breeze cycles. The longshore suspended sediment flux direction during the sea breeze cycles was toward the west with a mean of 0.4 $kgm^{-2}s^{-1} \pm 0.2$, except for station M3 which displayed a mean of 0.1 $kgm^{-2}s^{-1} \pm 0.06$. This difference in longshore current intensity between M3 and other stations was due to the different dynamics that are associated with the outer swash/inner-surf zone (detailed explanation can be found in Section 2.5.1) .Gaps in M3 observations seen in Figure 2.10a-b are a result from the quality control, where both the OBS or the ADVP had a high noise level or when instruments were exposed to atmosphere. The surf zone stations experienced intense eastward suspended sediment flux during the Norte event with a maximum value of 1.3 $kgm^{-2}s^{-1}$ observed at station M4, while station M3 registered a lower longshore suspended sediment flux magnitude with a mean of 0.14 $kgm^{-2}s^{-1} \pm 0.08$.

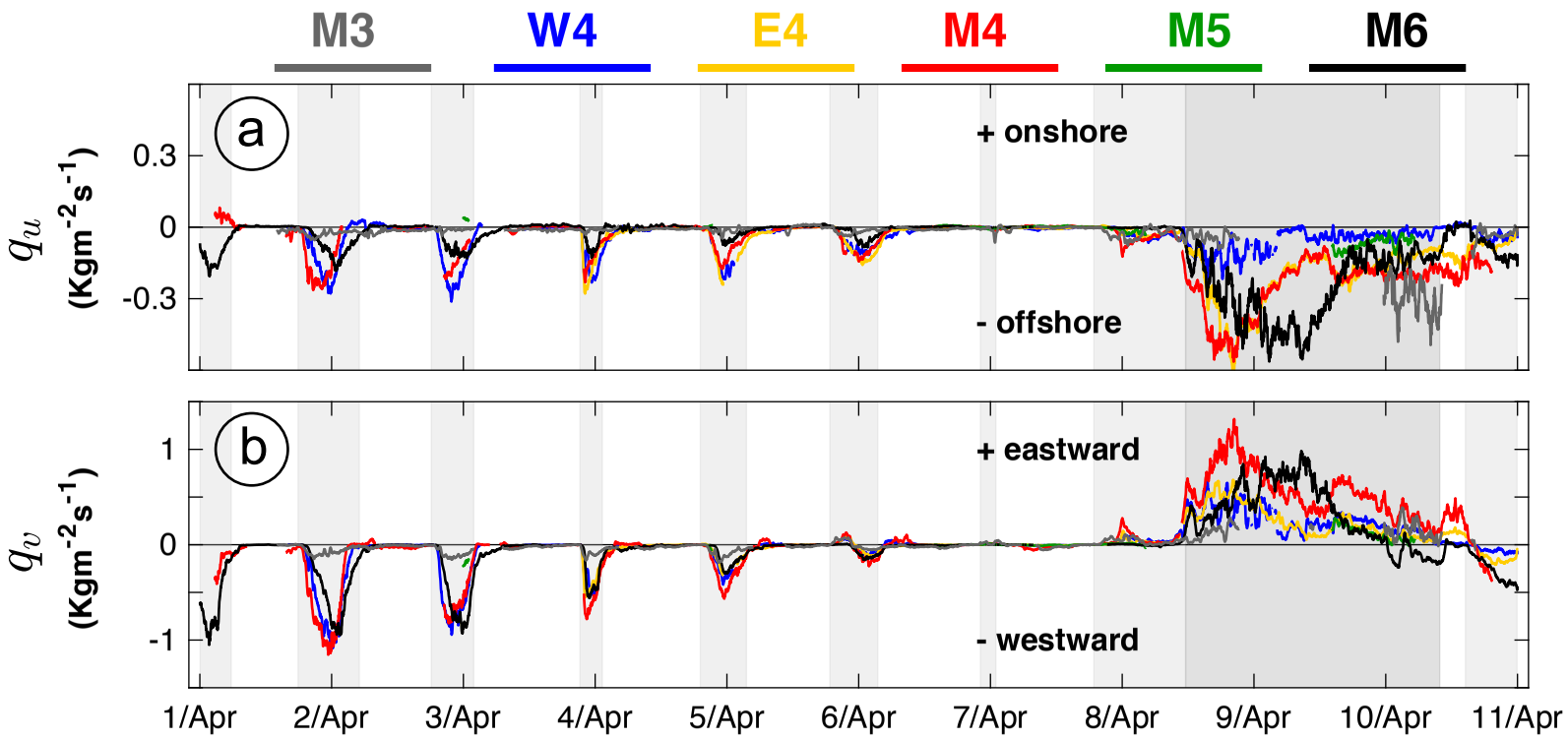

Figure 2.10. Measured time series of suspended sediment flux: (a) cross-shore (b) longshore. The light gray shaded areas represent sea breeze cycles, white areas refer to land breeze cycles and the dark gray shaded area indicates the Norte event.

Statistical analyses of both longshore and cross-shore suspended sediment flux for the middle transect are displayed in Figure 2.11 including each land and sea breeze cycle and the Norte event. The figure shows maxima, minima, and mean values with 95% confidence intervals. The Figure indicate that overall cross-shore suspended sediment flux has a higher variability during the sea breeze cycles compared to the land breeze cycles. This can be related to the abrupt increase in wave heights observed during sea breeze cycles when compared to the low wave energetic conditions experienced during the land breeze cycles. Moreover, observations suggest that highest variability was experienced during the third, fourth, and ninth sea breeze events at the inner sandbar stations (i.e. E4, M4, and W4). During the Norte event all stations encountered the highest cross-shore suspended sediment flux variability, except for W4. The low variability observed at W4 is due to the lower cross-shore velocity observed at the location. The low cross-shore velocity is high likely due to the lower wave heights compared to stations M5 and M7. Similar observations can be seen from the computed longshore suspended sediment flux but with higher magnitude. The largest variability values were followed by those measured at M5 and W4 in descending order. Nevertheless, it is worth mentioning that gaps in SSC and velocity measurements also effected the outcome for the sediment transport statistics.

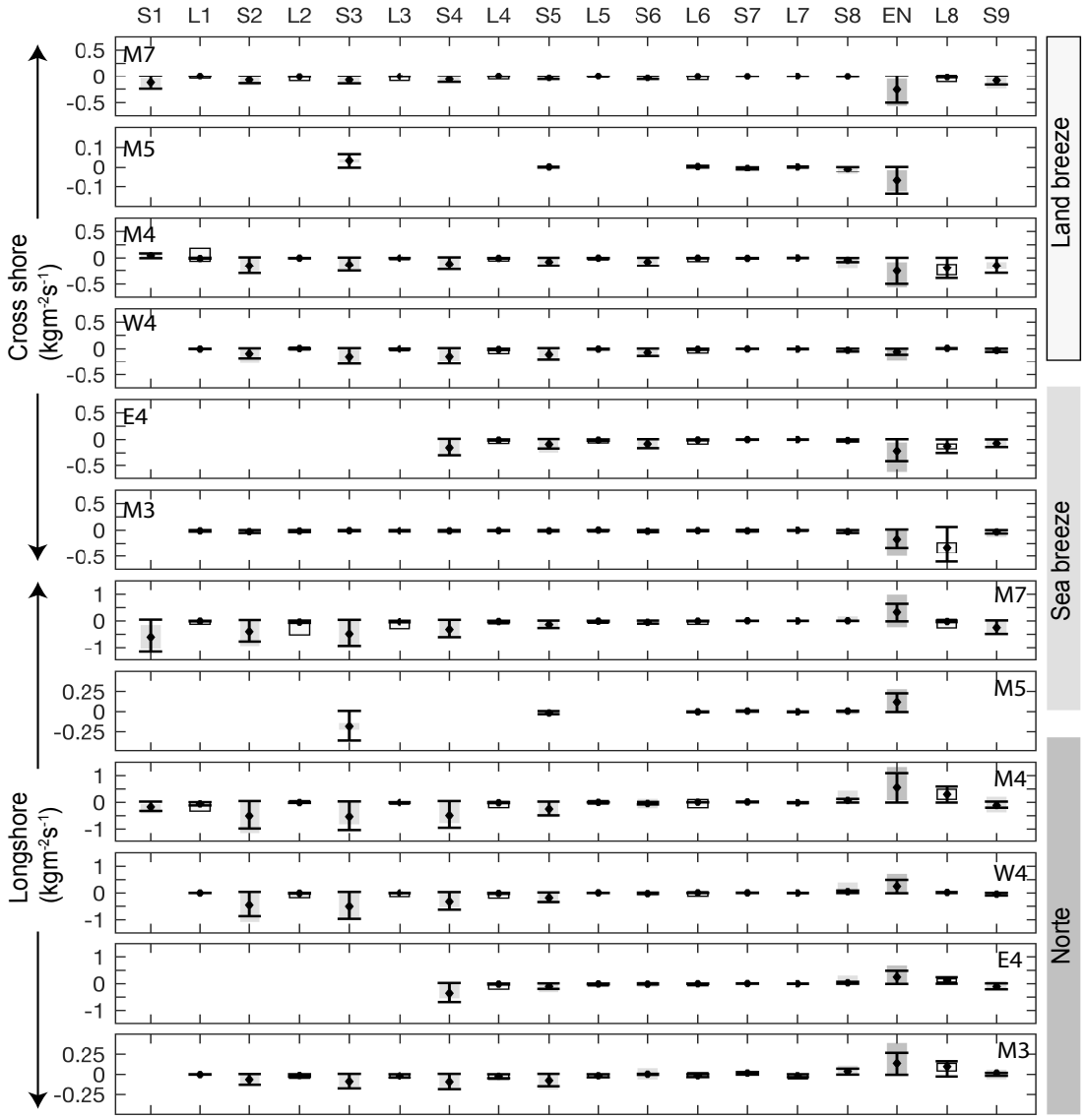

Figure 2.11. Cross-shore and longshore suspended sediment flux statistics for each land and sea breeze cycle and the Norte event. The shaded bars represent maximum and minimum values, while the whisker plots display mean values with 95% confidence intervals.

2.5 Discussion

This study compares the impact of diurnal wind system forcing (land and sea breezes) on nearshore processes to the impact of a cold front or Norte at the location of Sisal beach. Nearshore processes investigated via field measurements include currents, waves, turbulent kinetic energy and its dissipation rate, suspended sediment flux, and morphodynamics. Similarly to previous findings, a significant relationship between wind and nearshore processes is discovered. This has been confirmed by a recent study on nearshore circulation based on the same field experiment by Torres-Freyermuth et al. (2017). They suggest that within the surf zone and the outer swash/inner-surf zone, currents are mainly controlled by intense winds during Norte and sea breeze cycles. In the following, the new findings are discussed and placed into context.

2.5.1 Nearshore current response to changing wind forcing

The significant increase in surf zone current magnitude during the sea breeze cycles can be directly related to the increased incident wave energy levels. This energy increase resulted in sustained offshore and westward currents over the inner and outer sandbar stations, while the only station located within the trough region (M5) encountered onshore currents. This may be due to M5 located closer to the bed and deeper region compared to stations located on the sandbars. However, when the recorded significant wave height exceeded 0.3 m and was arriving from the north-west, all the surf zone stations had the same current direction. Therefore, it is suggested that within this study the direction of cross-shore currents within trough region were mainly controlled by the broken wave heights and direction. Similarly Wright and Short (1984) observed lower current magnitude recorded at the trough region and changes direction depending on the experienced waves parameters.

Current observations have been made by Masselink and Pattiaratchi (1998) and Pattiaratchi

et al. (1997) had a resemblance to currents experinced within this field study, with offshore currents ranging from 0.03 ms^{-1} to 0.15 ms^{-1} following the onset of a sea breeze cycle. During the regular land breeze cycles the waves energy impact on the nearshore currents were insignificant due to the diminished wind during the land breeze cycles. However, during the extended land breeze cycle currents magnitudes can increase as indicated in Figure 2.9a–b, suggesting some sort of minimum required duration of land breeze cycles to induce significant currents. Additionally, there was no difference in alongshore current magnitudes between sea breezes and the Norte, but current intensity was sustained longer during the Norte. Cross-shore current magnitude on the other hand was found to be higher during the Norte due to the increase in τ_w resulting in a higher waves. The shift in currents during the Norte correlates with the shift in wind direction from N-NE to N-NW (Figure 2.3b). However, the wave direction does not echo that, suggesting that during the Norte a wind-driven current component may be dominant over the wave-driven component.

During the sea breeze cycles the observed outer swash zone cross-shore current were approximately 60% lower than those measured at the surf zone. However, the difference in the cross-shore current magnitude between the outer swash and surf zone decreased during the onset of the Norte, as wave energy increased by 50%. Furthermore, the outer swash/inner-surf zone is more a complex region with several factors that impact current measurements such as water level, bore/wave energy levels, and the beach slope. This may explain the differences in current magnitude and direction between the surf zone and outer swash/inner-surf zone (e.g. sea breeze cycles 2 and 6, and land breeze cycles 3, 5, and 8). The bore heights decrease with decreasing water depth and becomes more oriented to the shore, therefore resulting in a different longshore characteristics from currents observed in the surf zone. Additionally, the processes of uprush and backwash at the swash zone may effect currents dynamics at the outer swash/inner-surf zone. The difference between the longshore current direction between the outer swash/inner-surf zone and the surf zone can

be a result of the different morphological feature at both of these zones. Previous study by Hoyt and Henry Jr (1963) suggests currents direction within the swash zone of a sandy beach can be affected by the slope of the beach and small washover ripples that are formed by the uprush and backwash processes.

2.5.2 Nearshore turbulence and bed shear stress response

Estimated turbulence parameters and bed shear stress (i.e. ε, TKE, and τ) in the surf and outer swash zones displayed a consistent pattern related to the fluctuation in wave climate and associated wind stress. During the sea breeze cycle and the Norte event, estimated surf zone energy dissipation rates values were higher than those observed in some previous studies (e.g. Ruessink, 2010; Feddersen et al., 2007), while other studies reported similar values (e.g. Feddersen, 2012; Grasso et al., 2012; Trowbridge & Elgar, 2001; Veron & Melville, 1999; George et al., 1994). For example, Feddersen et al. (2007) observed maximum ε values of 2.5×10^{-4} m^2s^{-3} , associated with a longshore velocity of 0.34 ms^{-1} and significant wave height of 1.2 m at a depth of 2.6 m. Feddersen (2012) however suggests that shallower regions have a higher ε than deeper regions and found magnitudes of ε as high as 3×10^{-3} m^2s^{-3} in a water depth of 1 m. This explains why stations located on the inner and outer sandbars feature higher values of ε than those obtained from M5. Outer swash zone ε values ranged from 10^{-4} m^2s^{-3} to 10^{-2} m^2s^{-3}. These relatively high values of ε are similar to reported values by Flick and George (1991). The lower observed ε values are likely linked to different environmental conditions (i.e. water levels, currents, waves, wind, and changing bathymetry). However, Lanckriet and Puleo (2013) observed ε values as low as 10^{-5} m^2s^{-3} within the swash zone. During increased water levels the cross-shore location of the outer swash zone could easily become the inner surf zone. Thus, the observed variation in ε values could be as a result of that transition.

Observed TKE values ranged from 10^{-5} m^2s^{-2} to 10^{-2} m^2s^{-2} within the surf zone and

from 10^{-4} m^2s^{-2} to 10^{-1} m^2s^{-2} within the outer swash zone. Surf zone TKE values in this study are similar to TKE values reported by Brinkkemper et al. (2017). The observed increases in TKE levels are a result of the increasing wave energy during the more intense wind events (sea breeze cycles and Norte). The higher TKE levels at the sandbar locations correspond nicely to more intense wave breaking at those locations. Huang et al. (2009) suggests that TKE levels are higher in the upper layer of the water column (up to 10^{-2} m^2s^{-2}) in the surf zone, specifically during passage of the wave crest. However, even higher surf zone TKE levels up to 10^{-1} m^2s^{-2} have been reported by Svendsen (1987) and (Aagaard & Hughes, 2010) with vertical velocities ranging from 0.12 ms^{-1} and 0.61 ms^{-1}.

The bed shear stress observed within the surf zone ranged from 0.1 Nm^2 to 26 Nm^2 compared to values between 0.2 Nm^2 and 42 Nm^2 observed in the outer swash zone. Higher values of τ during intense wind events are in agreement with previously reported numerical model results of surf zone dynamics during intense wind and wave events. Tomás et al. (2012) reported values between 2 Nm^2 and 50 Nm^2 using the SWAN model results and Dufois et al. (2008) presented values ranging from 0.8 Nm^2 to 10 Nm^2 by implementing field measurements data into MARS-3D model. Peaked bed shear stress levels found in this study were higher than those reported in other field studies (e.g. Ruessink, 2010), most likely due to stronger hydrodynamic forcing conditions combined with differences in beach morphology. However, (Aagaard & Hughes, 2010) reported bed shear stress up to 46 Nm^2 with offshore wave heights of 1.25 m.

2.5.3 Beach morphology

At the study site, the bathymetry was almost uniform in the longshore direction but fairly dynamic in the cross-shore. Analysis of bed level changes associated with sea breeze cycles suggest that sediment tends to accumulate after and before areas characterized by

sudden depth changes such as sandbars and the ephemeral beach step. This accretion is also likely to be as a result of the offshore-directed sediment transport observed in Figure 2.10a. However, the result from Figure 2.10a-b only represent a specific point in the water column which may make it difficult to infer profiles of sediment concentration and velocity over the entire water column. Additionally, bed-load may provide a significant (if not the most significant) mode of transport resulting in the observed morphological changes. However, bed-load was not measured explicitly in this study. Nonetheless, sea breeze cycles are considered net erosion events as the comparison of sediment volume gains and losses in Table2.2 and Figure 2.8d indicates. This also relates to the observed increases in ε and τ along with offshore-directed currents, resulting in fairly continuous suspension of sediment and offshore-directed flux. The erosion of the beach face (Figure 2.9, approximately between 45 m and 55 m) during sea breeze cycles (e.g. April 4 profile) was due to the increased wave energy levels and current magnitudes. Similar observations have been made by Masselink and Pattiaratchi (1998).

During April 6-7, the land breeze cycle dominated the area, leading to relatively low sediment suspension and weaker currents, resulting in significant accretion across the study site. The significant accretion was associated with τ less than 4 Nm^2. This suggests that in order for a significant accretion environment to occur for the selected study location it requires longer land breeze cycles (> 18 hours) and τ less than 4 Nm^2. 12 hours into Norte event, τ exhibited a 10-fold increase over the sea breeze cycles resulting in higher SSC values sustained for a longer period causing high levels of erosion up to 0.4 m around the trough and the outer sandbar. Additionally, results from Figure 2.8f suggest that areas of erosion and accretion alternate in the cross-shore direction, especially between 40 m and 70 m in the x-direction. Such patterns are more likely related to cross-shore sediment processes occurred during the Norte event where sediment eroded and moved seaward.

2.5.4 Suspended sediment flux response

Suspension of sediment from the seabed to the water column occurs when forces exerted by the fluid on the sediment particles increases. Herein, estimation of SSC were obtained by calibrating the OBS as introduced in Section 2.3.2. However, the estimated SSC values through the OBS calibration may not reflect the actual amount of suspended particles due to the difference between the sediment sample used for the calibration and the actual suspended sediment at the location of the measurement. For example, the sample used for calibrating the outer swash zone OBS was collected from the bed and ranged from moderately well sorted (1.92 $\phi \pm 0.68$) to very poorly sorted (-1.41 $\phi \pm 3.01$). On the other hand, sediment sample collected at the middle of the water column showed moderately well-sorted (2.39 $\phi \pm 0.68$) to well-sorted fine sand (2.84 $\phi \pm 0.27$). However, this method has been widely used and recognized through the coastal researchers community. The measured suspended sediment concentrations ranged from 0.1 gl^{-1} to 3 gl^{-1}. This is somewhat lower than SSC values reported from other field experiments. For example, Pattiaratchi et al. (1997) found SSC values derived from OBS measurements 0.27 m above the local bed ranging from 1 gl^{-1} prior to the onset of sea breeze winds to 6 gl^{-1} during sea breeze. However, values of significant wave height measured by Pattiaratchi et al. (1997) were up to 50% higher than the ones this study site has experienced and the beach composed of fine sand sediment with a mean grain size of 0.89 ϕ. Nonetheless, the factor of 6 increase in SSC between land and sea breeze events observed by Pattiaratchi et al. (1997) is low when compared to a factor of 25 increase from land to sea breeze cycles measured in this field study. Other factors potentially leading to differences in measured SSC ranges include sediment texture and grain size distribution.

The longshore and cross-shore suspended sediment fluxes were estimated using Eq.2.8 and Eq.2.9, respectively. The cumulative effects of the different wind systems on sus-

pended sediment transport are investigated using data from the middle transect. Essentially, a comparison of transported suspended mass and mean suspended sediment flux in the cross-shore as well as the longshore directions is performed to assess the relative importance of repeated sea breeze cycles versus a single Norte event. During sea breeze cycles, the total mass transported was highest at the inner sandbar location (station M4) with a magnitude of 1.8×10^4 kgm^{-2} and offshore-directed (Figure 2.12a). This maximum value was followed by those measured at M7, M3, and M5 in descending order with values of 1.3×10^4, 5×10^3, and 1.3×10^2 kgm^{-2}, respectively.

Total suspended mass transport significantly increased during the Norte event by up to 900% at station M5. This suggests that the total cross-shore mass transport during the Norte event is significantly higher than the sum of the 9 sea breeze cycles preceding it. The longshore total suspended transport (Figure 2.12b) was comparable between the sea breeze cycles and the Norte event, except for the reversal in direction in the surf zone, where transport was westward during sea breeze cycles and eastward during the Norte event. However, the increase in longshore total transport over the trough region (M5) was most notable during the Norte event with a 1100% compared to the the total suspended transport of the 9 sea breeze cycles preceding it. The overall mean cross-shore suspended sediment flux observations during all sea breeze cycles suggest that M4 had the highest maximum mean value (0.12 kgm^{-2}s^{-1}) followed by M7 stations with a maximum mean value of 0.1 kgm^{-2}s^{-1}. During the Norte event mean flux values at M4 and M7 experienced 130% increase in magnitude. Similar observation can be seen from the mean longshore suspended sediment flux with higher magnitude observed at sandbar stations (M4, M7). This increase can be a result of the increased turbulence intensity due to wave breaking resulting in a higher sediment suspension and higher current intensity.

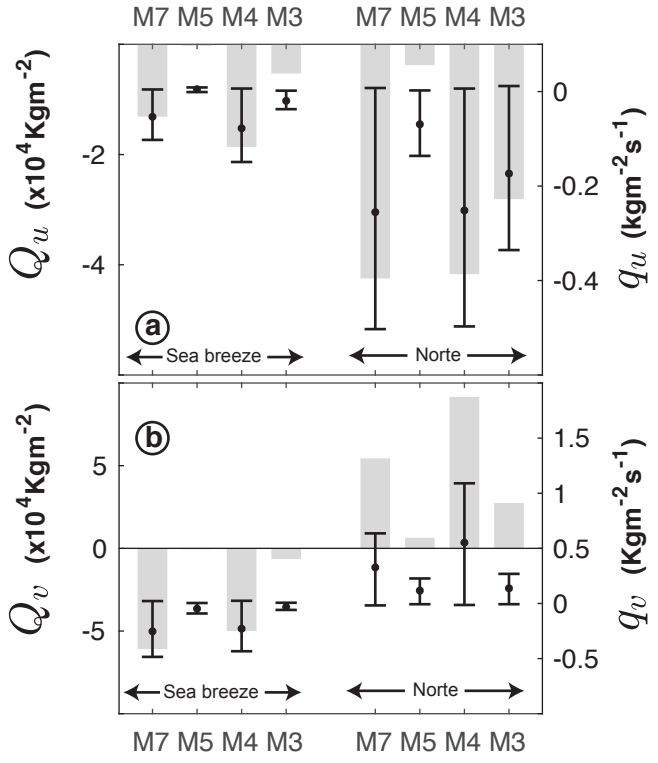

Figure 2.12. Overall sediment transport observations. The left vertical axis represents total suspended sediment mass transport (kgm^{-2}, gray shaded columns), while the right vertical axis display suspended sediment flux mean values with upper and lower 95% confidence intervals (kgm^{-2}s^{-1}, whisker plots) comparing all sea breeze cycles combined to the one Norte event. Values have been estimated from measurements at stations along the middle transect and are shown separately for cross-shore (panel a) and alongshore (panel b) components.

The comparison between total suspended sediment transport during sea breeze cycles and the Norte event as displayed in Figure 2.12 of course only covers the duration of the field measurements. Sea breeze cycles occur on a diurnal basis, and are approximately 25% more intense during the summer season (Torres-Freyermuth et al., 2017), while cold fronts (or Norte events) are less frequent that approximately 30 to 40 cold fronts cross the GoM in one year. Thus the cumulative effect of sea breeze cycles over an entire year can outweigh the effect of cold fronts. For example, if the presented volume loss during the

sea breeze cycle presented in Table 2.2 is assumed to be constant for 365 days, then the volume lost within the study site would be 2,87,620 m^3. Therefore it would takes 152 cold fronts with the same energy level as one observed in this study to overcome the effect of a year time sea breeze cycles. Taking Appendini et al. (2018) predication regarding the decrease of intense Norte events and replaced with more frequent Norte events in the far future into consideration, it is suggested that sea breeze cycles will still be the dominate wind forcing controlling the nearshore morphodynamics.

2.6 Conclusions

The nearshore response of a sea breeze dominated beach to alternating land and sea breeze cycles and one cold front (referred to as Norte) was investigated through detailed field measurements of wind, hydrodynamics, and morphodynamics over a period of 10 days. Wind intensity and direction changed significantly between the different forcing conditions leading to distinct responses in nearshore waves and currents as well as sediment transport and morphological evolution (i.e. formation and migration of a beach step/berm and sandbars). In the following, findings are summarized for each type of wind forcing condition, respectively:

[1] Land breeze cycles: Land breeze cycles featured relatively low prevailing wind velocities resulting in low wave energy levels with $H_s < 0.26$ m and weak onshore and westward-directed currents (maximum of 0.01 ms^{-1} and 0.1 ms^{-1}, respectively). These low energy conditions led to low values of ε, TKE, and τ both in the surf and the outer swash/inner-surf zone. This is approximately 900% less than those observed during the sea breeze cycles. Subsequently resulting in low SSC values less than 1 gl^{-1}. The combination of weak currents and low SSC created a mostly depositional environment across the study site resulting in a 87% volume gained (exhibiting a mean of 0.15 m, Figure 2.8e). However, this volume gain was a com-

bination of both suspended load and bed-load.

[2] Sea breeze cycles: A rapid increase in wind speed up to 11 ms^{-1} was observed at the onset of each sea breeze cycle. This increase in wind speed was followed by an increase in SSC, current magnitude, wave energy levels (0.2 m $< H_s <$ 0.43 m), and turbulence intensity of approximately 300%, 250%, 120%, and 900%, respectively. Surf zone cross-shore currents experienced an increase of 0.24 ms^{-1} (onshore directed), while longshore currents increased by 0.5 ms^{-1} (westward directed). The results indicated that currents during sea breeze cycles are more intense around the sandbars than the outer swash/inner-surf zone and trough region, approximately 70% and 35% higher, respectively. This leads to an increase in ε, TKE, and τ inducing sediment suspension across the surf zone up to 0.26 gl^{-1}. Consequently resulting in higher offshore and westward-directed suspended sediment flux with mean values of 0.1 $kgm^{-2}s^{-1}$ and 0.4 $kgm^{-2}s^{-1}$, respectively, that are 300% higher than observation made during the land breeze cycles. This is reflected in beach morphology changes, with a decrease of the inner sandbar height by 33% and an increase in the outer sandbar height by 25%. In addition, following each sea breeze cycle, the outer sandbar became pronounced and skewed landward (Figure 2.9). The diurnal cycle of the sea breeze system can play a major role in long-term sediment budget considerations consistent nature as also mentioned by Masselink and Pattiaratchi (1998).

[3] Norte event: The Norte event featured onshore wind speeds up to 15 ms^{-1}. This increase was reflected in nearshore currents with cross-shore currents approximately 125% higher than during sea breeze cycles. However, the longshore currents intensities were similar to those measured during sea breeze events.The main change was the shift in wave direction resulting in eastward longshore currents (Figure 2.3a).

Turbulence parameters showed higher values than those observed during sea breeze cycles and were sustained for longer periods of time. For example, TKE values increased one order of magnitude during the onset of the Norte and τ increased by a factor of ten. In response to this substantial increase, suspended sediment concentration was almost continuous with levels up to 2.8 gl^{-1}. Cross-shore suspended sediment flux was twice as high as during the sea breeze cycles. The Norte resulted in a significant erosion in comparison to the other events (Figure 2.9). This can be primarily attributed to the induced return flow (undertow current), proven to be effective in eroding sediment (Roelvink & Stive, 1989; Thornton et al., 1996).

To summarize, this study suggest that the cumulative impact of sea breeze cycles on the nearshore hydrodynamics and morphodynamics is comparable to the effect of onshore-directed cold fronts. As both of these system are considered to be erosive, it is believed that the land breeze cycle acts as the equilibrium factor in terms of cross-shore sediment transport. The interactions of different nearshore forcing mechanisms are complex and extrapolation to yearly averages is difficult from this fairly short-term field study. However, the collected data gives valuable insights into the relative importance of different wind forcing conditions that can help create a better understanding of nearshore dynamics and resulting morphology changes in general.

3. NEARSHORE CIRCULATION ON THE UPPER TEXAS COAST IN RESPONSE TO FLUCTUATING ONSHORE (GULF BREEZE) AND OFFSHORE (COLD FRONT) WIND

3.1 Introduction

In recent years, understanding nearshore circulation has been a primary focus in better constraining its impact on the coastal zones. This is due to the importance of nearshore circulation being a key factor in the exchange/transport of sediment, nutrients, and pollutants along and across the surf zone and the inner-shelf region (Hendrickson & MacMahan, 2009; S. B. Grant et al., 2005; Aagaard et al., 1997; Nittrouer & Wright, 1994). The influence of wind, waves, and tide on nearshore circulation has been documented in previous literature using both field observation and models (e.g. Torres-Freyermuth et al., 2017; Gallop et al., 2016; Mulligan & Hanson, 2016; Zhang et al., 2009; Zavala-Hidalgo et al., 2003; Noda, 1974). However, there is a dearth within the literature in comparing or investigating the spatial, across the surf zone and inner-shelf region, and temporal influence of both oceanographic and atmospheric forcing on the nearshore circulation.

Currents within the northwestern Gulf of Mexico (GoM), in particular the Texas and Louisiana Shelf (hereafter referred to as LATEX shelf) varies seasonally and are mainly wind driven (Zhang et al., 2009; Cho et al., 1998). During the summer and early fall, Gulf breeze (onshore wind) dominates along the upper Texas coast (W. Wang et al., 1998; N. P. Smith, 1977), resulting in a westward flow (Wallace et al., 2010; Nowlin et al., 2005), and onshore flow over the inner-shelf (Nowlin et al., 1998). Within this study the Gulf breeze events (GE) are defined as an onshore wind events that are associated with a high wind speed ($5\ ms^{-1} < GE < 11\ ms^{-1}$) and a mean duration of one day. In contrast, during the winter, northwesterly and northeasterly winds are more frequent, resulting in

eastward flow (Nowlin et al., 2005; W. Wang et al., 1998), and offshore flow over the inner-shelf (Nowlin et al., 1998).

The shift in wind direction during winter season is due to maritime polar and continental polar cold front events (CE) that enter between Corpus Christi and Galveston and propagate across the GoM (Henry, 1979). These synoptic-scale disturbances can be accompanied with a rapid increase in wind speed up to 16 ms^{-1} (Kineke et al., 2006), extreme temperature fluctuation (Huh et al., 1978), and contributes to 50 % of rainy events in the northwestern part of the GoM (Keim, 1996). Moeller et al. (1993) suggest that about 30 – 40 cold fronts pass over the Louisiana coast during the winter season. Additionally, studies by Henry (1979) and Hardy and Henderson (2003) reveled an average of five cold fronts passes the north GoM coast during each month from November to April. According to Dingler et al. (1993), cold fronts resulted in a significant wave height of 2 – 3 m, while Pepper and Stone (2004) observed a 0.4 ms^{-1} increase in near bed current velocity. Therefore, cold fronts are considered to be an important atmospheric forcing mechanism, due to their frequency of occurrence and large spatial coverage (Pepper & Stone, 2004; Stone et al., 2004; Moeller et al., 1993; Roberts et al., 1987).

The majority of field work conducted within the northern GoM investigated the impact of cold fronts over the northern coastal regions including, barrier islands (e.g. Dingler & Reiss, 1990), inner-shelf regions (e.g. Pepper & Stone, 2004; Pepper et al., 1999), micro-tidal lagoons (e.g. Carlin et al., 2016a). However, despite the considerable effort that has been invested in understanding the significant impact of cold fronts on nearshore hydrodynamics (e.g. Keen, 2002), sediment resuspension and transport (e.g. Dellapenna et al., 2006; Kineke et al., 2006; Stech & Lorenzzetti, 1992), beach morphology (e.g. Keen et al., 2003; Armbruster et al., 1995; Moeller et al., 1993; Dingler & Reiss, 1990), and nutrient transport (e.g. Gallucci & Netto, 2004; Madden et al., 1988), little has been done to investigate their impact on nearshore current circulation in the northwestern GoM.

Specifically, there is a need in understanding the influence of offshore cold fronts to the onshore Gulf breeze winds and the resultant nearshore current circulation.

Previous studies on nearshore circulation conducted within the northwestern GoM investigated seasonal shelf upwelling (e.g. Zavala-Hidalgo et al., 2006), inner-shelf current in response to winter cold fronts (e.g. Pepper & Stone, 2004), correlation between wind stress, currents, and suspended particulate matter concentration (e.g. Salisbury et al., 2004), the role of surface circulation on hypoxia, and red tide blooms (e.g. Bianchi et al., 2010; Tester & Steidinger, 1997). Nevertheless, to the authors knowledge, there has not been a study conducted in the northern GoM investigating the role of different physical processes such as wind, tide, waves, and LATEX shelf current on the nearshore circulation across the surf zone and the inner-shelf. However, Torres-Freyermuth et al. (2017) conducted a study on a sea breeze dominated beach (Sisal, Yucatan), to investigate the relative role of different physical forcing on nearshore circulation between the inner-surf zone and the inner-shelf region. The findings from Torres-Freyermuth et al. (2017) suggests that wind and shelf currents mainly control the inner-shelf circulation during the passage of cold front, while wind and waves were the main driving forces within the surf zone.

This paper replicates the work from Torres-Freyermuth et al. (2017) in order to understand the relative role of two different atmospheric phenomena, specifically cold front and Gulf breeze events along with the variation in the different forcing mechanisms such as winds, waves, tides, and LATEX shelf currents in the Texas upper coast. Therefore, this work aims to investigate the influence of physical processes (i.e. wind, waves, tide, and LATEX shelf current) associated with the offshore cold fronts and the onshore Gulf breeze on nearshore current circulation across the surf zone and the inner-shelf region.

3.2 Field experiment location description

The field experiment was conducted on Galveston Island , a barrier island located in the upper Texas Gulf coast (Figure 3.1). Galveston Island is known for its economic importance due to high tourism impact scale (John & Crompton, 1998). The island is also known for its 4.8 m $\times$ 5.4 m seawall that has a length of 16 km, which was built to protect the island from storm surges (Ravens & Sitanggang, 2007; Morton et al., 1995). The specific location of the instrument deployment site was 10 km west of the seawall and in front of Galveston Island state park beach. The location was selected based on the minimal anthropogenic interference (i.e. structures such as seawall, piers, and jetties), in order to obtain the most natural current circulation within the surf zone.

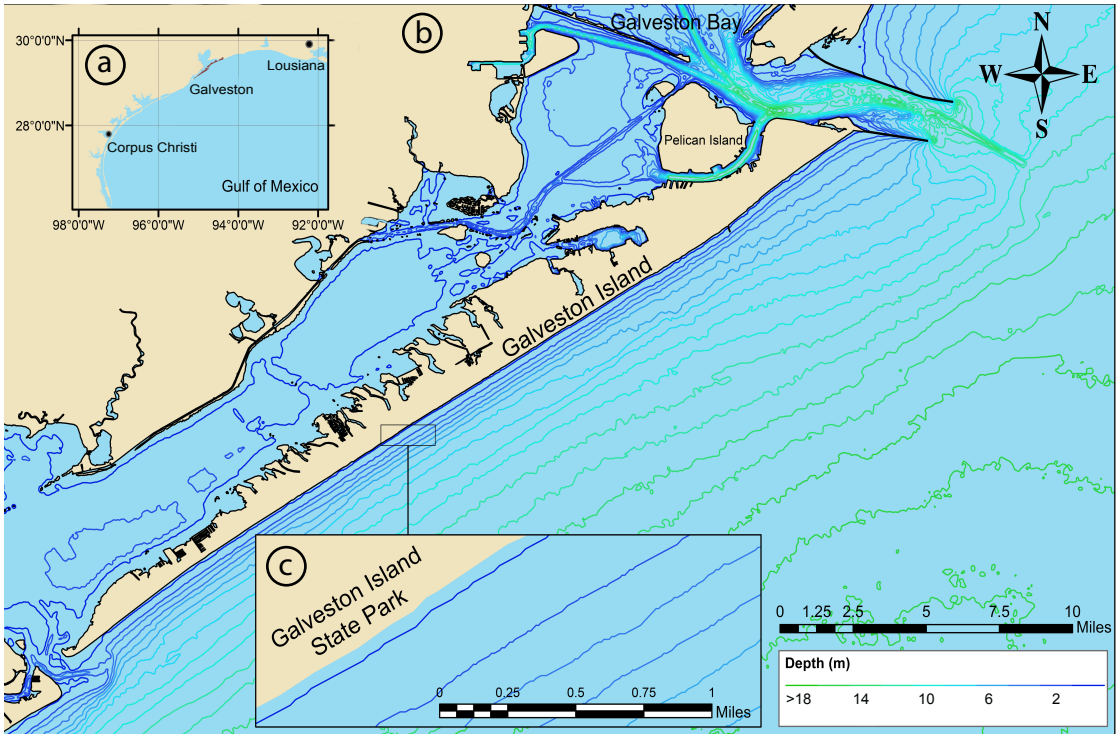

Figure 3.1. Map of study area showing: (a) location of Galveston Island within the upper Texas coast, (b) map of Galveston Island with depth contours, and (c) a zoomed-in view of the field experiment site.

The region is subtropical with hot summer and mild winter (Feagin et al., 2005). During the winter the area is subject to northeasterly cold fronts (W. Wang et al., 1998; Henry, 1979) associated with wind speed up to 16.5 ms^{-1}, while in the summer the area is subject to hurricanes and tropical storms. Galveston beach is microtidal with a tidal range of 0.3 m, and has a relatively low wave energy (Wallace et al., 2010; Rogers & Ravens, 2008).

The current flow regime is mainly wind driven; westward currents are generated by the prevailing southeasterly Gulf wind, while eastwards currents are generated by the passage of cold fronts during the winter season (Wallace et al., 2010; Darby, 2005). According to Brannstrom et al. (2014) and Brannstrom et al. (2015), rip currents are more frequent on the eastern portion Galveston, but can exist on the west side of Galveston with a lower frequency. During the field experiment two types of breakers were observed: spilling breakers covered the whole surf during low wind condition, and plunging breakers mainly seen over the sandbars during high wind events.

3.3 Data collection and analysis

3.3.1 Field setup

The field experiment included five current meters deployed in a cross-shore array covering the area from the surf zone to the inner-shelf region (Figure 3.2a). Measurements of currents, water free-surface elevation, atmospheric temperature, and wind were collected between November 16 to December 1, 2016. Table 3.1 provides detailed instrument setup and sampling parameters. In addition, mean spatial GoM surface wind data (10 m above sea level) has been obtained from Kalnay et al. (1996), covering the whole period of the experiment, to examine the cold fronts spatial extent and intensity over the region compared to the Gulf breeze events.

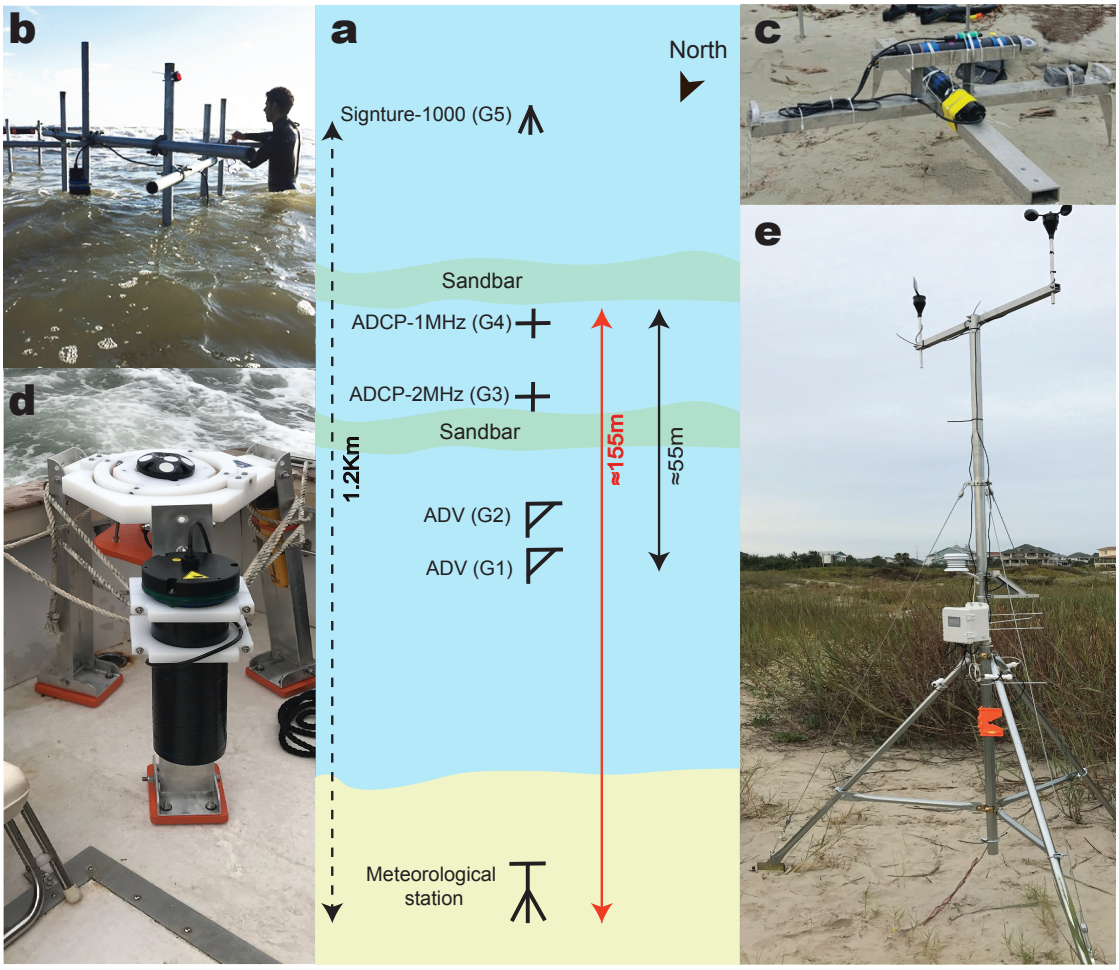

Figure 3.2. Field experiment setup and instruments: (a) plane view sketch of the instruments layout and sandbars locations, (b) frame used for mounting the ADVs, (c) pod used to hold the ADCPs, (d) Signature-1000 mounted on gimbal tripod, and (e) HOBO-U30-NRC on-land meteorological station.

The surf zone instruments included two Nortek Acoustic Doppler Velocimeters (ADV), that are 7 m apart (hereafter referred to as G1 and G2, respectively). Two sets of goalpost frames were made of galvanized steel pipes in a triangle shape used to mount the ADVs (Figure 3.2b). The ADVs were oriented downward and measured velocity at 0.15 m from the seabed. The ADVs were configured to record continuous pressure and velocity point measurements at 16 Hz using ENU coordinate system (i.e. East, North , Up) with an accuracy of $\pm$ 0.001 ms^{-1}.

Additionally, a 2 and 1 MHz Nortek High Resolution Acoustic Doppler Current Profiler (ADCP HR), were deployed within the mid surf zone and has an accuracy of $\pm$ 0.005 $ms^{-}1$ looking upward into the water column. The 2 MHz ADCP-HR (hereafter referred to as G3) was located on the outer edge of the inner-sandbar, and used to record velocity profiles (0.075 m bin over 13 cells), and pressure measurements at 8 Hz in burst mode (2 minutes of measurements every 3 minutes), using ENU coordinate system. The 1 MHz ADCP-HR (hereafter referred to as G4), was located at the far end of the trough before the outer-sandbar (Figure 3.2a), and was setup with the same configuration as G3, except the sampling rate was at 4 Hz and collecting 0.1 m bin velocity profiles over 8 cells. Two pods made of aluminum frame were used to hold both ADCPs to minimize magnetic interference. The pods used for the ADCPs included spiked legs to anchor the instrument on the seabed, preventing the pods from flipping over during energetic wave condition (Figure 3.2c). Unfortunately, around 21:00 on November 27 both G3 and G4 stations were buried, due to high sediment accretion. Therefore, measurements of pressure and velocity made between 21:00-November 27 and 00:00-December 1, 2016 were filtered out.

One Nortek advanced five beam current profiling system referred to as Signature-1000 (AD2CP, hereafter referred to as G5) was deployed further offshore at the inner-shelf region, approximately 1.2 km from the shoreline (Figure 3.2a). The instrument was mounted on a gimbal tripod made by durable aluminum in 8 m depth looking upward into the water

column (Figure 3.2d). The instrument was continuously recording velocity profiles sampled with 0.2 m bin spacing over 5.4 m with an accuracy of $\pm$ 0.003 ms^{-}1, and pressure measurements with a sampling rate of 8 Hz. The velocity measurements were recorded using ENU coordinate system. LATEX shelf surface currents measurements were obtained through NOAA national data buoy center Station-42043-GA-252-TABS . The buoy was developed and maintained by Texas A&M University.

Atmospheric measurements of temperature ($^{\circ}$C), relative humidity (%), wind speed (ms^{-1}) and direction (degree) were recorded using Onset Computer Corporation HOBO U30-NRC (meteorological station). The meteorological stations has a 1 Hz sampling frequency and report a mean of the recorded measurements every 30-seconds. The meteorological station sensors were mounted on a 3 m mast fixed to a tripod approximately 100 m from G1 (Figure 3.2e). Having the meteorological station near the study site provides accurate local atmospheric observations.

Table 3.1. Summary of the instruments used within the field experiment and instruments setup.

Instrument	Instrument position	Sampling intervals (seconds)	Sampling frequency (Hz)	Sensor elevation above/ bed and orientation	Measurement
Acoustic Doppler velocimeters (ADV)	G1 G2	continuous	16	0.3m/down	current, water level
High Resolution Acoustic Doppler Current Profiler (ADCP-HR 2MHz)	G3	180	8	0.3m/up	current, water level
High Resolution Acoustic Doppler Current Profiler (ADCP-HR 1MHz)	G4	180	4	0.3m/up	current, water level
Signature-1000 (AD2CP)	G5	continuous	8	0.75m/up	current, water level
Meteorological station	onland	30	1	-	temperature, relative humidity, wind speed and direction

3.3.2 Meteorological and hydrodynamics data

Recorded meteorological data were block-averaged every 2 minutes, than smoothed using a low pass filter over 40 minutes window. In addition, wind speed measurements were adjusted to the standard reference height of 10 m. The wind stress (τ_w) was estimated by the quadratic law (Eq. 3.1), to investigate the role of cold fronts and Gulf breeze wind on nearshore current circulation:

$$\tau_w = \rho_a \, C_D \, U_{10}^2 \tag{3.1}$$

Where ρ_a is the air density assumed to be constant at 1.2 kgm^3, C_D is the drag coefficient, which is a function of air density, temperature, and wind speed, and was estimated using S. D. Smith (1988) methods. U_{10} is wind speed (ms^{-1}) at 10 m elevation above ground. The alongshore component of wind stress was computed using the wind horizontal velocity (U), and the wind longshore velocity (v) using the definition:

$$\tau_y = \rho_a \, C_D \, U \, v \tag{3.2}$$

A directional wave spectrum Matlab toolbox (DIWASP) designed by Johnson (2002), was used to estimate the significant wave height (H_s), period (T_s), angle (θ), and provided directional wave spectrum analysis, by implementing Direct Fourier Transform Method (DFTM, see Eq.16 and Eq.45 within Barber (1963). DIWASP have been used in previous ocean and coastal studies for the purpose of computing directional wave spectrum (e.g. Fisher et al., 2017; Fedele et al., 2013; Ogawa et al., 2012; Bechle & Wu, 2011; Bever et al., 2011). The toolbox computed the directional wave spectrum using measured pressure/free-surface elevation (P), cross-shore (u) and longshore (v) current velocity (i.e. PUV method). Later, the alongshore component of the wave radiation stress (S_{xy}) was

computed using estimated breaking wave height (H_b) and angle (θ_b) derived from G5, by the following definition:

$$S_{xy} = \frac{1}{16}\,\rho_w\,g\,H_b^2\,\frac{c_g}{c}\,\sin(\theta_b)\,\cos(\theta_b) \tag{3.3}$$

where ρ_w is the density of sea water assumed to be constant at 1025 kgm^3, c_g is the group velocity, and c is the phase velocity. The breaking wave height and angle was estimated using liner wave theory and apply a shoaling, refraction, and a breaking index (γ) of 0.42 to G5 waves observation.

3.3.3 PCA method

The principal component analysis (PCA) method, also known as empirical orthogonal eigen function (EOF), was used to determine the local variability orientation of both the longshore and cross-shore velocities for each stations following Thomson and Emery (2014). This method has been widely used in atmospheric and oceanography studies to investigate the relative role of the driving forces and the variability of nearshore currents (e.g. Torres-Freyermuth et al., 2017; Prandle & Matthews, 1990), inner-shelf cross-shore exchange (e.g. Hendrickson & MacMahan, 2009), and wind patterns and sea surface temperature (e.g. Torres et al., 2003; Deser & Blackmon, 1995). The results of PCA analysis are uncorrelated, and refereed to as Principal Components (PCs), where the first mode represent the significant portion of total variance in the current data (Jolliffe, 2002).

Prior to PCA analysis, the longshore and cross-shore currents of G5 – G3 stations were depth averaged. Surf zone velocity measurements with correlation less than 60% were filtered out, whereas inner-shelf region velocity measurements with correlation less than 70% were filtered out (for details see Rusello, 2009). Additionally, recorded current data were block-averaged every 2-minutes and then smoothed using a low pass filter over a 40-minutes window. The new variables from PCA analysis were rotated along the direction of

maximum variance of the currents, usually refereed to as principal direction (PD). Figure 3.3a-e displays a scatter diagram of E – W and N – S currents, where the dominate current direction oriented in a nearly NE – SW direction for all stations. Moreover, the PCs (First mode) for G1 – G5 describes more than 95% of the variance of the EOF analysis for the whole period of the field experiment.

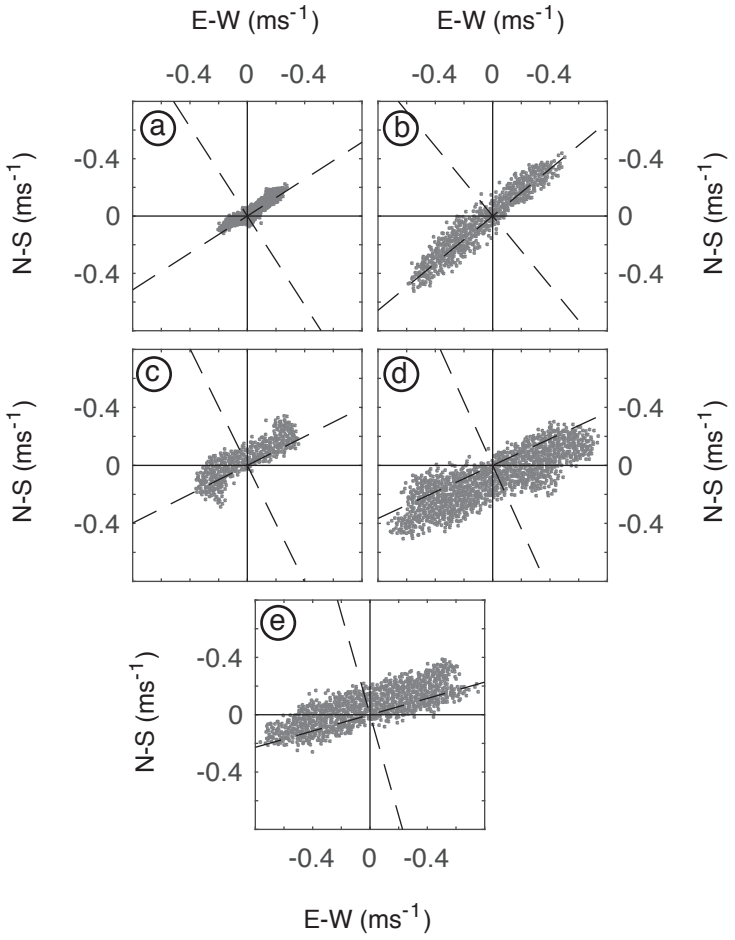

Figure 3.3. Scatter diagram of E – W, and N – S current components: (a) G5, (b) G4 , (c) G3, (d) G2, (e) G1. G5 – G4 stations values represent depth averaged velocity. The dashed line represent the rotated axes along the direction of maximum variance.

3.4 Results & discussion

3.4.1 Wind and wave observations

Over the duration of the field experiment the area experienced six main wind events. These events include the passage of three cold fronts (with mean wind speed: CE#1 $\approx$ 5.1 ms^{-1} blowing from NW – NE, CE#2 $\approx$ 3.3 ms^{-1} blowing from N – NE, and CE#3 $\approx$ 4.2 ms^{-1} blowing from NW – E). Additionally, three Gulf breeze events were observed (with mean wind speed: GE#1 $\approx$ 4.4 ms^{-1} blowing from SE – S, GE#2 $\approx$ 4.7 ms^{-1} blowing from SE – S, and GE#3 $\approx$ 7.9 ms^{-1} blowing from SE – W). Overall, results from Figure 3.4, suggest that Gulf breeze events tend to last for a longer period and are usually associated with higher winds than cold front events.

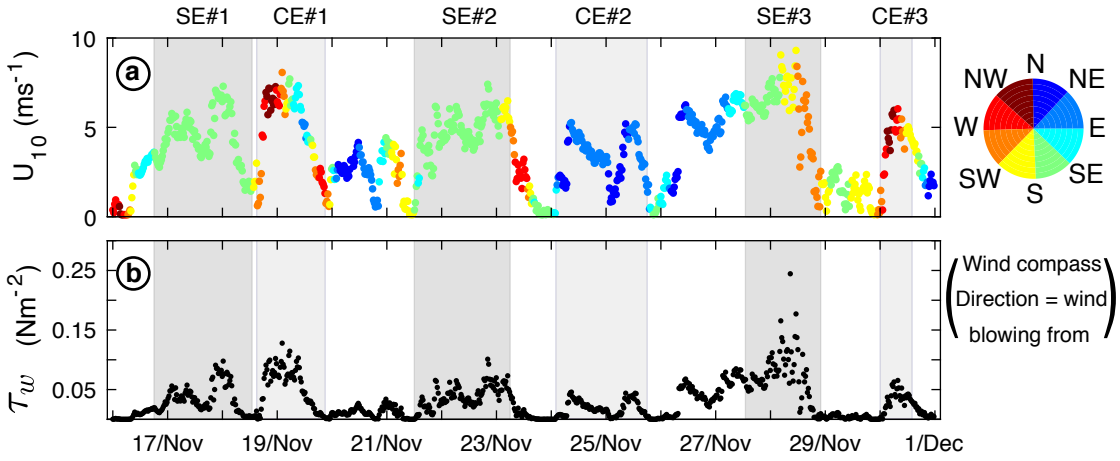

Figure 3.4. Measured time series of meteorological observations: (a) wind speed and direction, (b) wind shear stress. The light gray shaded areas represent cold front events, while the dark gray shaded area indicate Gulf breeze events.

High surface wind shear stress derived from the wind measurements (Figure 3.4b) were associated with Gulf breeze wind (approaching the coast from SE – S). The study site ex-

perienced the highest wind shear stress during GE#3, while the lowest surface wind shear stress was observed between the November 29 and November 30, 2016. Nevertheless, the wind shear stress experienced an immediate sharp increase following the onset of CE#1 (second highest wind stress value over the total period of the experiment). A summary of mean, max, and standard deviation (σ) of both τ and U_{10} are provided in Table 3.2.

Table 3.2. Mean, max, and σ of U_{10} and τ for the selected events, including upper and lower 95% confidence intervals in brackets.

	U_{10}			τ_w		
Event	Std Deviation	Average	Max	Std deviation	Average	Max
CE#1	1.8	5.08 [5.03, 5.14]	6.8	0.03	0.054 [0.053, 0.056]	0.09
CE#2	1.0	3.29 [3.26, 3.32]	4.8	0.01	0.0195 [0.0192,0.0197]	0.04
CE#3	1.2	4.23 [4.17, 4.29]	5.4	0.01	0.0343 [0.0336,0.0349]	0.05
GE#1	1.3	4.41 [4.37, 4.44]	6.6	0.02	0.0354 [0.0349, 0.0360]	0.08
GE#2	1.0	4.72 [4.69, 4.75]	6.3	0.01	0.0393 [0.0389, 0.0397]	0.07
GE#3	1.6	5.97 [5.92, 6.02]	7.9	0.03	0.0718 [0.0708, 0.0728]	0.12

Analysis of wind measurements suggest that southeasterly winds are the most dominant winds during the total period of the field experiment (Figure 3.5). Winds approaching the coast from 90° to 180° had a 12% frequency of occurrence with wind speeds up to 8 ms^{-1} (this represents GE#1 and GE#2). However, winds blowing from the southwest (180° to 270°) have a lower frequency of occurrence (between 3% and 1%), but with high wind speed reaching up to 8 ms^{-1} (this represents GE#3). On the other hand, wind blowing from 0° to 90° had a frequency of occurrence up to 11.8%, and associated with wind speed ranging from 1 to 6 ms^{-1} (this represents CE#2). However, wind blowing from

270° to 0° had the lowest frequency of occurrence (3%<), with wind speed ranging from 1 to 7 ms^{-1}.

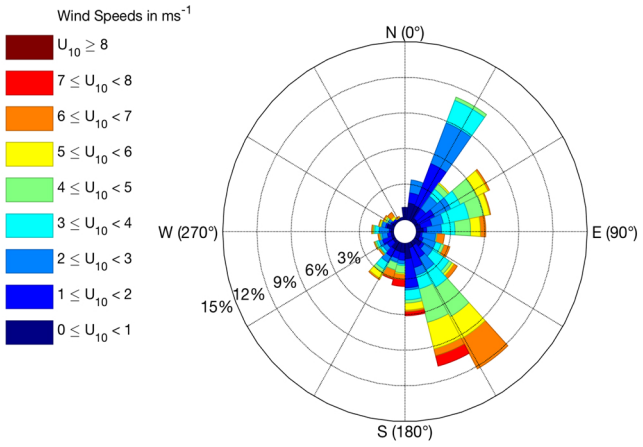

Figure 3.5. Hourly averaged variation in wind frequency rose generated by the recorded data from HOBO U30-NRC. The direction represent of where wind blows from.

Additional spatial and temporal wind observations for each selected event (i.e. GE#1, GE#2 ... etc) were obtained using NCEP Reanalysis data provided by Kalnay et al. (1996) and are illustrated in Figure 3.6. Observations suggest that offshore cold fronts passing approximately from north – northwest has a larger extent over the upper Texas coasts, and are associated with higher wind speed than northeasterly cold fronts (Figure 3.6,). On the contrary, Gulf breeze wind blowing from the south, had a larger extent and covered almost the whole northwestern GoM especially GE#3. Nevertheless, GE#1–2 had a more effect on the local wind, were the spatial extent did not revile its true strength.

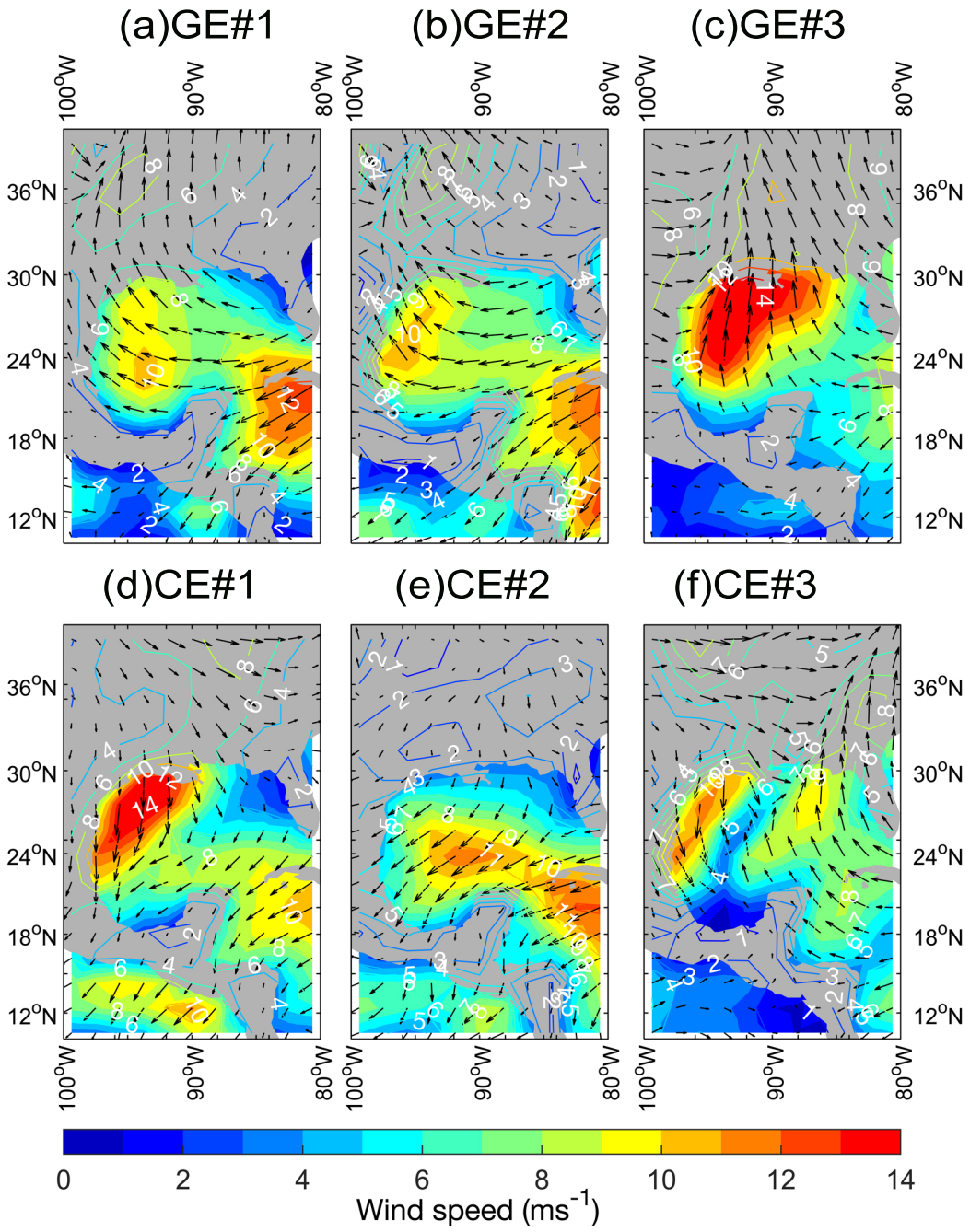

Figure 3.6. Mean surface wind (10 m) within the GoM of Gulf breeze events, (a) GE#1, (b) GE#2, (c) GE#3, and cold front events, (d) CE#1, (e) CE#2, (f) CE#3. The spatial wind data presented in this figure were obtained from Kalnay et al. (1996).

The variation in wind measurements were reflected in the inner-shelf and surf zone wave climate (i.e. H_s, T_s, Figure 3.7a-b). During the Gulf breeze events estimated significant wave height was almost 50% higher than cold front events observations. The most largest increase in significant wave height (1.5 m) was observed at G5 during GE#3, due to the increase in wind stress. The region between the sandbars experienced a significant wave height ranging from 0.13 to 0.5 m, and periods 4 to 7 seconds, where the maximum values were found during the GE#1-3. On the contrary, at G1 and G2 stations wave conditions were found to be approximately 40% lower than those observed at G3 and G4 stations, where the significant wave height ranged from 0.12 to 0.32 m, and periods from 2 to 8 seconds. Across all stations, easterly – southeasterly waves dominated during the GE#1-3, while during the CE#1-3 southeasterly – south waves dominated (Figure 3.7c). Unlike cold fronts, the Gulf breeze winds blow from the south where wind is not constrained by land topography along with large fetch length allows for higher waves to develop.

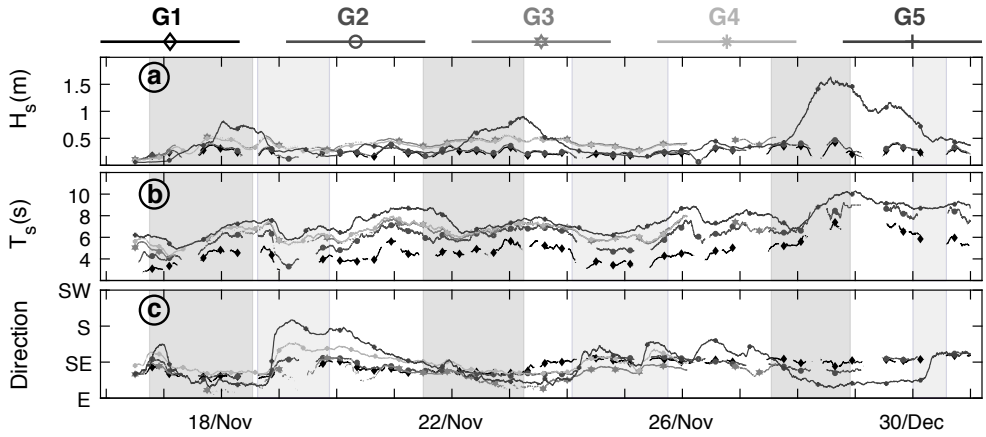

Figure 3.7. Measured time series of: (a) significant wave height, (b) significant wave period, and (c) wave direction. The light gray shaded areas represent cold front events, while the dark gray shaded area indicate Gulf breeze events.

The strongest current experienced within the inner-shelf region (up to 0.6 ms^{-1}) was during the Gulf breeze events (Figure 3.7a). The mean direction of the current was eastward during the cold front periods. Meanwhile, current directions were shifting frequently between eastward and westward, but westward currents were sustained for a longer period during GE#3 as wind shear stress exceeded 0.15 ms^{-1}. In comparison, the mean current magnitude recorded during the Gulf breeze was approximately 0.35 $ms^{-1} \pm 0.1$, while during the cold front events was 0.28 $ms^{-1} \pm 0.05$. The same observations are made by Nowlin et al. (2005), as after the passage of the cold front the currents encountered an abrupt increase in velocity and shift in current direction.

The region between the sandbars experienced current velocities up 0.7 ms^{-1} at G4 station during GE#1 (Figure 3.7b-c). On the other hand, G3 station experienced lower current velocity fluctuations than recorded current velocities at observed at G4 station. Currents within the surf zone are mainly induced due to waves motion and breaking. Therefore, the high currents observed at G4 station are likely due to the higher waves observed at the outer surf zone that might break before G3 station leading to lower current speed. However, both G4 and G3 stations had sustained southwestward flow and northeastward flow during the Gulf breeze and cold front events, respectively. In the inner-surf zone enhanced currents were observed over G2 and G1 stations, during GE#3 with a maximum of 0.8 ms^{-1} (Figure 3.7d-e). On average, measured currents within the inner-surf zone were higher than current values recorded in stations in deeper locations. The direction of currents across the surf zone was consistent, where northeasterly – northwesterly wind results in a eastward-directed flow, whereas southeasterly – southwesterly wind results in a westward-directed flow. Elevated current values recorded during GE#1, GE# 3, and CE#1, are likely due to the increase in both wind speed, and wave climate accompanied by a large tidal range (spring tide, see Figure 3.8c).

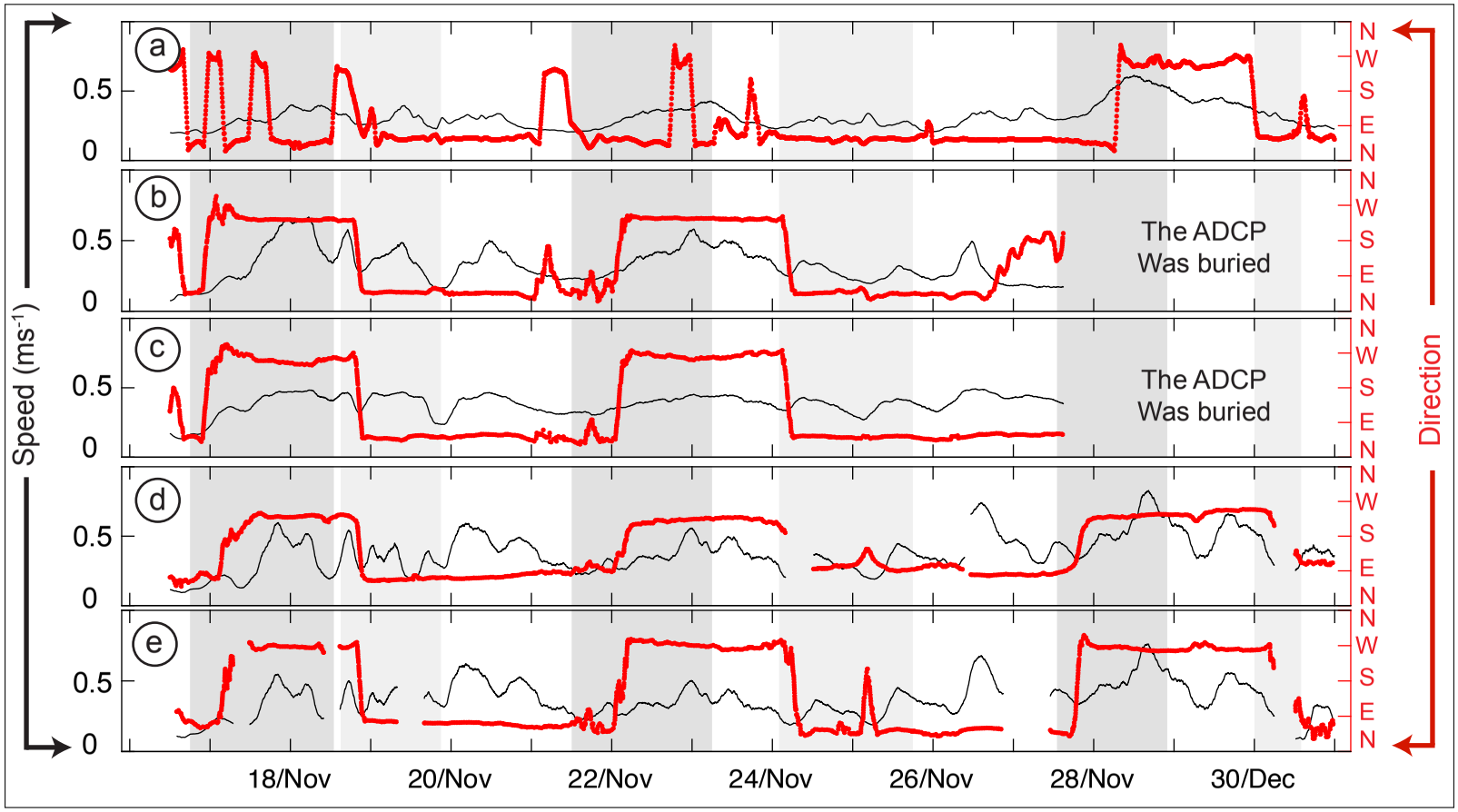

Figure 3.8. Measured time series of current speed (black) and direction (red) for station: (a) G5, (b) G4, (c) G3, (d) G2, (e) G1. Station G5 through station G3 values shows depth averaged current speed. The light gray shaded areas represent cold front events, while the dark gray shaded area indicate Gulf breeze events.

3.4.2 Nearshore circulation and forcing conditions

Following Torres-Freyermuth et al. (2017), LATEX shelf currents, alongshore wind stress, alongshore wave radiation stress, and tides were considered to be the main influence on nearshore current circulation across the surf zone and the inner-shelf region (Figure 3.9). The alongshore wind stress was found to be strongest during CE#1 and CE#3, where the highest magnitudes were found during the middle of the events (Figure 3.9a). During the cold front periods, the alongshore wind stress ranged from 3×10^{-6} Nm^{-2} to 9×10^{-2} Nm^{-2}, and ranged from -3×10^{-6} Nm^{-2} to -1×10^{-1} Nm^{-2} during the Gulf breeze periods .The recorded LATEX shelf currents were found to be higher than currents recorded at G5 station, especially during cold front periods (Figure 3.9b).

The recorded currents during Gulf breeze periods were almost twice as high at G5 station than the shelf current. This might be due to the location difference, as the buoy was approximately 22 km from the coast. This difference in distance will allow the offshore wind to develop enhanced current velocity, whereas G5 station was located closer to the coast so it has less distance for wind to develop high waves (i.e. fetch length effect). On the other hand, the estimated alongshore wave radiation stress values within the surf zone experienced small fluctuation during cold front periods, and higher magnitudes were observed during the Gulf breeze periods, especially during GE#3 (Figure 3.9d). This was likely due to the increase in breaking wave height and change in breaking wave angle.

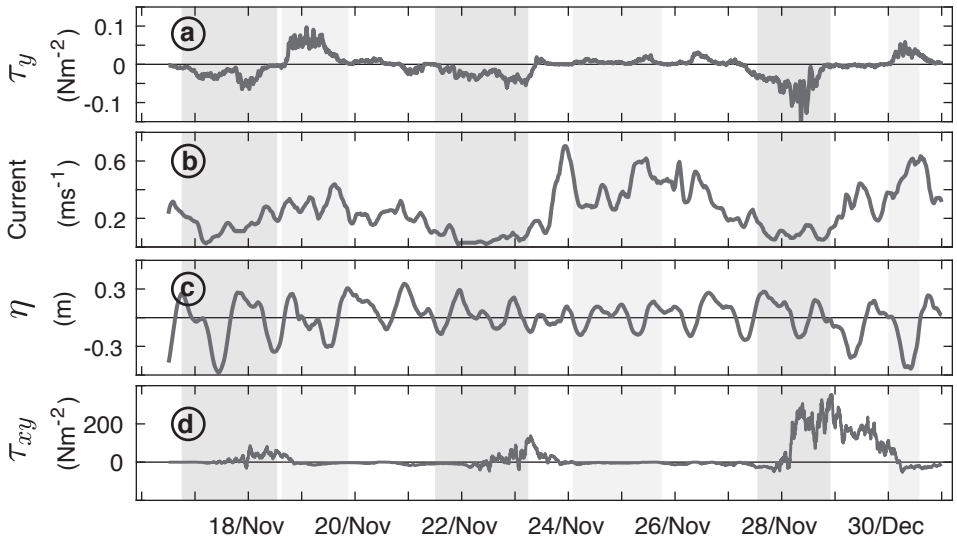

Figure 3.9. Measured/computed time series of the selected forcing mechanism: (a) alongshore wind stress, (b) recorded LATEX shelf current, (c) measured mean sea level at G5, (d) alongshore wave radiation stress. The light gray shaded areas represent cold front events, while the dark gray shaded area indicate Gulf breeze events.

The first EOF mode values for the inner-shelf region were ranging from -0.3 ms^{-1} to 0.25 ms^{-1}, and were mainly eastward-directed (Figure 3.10a). Meanwhile, stations within the surf zone had a higher range than the inner-shelf region, approximately between -0.6 ms^{-1} and 0.58 ms^{-1}, Figure 3.10b-e. Additionally, stations located within the surf zone displayed similar flow direction with a consistent pattern of westward-directed currents during the Gulf breeze events, and eastward-directed currents during the passage of cold fronts. Similar observations have been made by Torres-Freyermuth et al. (2017), as the first EOF mode for the inner-shelf region behaved differently than the surf zone. Additionally, Torres-Freyermuth et al. (2017) suggested that the rotation in EOF values within the surf zone correspond to wave breaking.

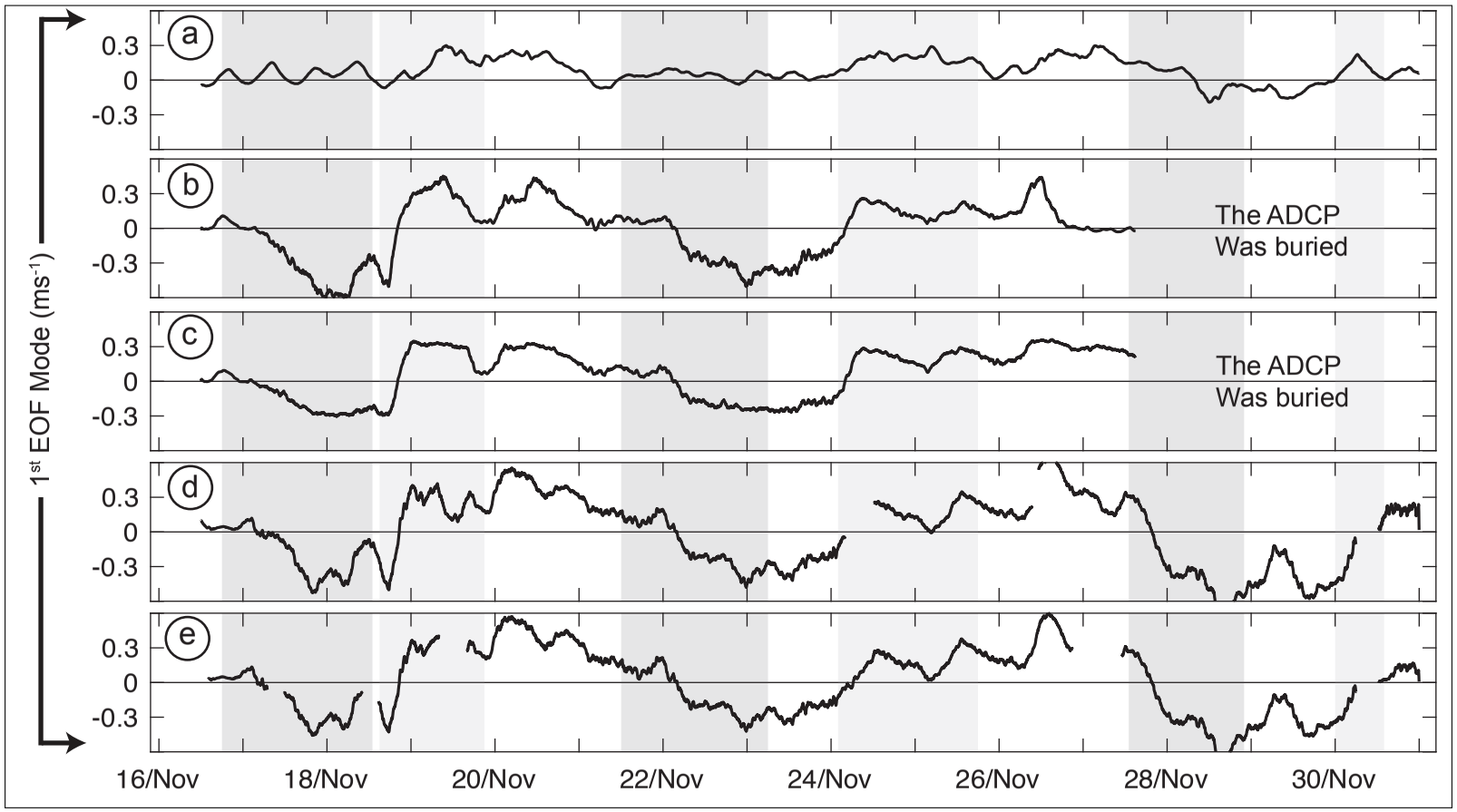

Figure 3.10. Measured time series of the velocity first EOF mode at: (a) G5, (b) G4, (c) G3, (d) G2, (e) G1.The light gray shaded areas represent cold front events, while the dark gray shaded area indicate Gulf breeze events.

In order to examine the influence of the forcing mechanism on nearshore current circulation across the surf zone and the inner-shelf region, the first EOF mode was correlated with selected forcing over a 12-hour moving window. The mean correlation coefficients $\bar{R}$ values of all Gulf breeze and cold front events were computed for all stations and are reported in Table 3.3. During the cold front events, the inner-shelf currents showed higher correlation with LATEX shelf current ($\bar{R}$ = 0.44) and tide ($\bar{R}$ = 0.45), than alongshore wind stress component ($\bar{R}$ = 0.41). Meanwhile stations within the surf zone correlated better with the alongshore component of wave radiation stress ($\bar{R}$ = 0.69) and tides ($\bar{R}$ = 0.62) compared to alongshore wind stress ($\bar{R}$ = 0.50).

Table 3.3. A summery of $\bar{R}$ (12 hours window moving correlation between alongshore wind stress, alongshore wave radiation stress, tide, and LATEX shelf currents with G1 – G5 first EOF mode during all cold fronts and Gulf breeze events

	Mean R values (CE#1-3)				Mean R values (GE#1-3)			
	Wind	Waves	Tide	Current	Wind	Waves	Tide	Current
G1	0.47	0.76	0.72	-	0.38	0.42	0.78	-
G2	0.41	0.61	0.64	-	0.42	0.41	0.74	-
G3	0.57	0.71	0.57	-	0.45	0.39	0.57	-
G4	0.53	0.71	0.56	-	0.43	0.40	0.67	-
G5	0.41	-	0.45	0.44	0.47	-	0.42	0.57

Stations located closer to shore (i.e. stations G1 – G2) displayed the highest correlation with tide, while stations between the sandbars were better correlated with alongshore wind stress. On the contrary, during the Gulf breeze events the inner-shelf region correlated better with LATEX shelf currents ($\bar{R}$ = 0.57), alongshore wind stress ($\bar{R}$ = 0.47), and tides

($\bar{R} = 0.42$) in descending order. Surf zone stations $\bar{R}$ values suggest that during gulf breeze periods alongshore wind stress ($\bar{R} = 0.42$) and the alongshore component of wave radiation stress ($\bar{R} = 0.40$) decrease in correlation, while tides ($\bar{R} = 0.69$) correlated better with the first EOF mode. In comparison, the circulation at the inner-shelf region was controlled by LATEX shelf currents during both wind events (i.e. cold fronts and Gulf breeze winds), whereas during the passage of the cold front wave breaking drives the current circulation within the surf zone.

Figure 3.11 display a 12-hour moving R^2 between the first EOF mode computed for stations G1 – G5 and the tested forcing mechanisms (i.e. alongshore wind stress-black line, alongshore wave radiation stress-blue line, tide-gray line, and LATEX shelf currents-green line). During energetic cold fronts (i.e. CE#1 and CE#3), the inner-shelf region currents were mainly influenced by the LATEX shelf currents and the alongshore wind stress. Meanwhile, during periods sustained wind direction (N – NE) and lower wind speed ($3 < U_{10} < 5$) LATEX shelf currents and tides are considered the main driving force (i.e. CE#2). It is also suggests due to that high tidal range recorded during spring tides tidal forcing dominate over the LATEX shelf currents. Therefore, high sea level fluctuation can play a role in inner-shelf region current circulation. During the Gulf breeze periods, the LATEX shelf currents and alongshore wind stress controls the current circulation within the inner-shelf region. This was noticed especially during the GE#1 and GE#3 as alongshore wind stress experienced increased in magnitude.

Moreover, observations of the mid-surf zone (i.e. G3 and G4 stations) suggests that during the cold front events waves breaking and alongshore wind stress are the main driving force, but the influence of the tides can become as important during the spring tide. Additionally, the importance of the tide is mainly dependent on the wave height and the alongshore wind stress conditions. For example, tides were found to be the dominate forcing mechanism when less intense wave heights and alongshore wind stress conditions

exist (i.e. CE#2). Similar to Torres-Freyermuth et al. (2017) findings, tides became more important to current circulation during the spring tidal cycle. Recorded observations at G1 and G2 stations suggests that during the cold front events the inner-surf currents were influenced by all forcing mechanisms, but tides and waves were the dominate controlling forces. These findings contradict with Torres-Freyermuth et al. (2017) observations, as their data suggest that the main driving forces within the surf zone are breaking waves and wind. This contradiction is likely due to the difference in study site locations and meteorological environment (i.e. wind speed and direction). For example, the tidal range in Galveston Island is 0.5 m lower than the tidal range in Torres-Freyermuth et al. (2017) study site. Additionally, Torres-Freyermuth et al. (2017) field experiment site experienced higher wind conditions than what was observed within this study.

In the surf zone the relative importance of tides becomes more visible during the period of Gulf breeze events, and unlike the cold front events waves breaking has relatively similar influence as the alongshore wind stress. Overall during the Gulf breeze events, the tidal force is considered the main driving mechanism for surf zone current circulation, followed by wind. In addition, surf zone stations had a significant portion of data gaps. This definitely has affected the statistical analysis of $\bar{R}$ between the first EOF mode and the selected forcing mechanisms.

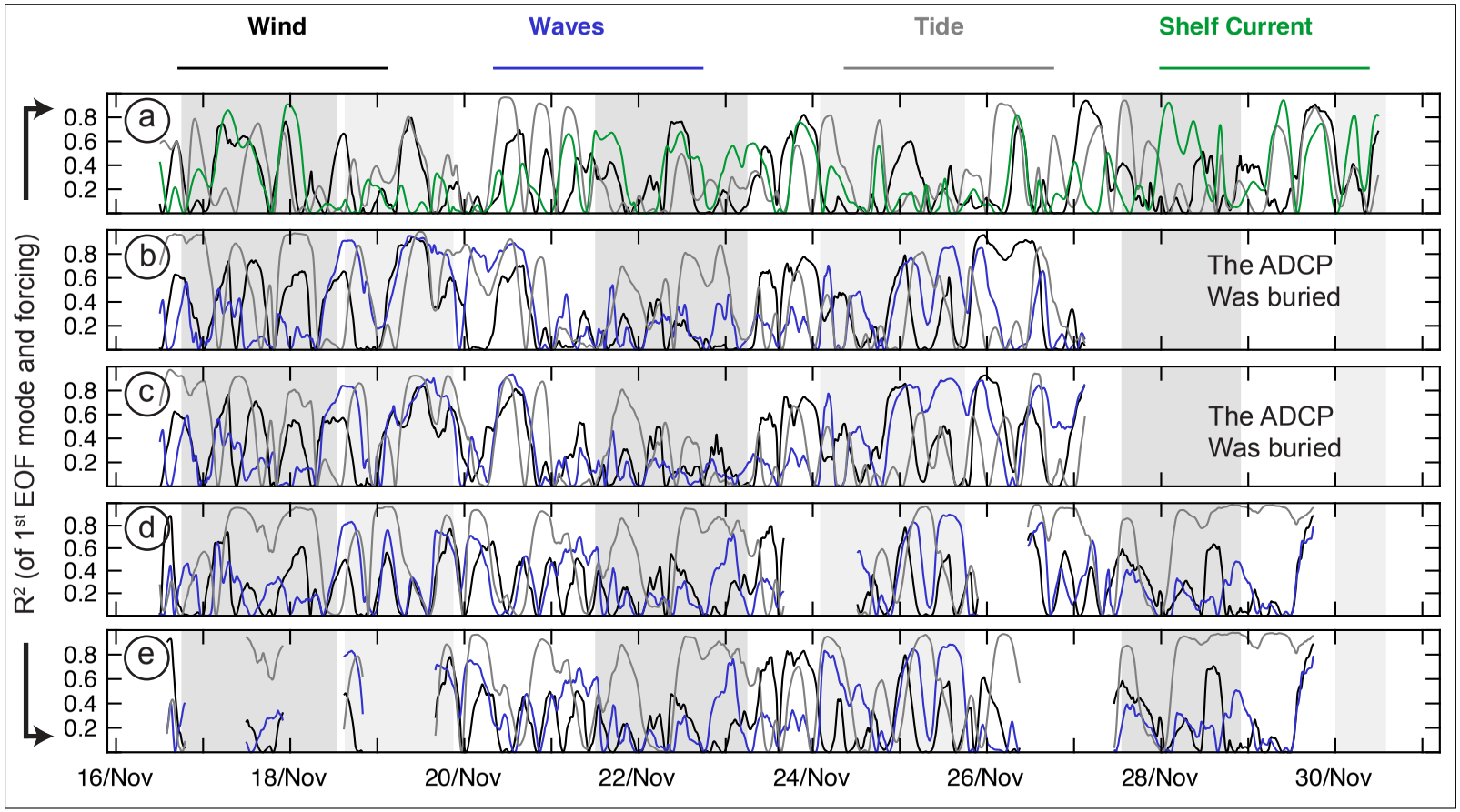

Figure 3.11. R^2 time series computed using a 12 hour window moving correlation between the selected forcing mechanisms and the first EOF mode of the current at: (a) G5, (b) G4, (c) G3, (d) G2, (e) G1.The light gray shaded areas represent cold front events, while the dark gray shaded area indicate Gulf breeze events.

3.5 Summary

The present study has investigated the influence of alongshore wind stress, alongshore wave radiation stress, tide, and LATEX shelf currents on nearshore current variability. This included both spatial and temporal scales, during the passage of three cold front and three Gulf breeze events. Results shows that nearshore currents are intensified during both the passage of cold fronts and during the Gulf breeze events. The findings of this study are summarized in the following three points:

[1] During the cold fronts passage ($2 \leq U_{10} \leq 7$, offshore-directed wind) currents were mainly eastward-directed from the inner-shelf region to the surf zone. During energtic cold fronts the inner-shelf circulation was mainly driven by the tide and wind, whereas less energtic condations the main driving forceses are LATEX shelf current and wind. Meanwhile, the surf zone current circulation was mainly influenced by tides and waves (Figure 3.11b-e).

[2] During the Gulf breeze events ($3 \leq U_{10} \leq 8$, onshore-directed wind), westward-directed currents dominate over the surf zone, while the inner-shelf region current direction varied, and became sustained when wind shear stress levels increased (τ_w > 0.13 Nm^{-2}). It is suggested that the inner-shelf region current circulation was controlled by both wind and LATEX shelf currents. On the other hand, tides and waves combined are considered the main driving forces controlling surf zone current circulation. The consistency of current flow within the surf zone, is likely due to waves arriving from ESE breaks resulting in a westward flow.

[3] During the fall season, both cold front and Gulf breeze events can significantly influence the nearshore circulation, by reversing the mean direction of the current flow. Therefore, this can determine the main transport direction of the sediment,

pollutants, and nutrients. However, the analysis herein does not provide a long term influence of the tested forcing mechanisms. This may result in either underestimating the influence of the forcing mechanisms during both gulf breeze and cold front events.

4. NEARSHORE HYDRODYNAMICS AND SEDIMENT DYNAMICS ON THE UPPER TEXAS COAST IN RESPONSE TO FLUCTUATING ONSHORE (GULF BREEZE) AND OFFSHORE (COLD FRONT) WIND: A SANDY MICROTIDAL BEACH FIELD STUDY

4.1 Introduction

Human beings favor settlement around coastal areas, because of the economical value, ecological, and social importance they have to offer (Costanza, 1999; Culliton et al., 1990). However, coastal erosion is a growing worldwide problem. According to Bird (1985) coastal erosion has affected almost 70% of the world sandy beaches. In addition, coastal erosion can caused by anthropogenic interference by placing artificial structures (e.g. sea-wall, piers, and dams), altering the sediment supply (Morton, 1988). Syvitski et al. (2005) suggest that humans impact have reduced sediment flux to the world coast by 1.4 ± 0.3 billion metric tons per year. In the Gulf of Mexico (GoM) coastal erosion/retreat is a significant problem facing Texas coast, especially from Galveston Island to Padre Island (Morton & McKenna, 1999). This is due to storm activity (Sebastian et al., 2014; Morton et al., 1995), sea level rise (Feagin et al., 2005), and human interference altering the sediment supply (Morton, 1988).

During late fall and early winter months, the northern GoM is subject to synoptic-scale disturbance events (i.e. cold fronts), that are considered to be highly energetic and covers a large spatial extent. An eleven-year analysis of cold fronts by Henry (1979) suggests that on average five fronts pass the GoM between November and April. Approximately 50% of these cold fronts are considered continental polar and enters the GoM between Galveston and Corpus Christi (Henry, 1979). This is similar to what has been reported by Moeller et al. (1993) with an average of 35 cold fronts passing over the Louisiana coast during the

winter months. Cold fronts are characterized by an abrupt increase in wind speed (up to 16 ms^{-1}), reversal in wind direction, and accompanied with high precipitation (Kineke et al., 2006; Keim, 1996; Huh et al., 1978). This can reflect on the wave field, for example, Dingler et al. (1993) reported an increase of significant wave height of 2-3 m in the north of GoM, while Pepper and Stone (2004) reported a 1 m increase in significant wave height and a 3-second decrease in peak wave period. Additionally, Pepper and Stone (2004) observed a 1.5 ms^{-1} increase in near bed current velocity shortly after the passage of a cold front .

Studies by Dingler et al. (1993) and Moeller et al. (1993) suggest that cold fronts are more effective in sediment re-suspension and transport than tropical storms due to their high frequency of occurrence. Therefore, cold fronts are found to be highly effective in sediment re-mobilization (Stone & Wang, 1999; Chaney & Stone, 1996). Pepper and Stone (2004) reported an increase of 0.6 $gm^{-1}s^{-1}$ in cross-shore suspended sediment transport right after the passage of a cold front. Moreover, Dingler et al. (1993) suggested that beach face erosion and overwash deposition are likely to occur during a cold front passage. In contrast, Kineke et al. (2006) results regarding the effect of cold fronts passage over the chenier-plain coast of Louisiana, suggest sediment accretion events are likely to occur following an offshore cold fronts. Therefore, cold fronts can result in both accretion and erosion of sediment within the nearshore region. The impact of cold fronts on nearshore sediment dynamics depends on the wind speed and the cold fronts orientation in regards to the coast (Curtarelli et al., 2013; Garreaud, 2000).

Adding to their critical impact on sediment transport, cold fronts also have an impact on biogeochemical fluxes (e.g. Booth et al., 2000), nutrient transport (e.g. Gallucci & Netto, 2005), and pollution transport (e.g. Michel et al., 2013; Balseiro et al., 2003). The most outstanding impact of cold fronts within the nearshore current circulation on the northern GoM is reversing the westward current resulted from the Gulf breeze wind

events to eastward flow (Wallace et al., 2010; Nowlin et al., 2005; W. Wang et al., 1998; N. P. Smith, 1977). Herein, the Gulf breeze wind events are defined as an energetic wind events, which has a mean duration of one day and blowing onshore with wind speeds more than 5 ms^{-1} and less than 11 ms^{-1}.

Studies addressing the impact of seasonal meteorological events such as cold fronts on coastal regions have been growing in the GoM. A considerable amount of research has covered the cold fronts impact on re-suspension of sediment in lagoons (e.g. Carlin et al., 2016b; Dellapenna et al., 2006), barrier island erosion and overwash (e.g. Keen et al., 2003; Moeller et al., 1993; Dingler & Reiss, 1990), inner-shelf waves and currents (e.g. Keen, 2002), inner-shelf sediment transport (e.g. Kineke et al., 2006; Pepper & Stone, 2004; Stech & Lorenzzetti, 1992), and bay foreshore erosion (e.g. Armbruster et al., 1995). However, there is a sparse regarding the impact of cold fronts on the hydrodynamics and sediment dynamics within the surf zone, despite the widespread recognition of cold fronts impact on the coastal region. Therefore, this paper aims to provide a better understanding of offshore directed cold fronts compared with the onshore winds associated with the Gulf breeze events within the surf zone. The was conducted by comparing cold fronts and Gulf breeze events impact on the surf zone hydrodynamics and sediment dynamics.

4.2 Study site

The field experiment was located on Galveston Island (29°14′27.62″N 94°54′32.88″W, see Figure 4.1), approximately 10 km west of the seawall and in front of Galveston Island State Park. The site can be considered as a natural beach with no human interference. The island is 50 km long and well known to coastal engineering committees because of the 16 km seawall (4.8 m $\times$ 5.4 m) built to protect the island after the 1900 hurricane that resulted in the loss of both lives and properties (Ravens & Sitanggang, 2007; Morton et al., 1995). The study location has the highest shoreline loss of 1.5 – 2.5 m/y within the

upper Texas coast (Paine et al., 2012). Some studies have suggested that the key reason behind Galveston Island shoreline loss is due to the influence of human structures, such as the seawall and jetties, which altered the littoral drift system (e.g. Ravens & Sitanggang, 2007; Morton et al., 1995; Morton, 1988). Another reason can be due to the extreme storm events such as hurricanes (Wallace et al., 2010). However, Galveston Island has an important economic value to the state of Texas. This is due the island location relatively in the center of northwestern GoM with open accesses to sea provided ease of transport for trades via vessels and ports, and high revenue from tourists attraction (Sen & Mayfield, 2004). Therefore, the government spends a huge amount of money heavily to compensate the loss of sediment by beach nourishment. According to Trembanis and Pilkey (1998) 5.9 million dollars have been spent in 1994 – 1995 in order to provide Galveston Island coast with 542834 m^3 of sand.

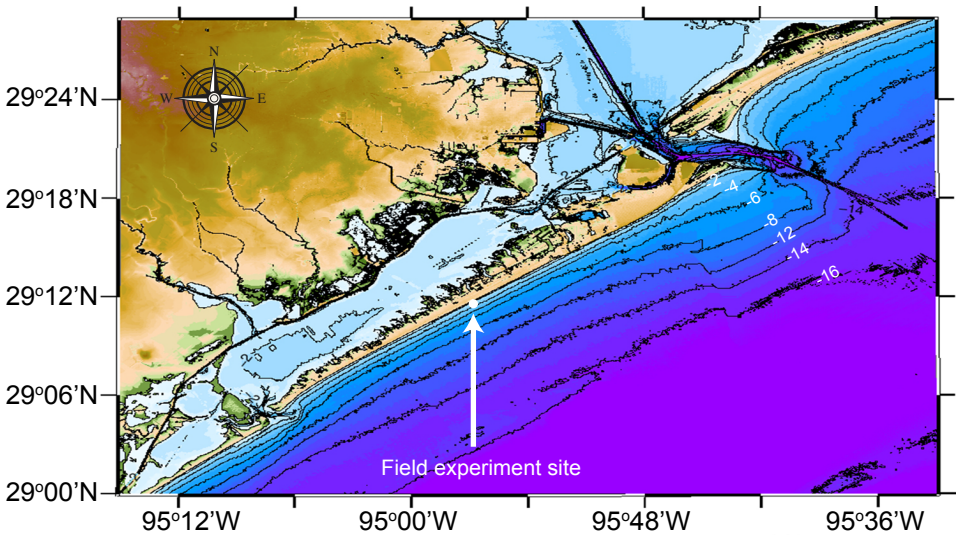

Figure 4.1. Map of the Galveston Island with depth contours. The white circle represents the field experiment location.

Galveston Island has a subtropical climate with hot summers and mild winters (Feagin

et al., 2005). During the summer season the area is subject to the Gulf breeze winds resulting in a westward current flow, while in the winter season the area is subject to frequent cold fronts resulting in an eastward current flow (Wallace et al., 2010; Nowlin et al., 2005, 1998; W. Wang et al., 1998; Henry, 1979).

Galveston beach is microtidal with a tidal range of 0.3 m and a relatively low wave energy (Wallace et al., 2010; Rogers & Ravens, 2008). The reported mean grain size in the surf zone was approximately 0.13 mm (Rogers & Ravens, 2008). The available sediment within the study area is 10-25% calcium carbonate (Balsam & Beeson, 2003), and abundant quartz sand on the Texas shelf, while high percentage of terrigenous silt is available near the coast (Ellwood et al., 2006). Additionally, surf zone sub-tidal sandbars are common within the upper Texas coast (Anderson, 2007), with two sandbars present during the field experiment.

4.3 Data collection and analysis

4.3.1 Field setup

The data used in the present study was collected from November 16 to December 1, 2016, where the field experiment included a cross-shore array of current meters that covered the surf zone (1 m – 2 m depth) and extended to the inner-shelf region (8 m depth). Surf zone currents were measured using two Nortek Acoustic Doppler Velocimeters (ADV) with a 7 m spacing between the two stations. The ADVs were mounted on a triangle frame made on site using galvanized steel pipes as shown in Figure 4.2b. The ADVs, hereafter referred to as G1 and G2, respectively, were oriented downward targeting current measurements at 0.15 m from the seabed. Additionally, the ADVs were able to be vertically adjusted to the targeted depth if needed. Both stations were configured to record continuous pressure and velocity at 16 Hz using the ENU coordinate system (i.e. East, North , Up) with an accuracy of $\pm$ 0.001 ms^{-}1.

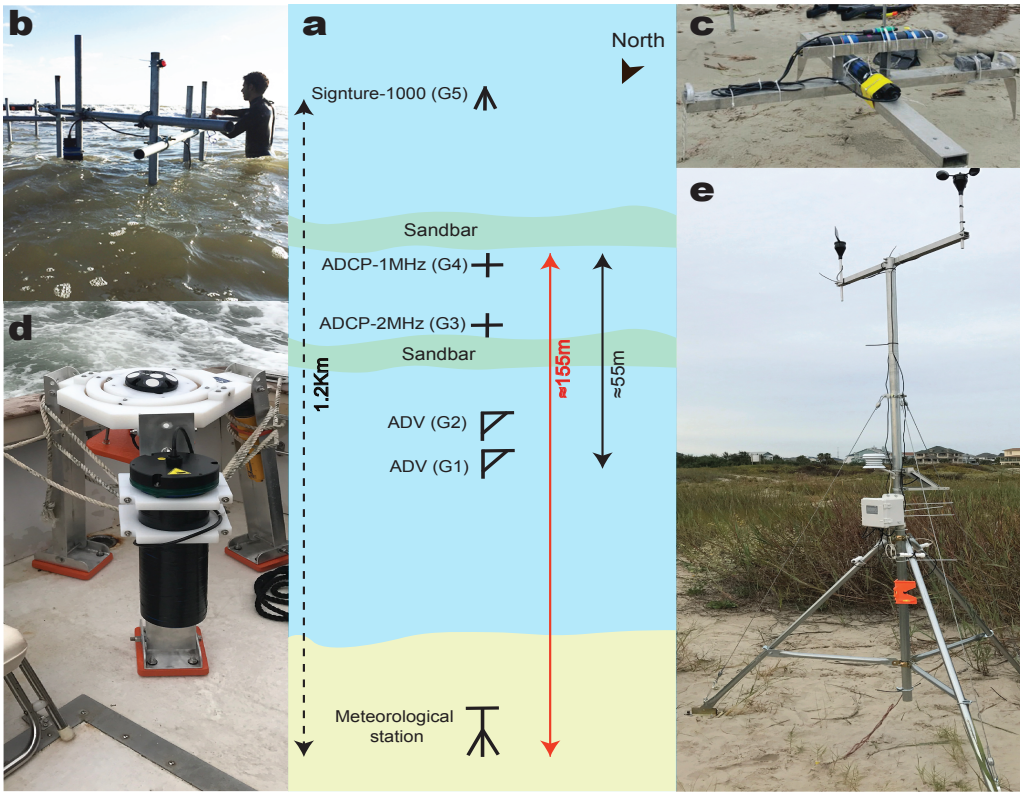

Figure 4.2. Setup and field experiment instruments: (a) plan view schematic of the study area showing instruments locations and layout, (b) frame used for mounting the ADVs , (c) an ADCP mounted on the aluminum pod, (d) gimbal tripod used to mount the Signture-1000, and (e) ONSET meteorological station.

Both G1 and G2 stations were equipped with optical backscatter sensor (OBS), fixed at 0.15 m from the seabed next to the ADVs. However, the OBS failed to record data; therefore, another deployment was conducted to calibrate the Suspended Sediment Concentration (SSC) using G2 station only (will be further discussed in 4.3.4).

Additionally, two pods, holding a 2-MHz and 1-MHz Nortek High Resolution Acoustic Doppler Current Profiler (ADCP HR), were deployed between the inner and the outer-sandbars (Figure 4.2a). The ADCPs provided a measurements of pressure and velocity profile using the ENU coordinate system with an accuracy of $\pm$ 0.005 ms^{-1}. To reduce

magnetic interference, the pods used here were made by aluminum frames, and were anchored to seabed using spiked legs (Figure 4.2c). The 2-MHz ADCP-HR, hereafter referred to as G3, was placed right after the inner-sandbar, and was configured to record 2-minute velocities profile (0.075 m bin over 13 cells) and pressure measurements at 8 Hz every 3-minute. Meanwhile, the 1-MHz ADCP-HR, hereafter referred to as G4, was deployed just before the outer-sandbar, and had the same configuration as G3, but sampled at 4 Hz with cell resolution of 0.1 m (i.e. bin size) over 8 cells. Both G3 and G4 stations were oriented upward, and each were equipped with an OBS; however, the OBS failed to record any measurements. Additionally, measurements of both pressure and velocities from G3 and G4 stations recorded between 21:00-November 27 and 00:00-December 1 2016 were deleted, as the ADCPs were buried under the sandbars.

Furthermore, one Nortek advanced-five-beam current profiling system referred to as Signature-1000 (AD2CP), hereafter referred to as G5, was deployed approximately 1.2 km from the shoreline. The AD2CP was deployed in an 8 m depth using a gimbal tripod. G5 station was configured to record continuous pressure and velocity profile measurements at 8 Hz with 0. 2 m spacing over 5.4 m, using the ENU coordinate system with an accuracy of $\pm$ 0.003 ms^{-1}(Figure 4.2d).

Finally, atmospheric observations were collected using Onset Computer Corporation HOBO U30-NRC (meteorological station) and was setup on the beach approximately 100 m from G1 station. The meteorological station was configured to record measurements of temperature ($^{\circ}$C), relative humidity (%), wind speed (ms^{-1}) and direction (degree) at 1 Hz, and produced an average value every 30 seconds. The meteorological station sensors were mounted on a 3 m mast (Figure 4.2e), and the calibration of wind direction sensor was performed on site. A summary of instrument configuration and sampling parameters are provided in Table 4.1.

Table 4.1. Summary of overall instrumentation and the configuration used within the field experiment.

Instrument	Instrument position	Sampling intervals (seconds)	Sampling frequency (Hz)	Sensor elevation above/ bed and orientation	Measurement
Acoustic Doppler velocimeters (ADV)	G1 G2	continuous	16	0.15m/down	current, water level
High Resolution Acoustic Doppler Current Profiler (ADCP-HR 2MHz)	G3	180	8	0.3m/up	current, water level
High Resolution Acoustic Doppler Current Profiler (ADCP-HR 1MHz)	G4	180	4	0.3m/up	current, water level
Signature-1000 (AD2CP)	G5	continuous	8	0.75m/up	current, water level
Optical Backscatter Sensor (OBS)	G2	the same as attached instrument	the same as attached instrument	positioned with the same target depth of other instruments	scattered infra-red radiation
Meteorological station	onland	30	1	-	temperature, relative humidity, wind speed and direction

4.3.2 Wind, currents, and waves analysis

Prior to data analysis, wind measurements were adjusted to the standard reference height of 10 m. Later, the recorded wind speed and direction were block-averaged every 2 minutes, then smoothed using Savitzky-Golay filter over a 10-minute window (Savitzky & Golay, 1964). Additionally, the magnitude of wind stress (τ_w) was estimated using the quadratic law by the following definition:

$$\tau_w = \rho_a \, C_D \, U_{10}^2 \tag{4.1}$$

where ρ_a is the air density, assumed to be constant at 1.2 kgm^3, the drag coefficient (C_D) is a function of air density, temperature, wind speed, and was estimated following S. D. Smith (1988) methods. U_{10} in Eq.4.1 is wind speed at the standard reference height.

During the post processing phase all velocity measurements from station G1 to G5 were converted from the earth coordinate system (i.e. North-South and East-West) into cross-shore and longshore, according to the coastline orientation. Measurements of velocity with correlation less than 60% were filtered out for stations located within the surf zone and correlation less than 70% for the inner-shelf station (for description refer to Rusello, 2009. Later, velocity and pressure measurements were block-averaged every 2 minutes, then smoothed using a low pass filter over a 10-minute window.

Wave analysis was carried out using a directional wave spectrum Matlab toolbox referred to as DIWASP (Johnson, 2002). The toolbox has been used in previous studies to investigate wave dynamics within oceans and coastal regions (e.g. Fisher et al., 2017; Fedele et al., 2013; Ogawa et al., 2012; Bechle & Wu, 2011; Bever et al., 2011). DIWASP output provides an estimate of significant wave height (H_s), period (T_s), angle (D_w), and also provides a directional wave spectrum analysis. This was carried out by implementing the Direct Fourier Transform Method (DFTM, see Eq.16 and Eq.45 within Barber (1963)).

The toolbox computes the wave direction similar to Gordon and Lohrmann (2001) methods (Eq.4.2) by using the pressure recording and both the cross-shore and the longshore velocity cross spectra (Φ_{pu} and Φ_{pv}, respectively, usually referred to as PUV method):

$$D_w = \text{atan2}(\Phi_{pu}, \Phi_{pv}) \tag{4.2}$$

4.3.3 Turbulence

Shear stress produced by wind increases surface wave height. Therefore, it is directly linked with enhancing Turbulent Kinetic Energy (TKE). TKE dynamics can be quantified by measurements of TKE dissipation rate (ε). Both TKE and ε were estimated using the velocity measurements recorded using the current meters. In this paper, TKE was computed using the variance method (Eq.4.3), that has been previously used within the surf zone region (e.g. Butt et al., 2004; Svendsen, 1987):

$$\text{TKE} = \frac{1}{2}\left(\overline{u'^2} + \overline{v'^2} + \overline{w'^2}\right) \tag{4.3}$$

the right hand side of Eq.4.3, $\overline{u'^2}$, $\overline{v'^2}$, and $\overline{w'^2}$, corresponds to cross-shore, longshore, and vertical mean velocity variances, respectively. Furthermore, ε can be estimated by fitting the Kolmogorov -5/3 slope within the inertial subrange of Power Spectral Density (PSD) plot of velocity fluctuations (Eq.4.4). This method was developed by Kolmogorov (1941), and it assumes the turbulence to be homogeneous and isotropic and can be computed using the following:

$$E(k) = \alpha \varepsilon^{2/3} k^{-5/3} \tag{4.4}$$

where $E(k)$ is isotropic energy spectra, k is the wavenumber, α is the empirical Kolmogorov constant ≈ 1.5 (H. Grant et al., 1962). Additionally, a robust regression algo-

rithm (Huber, 1964) can be used for fitting the $-5/3$ slope into the spectra, as this method helps in reducing the error produced by the least square fit. However, within this paper a modified version of Eq.4.4 by Trowbridge and Elgar (2001) was used to compute ε (Eq.4.5). Trowbridge and Elgar (2001) version filters out the energy signature of wind and waves on the PSD, thus providing accurate estimate of turbulence, and was computed as follows:

$$E(k) = \frac{12}{55}\alpha\varepsilon^{2/3}k^{-5/3}V^{2/3}I\Big(\frac{\sigma}{V},\theta\Big) \tag{4.5}$$

where V is defined as the magnitude of the current, θ is the angle between the wave and current, and σ is the variance of the wave induced horizontal velocity. Trowbridge and Elgar (2001) defined the term $I\Big(\frac{\sigma}{V},\theta\Big)$ as follows:

$$I\Big(\frac{\sigma}{V},\theta\Big) = \frac{1}{\sqrt{2\pi}}\Big(\frac{\sigma}{V}\Big)^{2/3}\int_{-\infty}^{+\infty}\Big[x^2 - 2\frac{V}{\sigma}\cos(\theta)x + \frac{V^2}{\sigma^2}\Big]^{1/3}\exp\Big(-\frac{1}{2}x^2\Big)dx \tag{4.6}$$

a detailed explanation of Eq.4.6 can be found in Trowbridge and Elgar (2001). The cross-shore bed shear stress (τ_b) was estimated using the covariance method (e.g. Pope et al., 2006; Biron et al., 2004; Babaeyan-Koopaei et al., 2002; Kim et al., 2000) by using the cross-shore and vertical velocity fluctuations ($\overline{u'w'}$):

$$\tau = \rho_w\overline{u'w'} \tag{4.7}$$

herein ρ_w is the density of the salt water and assumed to be constant ($\approx$ 1025 kgL^{-1}).

4.3.4 Beach profile survey and suspended sediment flux

Beach topographic surveys were made using Real Time Kinematic (RTK) Differential Global Positioning Systems (DGPS) that has a horizontal accuracy of $\pm$ 10 mm and a ver-

tical accuracy of $\pm$ 20 mm. Due to some limitations, the surveys were only conducted on November 17, 21, and 30 2016, and December 1, 2016. However, due to technical issues with the RTK discovered later after the experiment for profiles taken after November 21. Thus, profiles taken on November 17 and November 21 were used for analysis. Moreover, due to the failure of the OBSs to operate during period of the experiment, another deployment was conducted on the same site using only G2 station. The new deployment lasted a week and had experienced similar atmospheric wind events (i.e. cold fronts and Gulf breeze events).

In order to compute suspended sediment flux, SSC was derived from G2 station backscatter measurements. Doppler velocity instruments were mainly designed to measure current velocity, but also can be used as a surrogate to measure SSC by backscatter intensity. Researchers have adopted this acoustical technique to aid in investigating sediment transport processes (e.g. Ha et al., 2011; Thorne et al., 2011; Hill et al., 2003; Jay et al., 1999; Thorne et al., 1993). Later, the technique had improved to account for sound attenuation (e.g. Sassi et al., 2012; Lee & Hanes, 1995; Thorne et al., 1993), and the impact of site environment on the backscatter calibration (e.g. Hoitink & Hoekstra, 2005; Gartner, 2004). The method used to derive SSC from G2 station followed Deines (1999) technique by using the simplified version of the sonar equation, as follows:

$$S_v = C + 10\log_{10}(R^2) - L_{DBM} - P_{DBW} + 2\alpha_{ab}R + K_c(E_i - E_r) \tag{4.8}$$

herein, S_v correspond to the volume backscatter strength, R is slant range ($R = \mathrm{z}/\dfrac{180 \times \theta}{\pi}$, θ is the transducer angle and z is the cell depth), L_{DBM} is the transmitted pulse length, P_{DBW} is the transmitted power, α_{ab} represent the absorption coefficient, E_i and E_r are the echo intensity/strength and the Received Signal strength Indicator (RSSI) reference level under no signal present. Moreover, once the RSSI scale factor (K_c) and the calibration

constant (C) were obtained using a linear regression of E and SSC obtained from the OBS, the inversion can be estimated using the following definition:

$$SSC_{ADV} = 10^{\left(20\log_{10}(R) - L_{DBM} - P_{DBW} + 2\alpha R + K_c(E_i - E_r)/10\right)} \tag{4.9}$$

where SSC_{ADV} is the SSC measured by the ADV. Computation of time averaged longshore and cross-shore sediment flux (q_v, and q_u, respectively) , were carried out following Jaffe et al. (1984) method, a well known method that has been used by several coastal researchers (e.g. Williams et al., 2015; Pattiaratchi & Masselink, 1996; Aagaard & Greenwood, 1994; Osborne & Greenwood, 1993; Russell, 1993):

$$q_v = \frac{1}{N}\sum_{i=0}^{i=n} v_{in}(SSC)_{in} \tag{4.10}$$

$$q_u = \frac{1}{N}\sum_{i=0}^{i=n} u_{in}(SSC)_{in} \tag{4.11}$$

The total suspended sediment transport in both the longshore and cross-shore direction was computed using Eq.4.10 and Eq.4.11 results, as follows:

$$Q_v = \sum_{i=0}^{i=n} \int_{t_1(i)}^{t_2(i)} q_v(t)dt \tag{4.12}$$

$$Q_u = \sum_{i=0}^{i=n} \int_{t_1(i)}^{t_2(i)} q_u(t)dt \tag{4.13}$$

herein Q_v and Q_u represent the total suspended transport in the longshore direction and the total suspended transport in the cross-shore direction, respectively. The term i represents the number of events, t_1 and t_2 are the beginning and end of the event period, respectively, and t is the time.

4.4 Results

4.4.1 Atmospheric observations and inner-shelf oceanographic forcing

Time series measurements of wind speed and direction in Figure 4.3a, display three Gulf breeze events, hereafter referred to as GE#1–3, and three cold front events, hereafter referred to as CE#1–3. Overall during the Gulf breeze events, wind speed was found to be slightly stronger than those experienced during cold front event winds. Meanwhile, changes in wind speed and direction over the course of cold fronts were almost instantaneous. Wind speed during the Gulf breeze events ranged between 2 ms^{-1} and 8.3 ms^{-1}, with a mean wind speed of 4.4, 4.7, and 5.9 ms^{-1}, experienced during GE#1, GE#2, and GE#3, respectively. Wind direction was sustained during GE#1, GE#2 and mainly blowing from the southeast, while GE#3 had a southwest wind component. On the contrary, cold front events had a lower duration and weaker winds, where wind speed ranged between 1.5 ms^{-1} and 6.8 ms^{-1}, with a mean wind speed of 5.1, 3.3, 4.4 ms^{-1}, during CE#1, CE#2, and CE#3, respectively. Over the course of Gulf breeze events, wind shear stress experienced the highest increase, with a maximum wind shear stress observed during GE#3 (0.185 Nm^{-2}), while cold fronts displayed lower values, except during CE#1 (Figure 4.3b). The characteristics of the wind events experienced during the field experiment are summarized in Table 4.2.

Water level (η) measurements display two spring tidal cycles at the start and end of the experiment, while neap cycle occurred between November 21 and November 26 (Figure 4.3c). A prediction of water level data was generated using T_Tide (Pawlowicz et al., 2002). Gulf breeze events associated with a wind speed of more than 6 ms^{-1}, the observed water level exhibited an increase of 0.13 m higher than the predicted water level (Figure 4.3c). However, during the cold front events, the observed water level was suppressed up to 0.12 m compared to the predicted water level, as the wind direction was rotated.

Table 4.2. Measured wind speed and direction, and total duration of GE#1–3 and CE#1–3.

Events	Duration (hour)	Max U_{10} (ms^{-1})	Wind direction
CE#1	30	6.8	NW-NE
CE#2	38	4.8	N-NE
CE#3	14	5.4	NW-N
GE#1	43	6.6	SE-S
GE#2	42	6.3	SE-S
GE#3	33	8.3	SE-SW

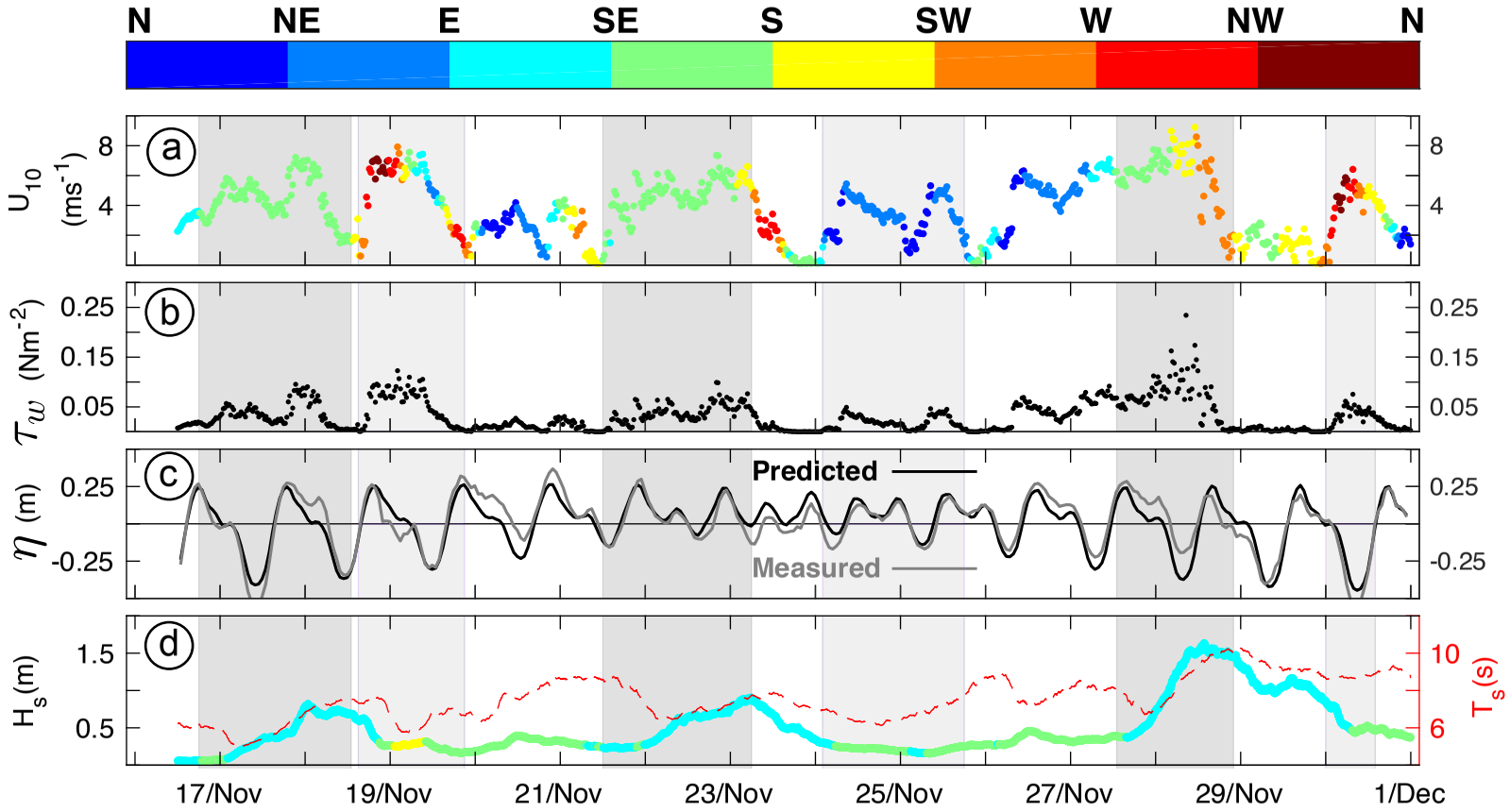

Figure 4.3. Measured time series of: (a) wind speed and direction, (b) wind shear stress, (c) predicted water level indicated by the black line (computed from G5 using T_Tide (Pawlowicz et al., 2002), and observed water level indicated by the gray line, (d) significant wave height and direction (left axis), and significant wave period (right axis, indicated by dashed red line). The color-bar represent direction of wind and waves as coming from. The light gray shaded areas represent cold front events, while dark gray shaded area indicate Gulf breeze events.

Moreover, during the Gulf breeze events, offshore waves arrived from E-SE, while during the cold front events, waves mainly arrived from SE-S (Figure 4.3d).The significant wave height was higher during the Gulf breeze events compared to cold front observations. The most outstanding increase in wave climate was experienced during GE#3, with a 1 m and 3.5 seconds increase in significant wave height and period, respectively. However, cold fronts displayed a weaker wave climate, with a mean significant wave height and period of 0.4 m and 6.5 seconds, respectively. The low wave energy experienced during the cold fronts can be a result of the low wind shear stress caused by the land topography. The average directional wave spectrum of all Gulf breeze events (Figure 4.4a) depicts a peak period of 4.5 seconds and a peak direction at 110°, while the mean directional wave spectrum of all cold fronts events (Figure 4.4b) display a peak period of 5 seconds and a peak direction at 150°.

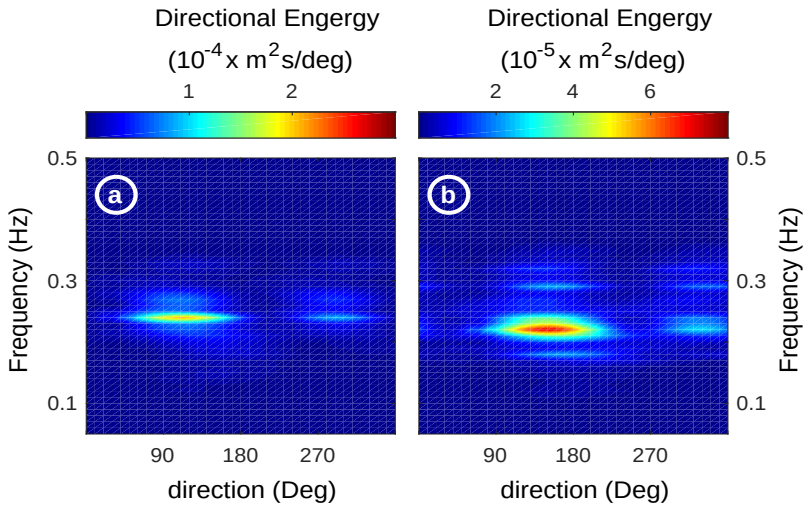

Figure 4.4. Mean directional wave spectrum for combined: (a) Gulf breeze events, (b) cold front events.

The recorded cross-shore and longshore currents within the inner-shelf display higher

magnitudes during the cold front events than the ones observed during the Gulf breeze events (Figure 4.5a-b). The current profile was relatively homogeneous through the water column, except for CE#2, which may be due to the low wave energy conditions. The mean depth averaged cross-shore currents experienced during the CE#1–3 was approximately 0.15 ms^{-1}, while the mean depth averaged lonshore current was approximately 0.18 ms^{-1}. On the other hand, Gulf breeze events depth averaged cross-shore current ranged between -0.08 ms^{-1} and 0.1 ms^{-1}, while the longshore currents ranged between -0.17 ms^{-1} and 0.18 ms^{-1}. Note that current direction was more consistent during the cold front events, with onshore and eastward currents. However, offshore and westward currents were enhanced and sustained for a longer period during GE#3 compared to GE#1–2.

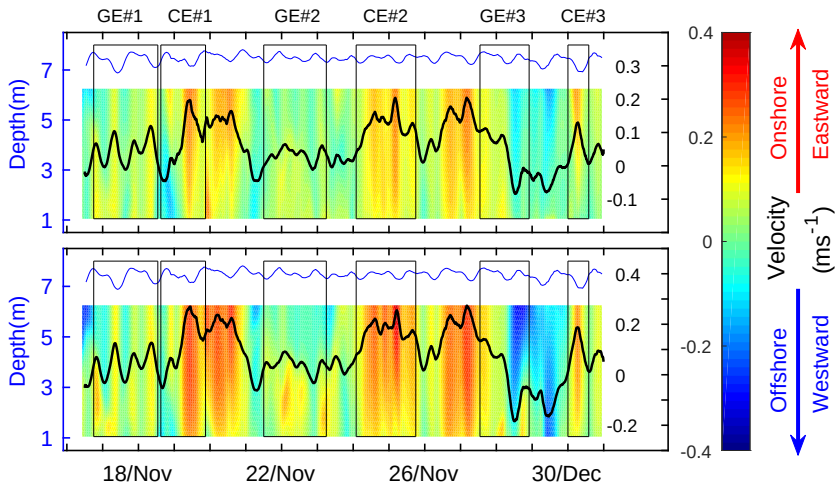

Figure 4.5. Measured time series current velocity at G5 station: (a) cross-shore component, (b) longshore component, the positive values indicate onshore and eastward flow, while negative values indicate offshore and westward flow. Blue line represent water level, black line represent depth averaged velocity, and wind events are reprsented by the rectangles.

4.4.2 Surf zone currents and waves

The surf zone significant wave heights and periods were lower than the wave climate experienced at G5 station (Figure 4.6a-b). The highest waves were recorded within the area between the sandbars, where G3 and G4 stations experienced similar wave height and period. In comparison, wave parameters during the Gulf breeze events were found to be higher than wave parameters experienced during cold fronts events. During the Gulf breeze events, G3 and G4 experienced a maximum significant wave height and wave period of 0.57 m and 7 seconds, respectively. On the other hand, during the beginning of the cold front events, an increase in wave climate was observed followed by a decline as the fronts passed the area. On the contrary, G1 and G2 stations wave climate were almost 40% lower than what was experienced at G3 and G4 stations, with significant wave heights ranging between 0.12 m and 0.32 m, and periods ranging between 2 seconds and 8 seconds. Nevertheless, all stations displayed a similar pattern in both wave height and period during the total period of the field experiment.

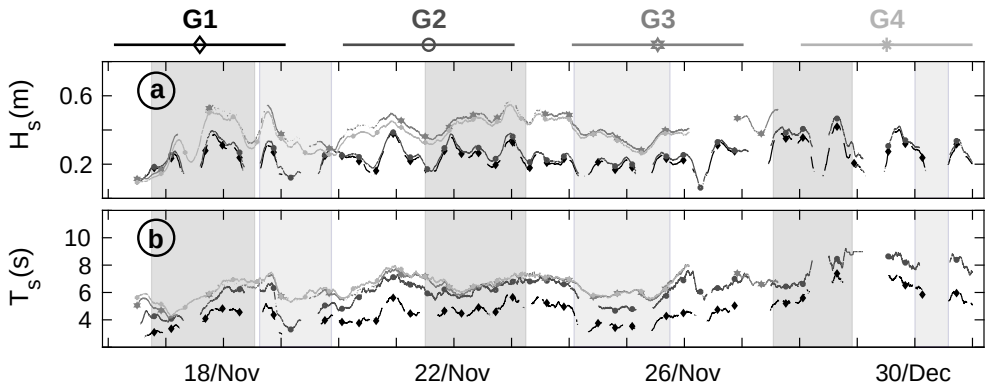

Figure 4.6. Measured time series of: (a) significant wave height, (b) significant wave period. The light gray shaded areas represent cold front events, while dark gray shaded area indicate Gulf breeze events.

Unlike the inner-shelf region, the surf zone cross-shore and longshore current profiles recorded at G3 station were homogeneous throughout the entire water column (Figure 4.7a-b). This homogeneity in the current profile is due to the waves energy distributed across the entire water column in shallower waters, where the inner-shelf region currents homogeneity can only be observed at the top layer of the water column. Overall, measured surf zone currents were found to be approximately 90% stronger than measured currents at the inner-shelf region (Figure 4.8). In comparison, the characteristics of the cross-shore current over G2 and G4 stations were found to have a similar current intensity and pattern (Figure 4.8a). Additionally, the same can be seen from the recorded cross-shore current between G1 and G3 stations.

During CE#1, the experienced cross-shore current between the sandbars were found to be approximately 0.13 ms^{-1} higher than those observed at G2 station. Meanwhile, during the GE#2, the cross-shore current at G2 station increased in magnitude with a maximum value of 0.48 ms^{-1}. On average, the cross-shore current across all stations was directed offshore during GE#1–3 and mainly directed onshore during the CE#1–3. Similarly, the longeshore current had a consistent pattern with eastward current during CE#1–3, and sustained westward current during GE#1–3. The recorded longshore current intensity at G1 and G2 stations were slightly higher than the recorded longshore currents at G3 and G4 stations, with a mean longshore current of 0.43 ms^{-1} and 0.35 ms^{-1}, during GE#1–3, and CE#1–3, respectively.

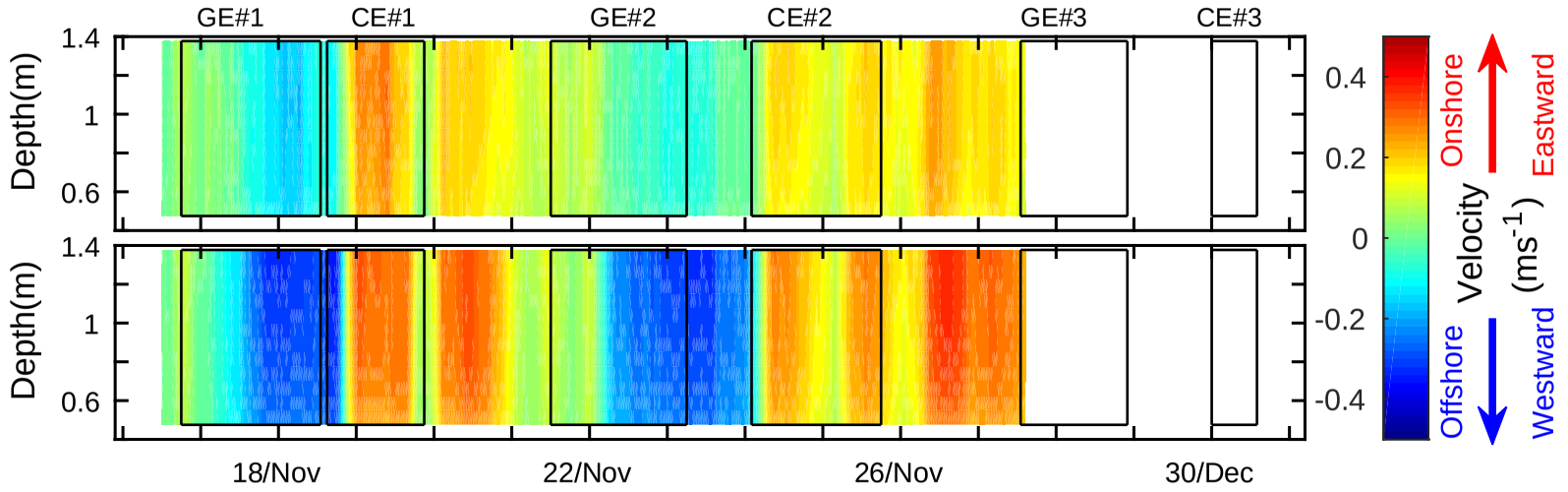

Figure 4.7. Measured time series current velocity at G3 station: (a) cross-shore component, (b) longshore component. The black rectangles reprsent cold fronts and Gulf breeze events.

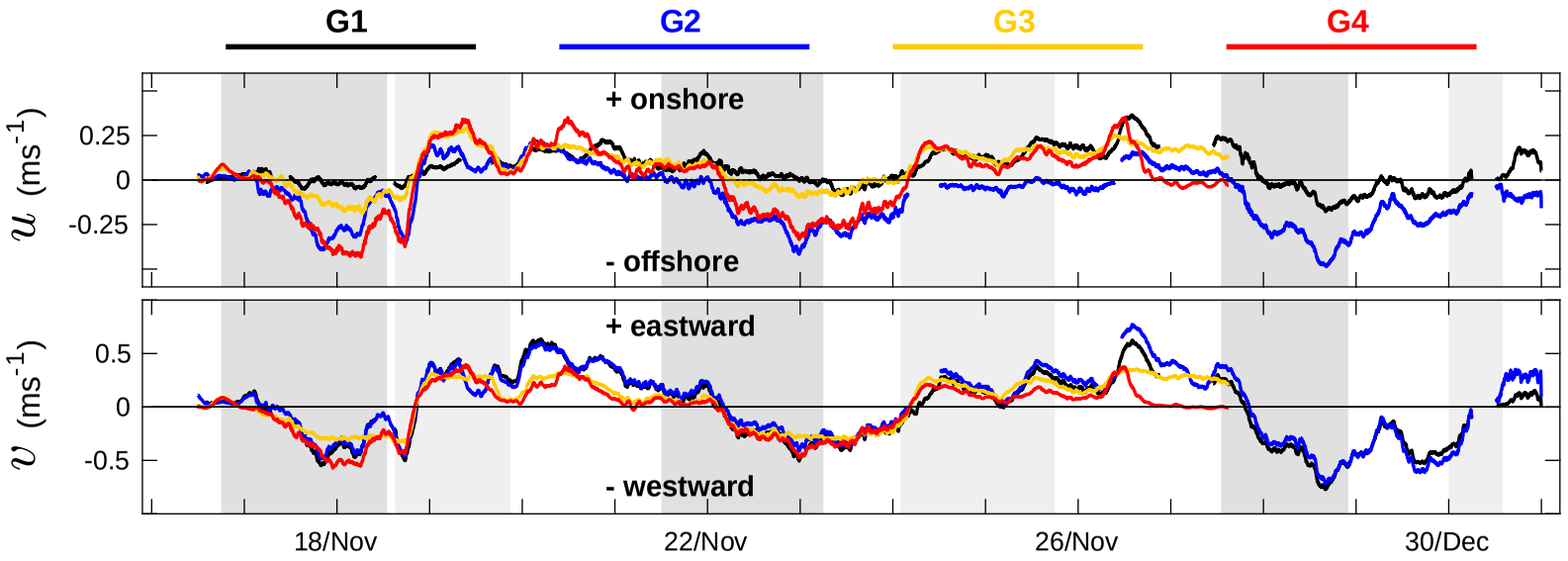

Figure 4.8. Measured time series of current observations: (a) cross-shore currents, (b) longshore currents. positive values indicate onshore and eastward flow, while negative values indicate offshore and westward flow. The light gray shaded areas represent cold front events, while dark gray shaded area indicate Gulf breeze events.

4.4.3 Turbulence within the the surf zone

In terms of suspended sediment concentration, it is essential to investigate the energy levels associated with each wind event, where higher values of TKE and ε are considered the main factors for sustaining the suspension for longer periods. Overall, the site experienced ε values ranging from 10^{-5} m^2s^{-3} to 10^{-3} m^2s^{-3} and TKE values ranging from 10^{-4} m^2s^{-2} to 10^{-2} m^2s^{-2}. Despite the high energetic conditions observed from this study, these observations falls within the range of previously reported values of ε and TKE within the surf zone region (e.g. Brinkkemper et al., 2017; Ruessink, 2010; Feddersen et al., 2007). Time series of estimated ε displays higher values during the Gulf breeze events and increases in magnitude as it gets closer to the coast (Figure 4.9a). The mean estimated ε during the Gulf breeze events was 2×10^{-4} m^2s^{-3}, while the maximum value of ε was observed during GE#3 (1.5×10^{-3} m^2s^{-3}). It can be noted that the high magnitude in ε experienced during GE#3 was associated with both high wave conditions accompanied by low or high tidal levels during the spring tidal cycle. Meanwhile, the lowest ε value was observed at G3 during the CE#2 (9×10^{-6} m^2s^{-3}). Additionally, it can be noted that during the Gulf breeze events, the differences in ε values between the stations were relatively high, whereas during the passage of cold fronts the differences between the stations ε values were reduced. This can be correlated to the wave energy conditions observed during both wind events, as low energetic conditions experienced with cold front events resulted in lower magnitudes of ε.

Moreover, the estimated TKE values at G1 station display similar characteristics to values experienced at G2 station (Figure 4.9b). However, between November 16 and November 24, the estimated TKE values at G1 station were found to be the highest compared to the other stations. On the other hand, TKE values at stations G3 and G4 were approximately the same throughout the total period of the field experiment. Mean TKE values

were similar during both the cold fronts and Gulf breeze events (3×10^{-3} m^2s^{-2}). During the Gulf breeze events, the maximum TKE was experienced in GE#3 with TKE values up to 8×10^{-3} m^2s^{-2} at G1 station. On the other hand, during the cold front events the maximum TKE was experienced in CE#1 up to 7×10^{-3} m^2s^{-2} at G1 station. Lower TKE values experienced between the sandbars and ranged from 7×10^{-4} m^2s^{-2} to 2×10^{-3} m^2s^{-2}, at G4 and G3 stations, respectively.

Near bed shear stress is an important parameter that is used in almost every sediment transport studies, where it provides an indication or a threshold for sediment movement within the coastal regions. Depending on sediment properties , wave activity, and the methods used, the computed τ values will range significantly. For example, values of surf zone reported τ values for both modeled and observed ranging between 0.8 Nm^2 and 50 Nm^2 (Tomás et al., 2012; Aagaard & Hughes, 2010; Ruessink, 2010; Dufois et al., 2008). Within this field experiment, the surf zone τ values were similar across all stations during the field experiment and ranged from 1.5 Nm^{-2} to 19.8 Nm^{-2} (Figure 4.9c). Generally, τ values were elevated during the Gulf breeze events and experienced a decline during the cold front events. The largest increase in τ levels was recorded during GE#3 with a maximum value of 19.8 Nm^{-2} observed at G2. In comparison, the lowest observed τ during the cold front events was experienced during CE#2 (2.7 Nm^{-2}) at G4 station. The mean τ experienced during the Gulf breeze events was 9 Nm^{-2}, whereas 6.6 Nm^{-2} was experienced during the cold front events. During the Gulf breeze events, the surf zone energy levels were found to be higher, which explains the difference between the observed τ values when comparing cold fronts to the Gulf breeze events.

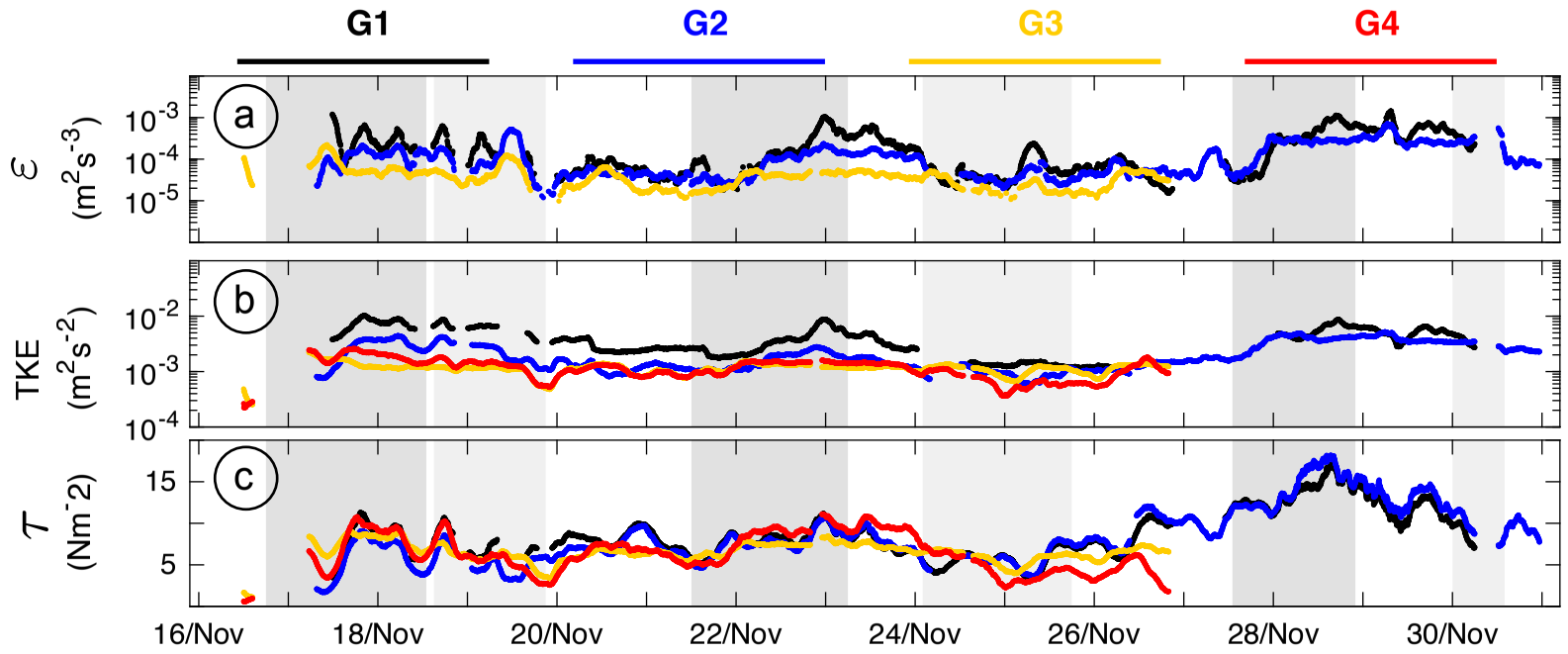

Figure 4.9. Time series of turblance quntities within the surf zone: (a) estimated ε, (b) estimated TKE, (c) τ. The light gray shaded areas represent cold front events, while dark gray shaded area indicate Gulf breeze events.

4.4.4 Beach morphology and suspended sediment

Examining the cross-shore beach profile for pre-GE#1 and post-CE#1, display relatively drastic changes in the profile morphology (Figure 4.10a). Post-CE#1, a 0.16 accretion of sediment was observed within the foreshore region (0 m – 8 m) and 0.14 m between the sandbars (70 m – 95 m). On the other hand, an erosion of 0.24 m was observed at the beach berm (18 m – 26 m). Meanwhile, an erosion of 0.14 m was observed at the inner-sandbar and erosion 0.16 m observed at the outer-sandbar. Comparing both cross-shore beach profiles and the associated prevailing hydrodynamics during GE#1 and CE#1, it can be noted that the eroded sediment was deposited landward. Nevertheless, this does not indicates sandbar migration phenomena, but suggests that due to the cross-shore velocity a re-mobilization of sediment will take place and will be transported landward. However, this is limited to the selected events (i.e. the cross-shore beach profile for pre-GE#1 and post-CE#1) and might not reflect the morphodynamics that will be associated with future cold fronts. Moreover, the passage of the cold front resulted in 0.3^o increase mean beach slope and an increase of 1.2^o in the foreshore slope. Similarly, the passage of the cold front resulted in 0.2^o decrease in the inner-sandbar slope.

The elevation Difference (Δ) between pre-GE#1 and post-CE#1 is shown in Figure 4.10b. Observations from Figure 4.10b suggests that distinct topographic features such as the sandbar and the beach berm will be eroded during the passage of offshore cold front, whereas sediment deposition will take place at the trough or trough-like regions.

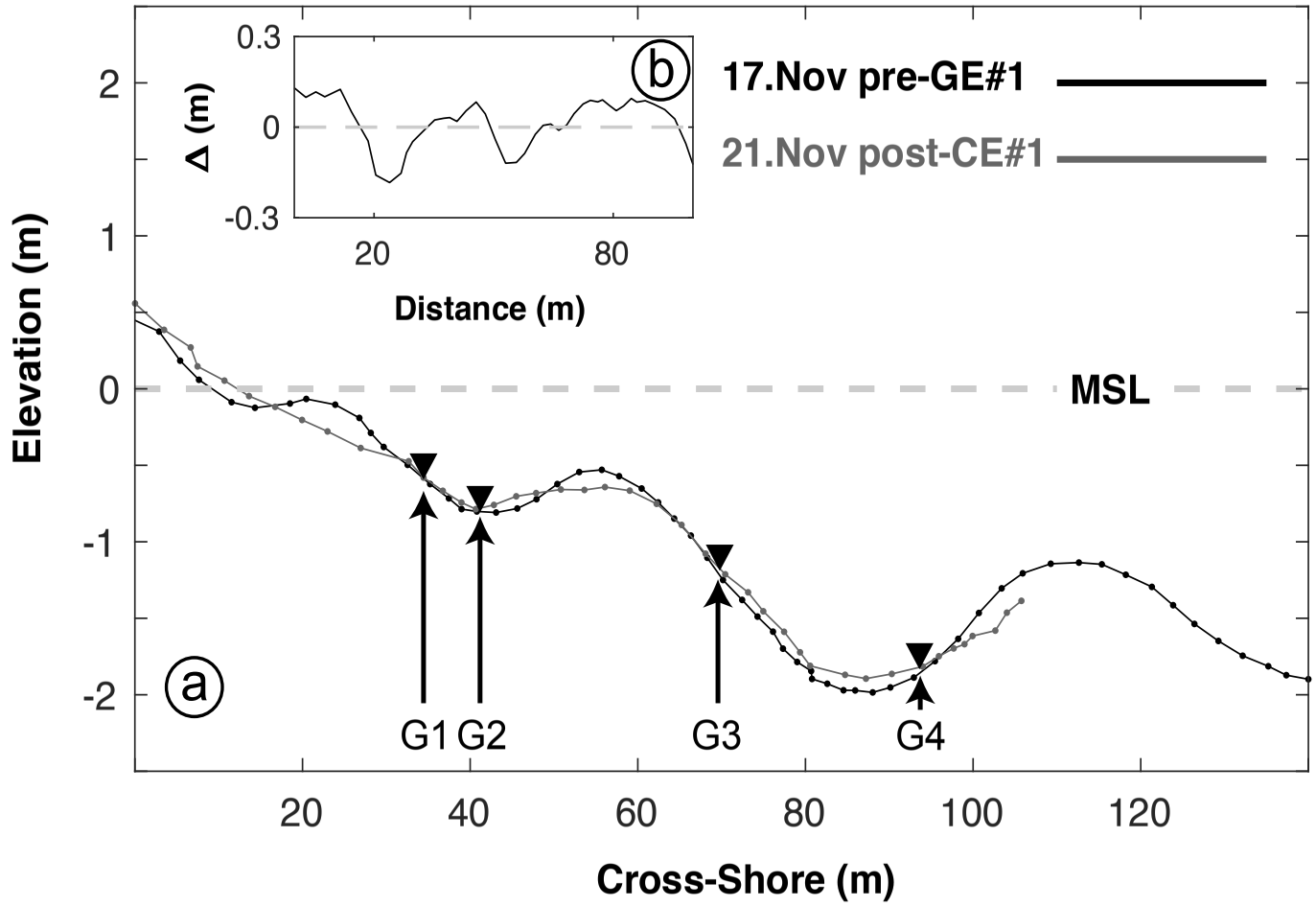

Figure 4.10. Measured beach profile for pre-GE#1 (black line) and post-CE#1 (gray line): (a) cross-shore profile of the site with instruments position, (b) difference between pre-GE#1 and post-CE#1. Dots indicate RTK measurements position.

Overall, the estimated SSC levels experienced within the total period of the experiment ranged between 1 gl^{-1} and 3.4 gl^{-1}, where higher concentrations were recorded during the Gulf breeze events (Figure 4.11a). During the Gulf breeze events, SSC levels experienced some variation, where spiked levels were seen at the beginning of the events, except during GE#3 where SSC levels were gradually increasing throughout the event. This increase can be a result of the combination in the increasing levels of τ and turbulence at G2 station, as can be seen from Figure 4.9. On the contrary, spiked SSC levels during CE#1–2 occurred approximately in the middle of the events. The mean SSC experienced throughout the total period of the experiment was 2.6 gl^{-1}.

The cross-shore suspended sediment flux was higher during the Gulf breeze events and ranged between 0.12 $kgm^{-2}s^{-1}$ and -1 $kgm^{-2}s^{-1}$, and was mainly directed offshore (Figure 4.11b). Meanwhile, cold front events cross-shore suspended sediment flux was mainly weaker. During the CE#1, the flux was mainly onshore directed exhibiting a mean of 0.1 $kgm^{-2}s^{-1} \pm 0.2$, while during CE#2, the flux was mainly offshore directed with a mean of -0.1 $kgm^{-2}s^{-1} \pm 0.1$. The direction of the cross-shore suspended sediment flux during CE#2 could be due to local generated undertow currents, as all other stations exhibited an onshore current direction. Unlike the cross-shore suspended sediment flux, the longshore flux experienced higher values with higher variation during cold front events (Figure 4.11c). Overall, westward-directed suspended sediment flux was dominating during the Gulf breeze events. On the other hand, a eastward-directed suspended sediment flux was consistent during the cold front events. During the cold front events, the maximum longshore suspended sediment flux reached up to 0.78 $kgm^{-2}s^{-1}$ (recorded during CE#1). Alternatively, the maximum longshore suspended sediment flux experienced throughout the experiment was recorded during GE#3 with a value of -1.5 $kgm^{-2}s^{-1}$.

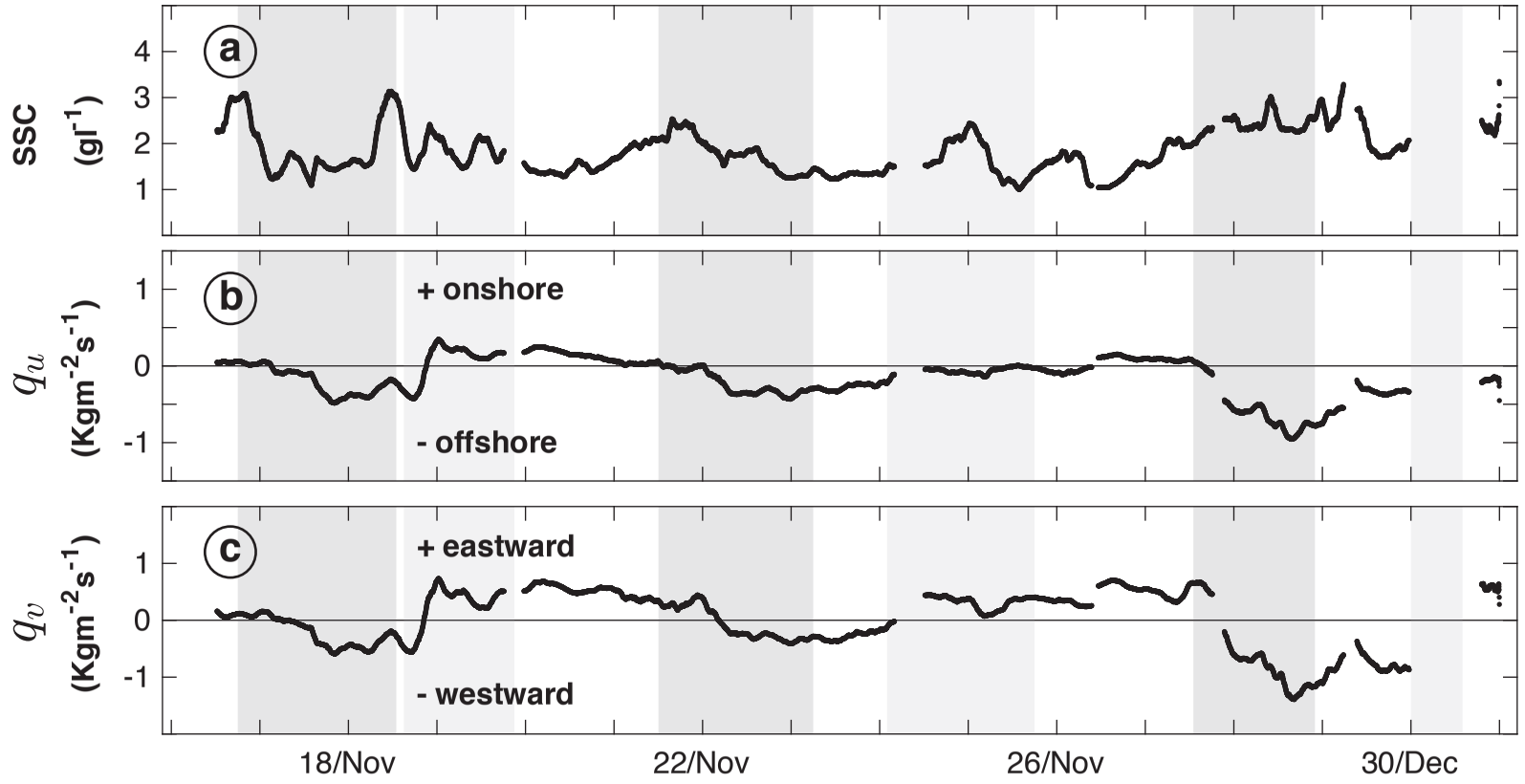

Figure 4.11. Measured time series of: (a) suspended sediment concentration (b) cross-shore suspended sediment flux, (c) long-shore suspended sediment flux. The light gray shaded areas represent cold front events, while dark gray shaded area indicate Gulf breeze events.

4.5 Discussion

The recorded oceanographic conditions were coupled with recorded sediment dynamics using in-situ data over a 14 day period. Oceanographic forcing (i.e. waves, currents, and turbulence parameters) within this study were similar to what has been reported with previous studies. Current characteristics during the shift between the onshore wind periods and the passage of offshore cold fronts were also in agreement with Nowlin et al. (2005) and W. Wang et al. (1998) observations.

4.5.1 Nearshore currents in response to Gulf breeze and cold front events

Overall, temporal observations of current velocities over the Gulf breeze events displayed a gradual and steady increase in velocity, and once wind was rotated it resulted in a more dramatic shift and increase in current velocity. However, the difference between the cold front events and the Gulf breeze events current intensity was mainly due to the sustainability in wind speed and direction. During the Gulf breeze events, winds were more sustained resulting in higher wave energy levels. On the other hand, the spatial variation in cross-shore current velocity is likely due to wave breaking before G4 and G2, resulting in higher offshore currents.

The Gulf breeze events produced similar characteristics to cross-shore currents seen in previous studies focused on the role of intense onshore winds (i.e. sea breeze cycle) on the surf zone hydrodynamics. For example, observations by Masselink and Pattiaratchi (1998) and Pattiaratchi et al. (1997), suggest that during periods of high onshore winds, the resultant cross-shore current was mainly offshore directed. In contrast, unlike the findings of Pepper and Stone (2004), the prevailing currents during the cold front events compared with the Gulf breeze events within this study were to be weaker. This is due to the difference of the cold front wind intensities the two studies experienced, as with Pepper and Stone (2004) study, the recorded wind speed exceeded 10 ms^{-1}, whereas within this

study, the maximum recorded wind speed was approximately 8 ms^{-1}. Meanwhile, the recorded longshore and cross-shore currents were in agreement with Kineke et al. (2006) observations with weaker onshore current and induced eastward current.

4.5.2 Nearshore turbulence in response to Gulf breeze and cold front events

The estimated ε within this study ranged between 10^{-5} m^2s^{-3} and 10^{-3} m^2s^{-3}, where the temporal fluctuations in ε were similar to fluctuations in wave climate and wind shear stress. The range of ε recorded within this study was also similar to previous surf zone studies (e.g. Ruessink, 2010; Feddersen et al., 2007; Trowbridge & Elgar, 2001; George et al., 1994). During the Gulf breeze events the recorded wave heights increased as the wind stress increased, therefore inducing ε values. In contrast, before the cold front's passage, the wind speed experienced abrupt decrease followed by a rapid increase in wind speed and a reverse in wind direction. Therefore, wave climate decreased at the beginning of the cold front events, and as the waves energy increased the ε values increased. Additionally, it is suggested that northwesterly–north fronts are more energetic than north-northeasterly fronts. The spatial variation in ε values is due to the difference in depth between the stations. In other words, within deeper waters ε values decays with depth, as the waves energy is disspated within the upper water column. Alternatively, within shallower regions such as the surf zone the waves breaking induces ε values, as observed from G1, and G2 stations compared to G3 and G4 stations. Similar observations have been recorded by Feddersen (2012), where stations located in shallower regions experienced higher ε than the stations located in deeper regions (3×10^{-3} m^2s^{-3}, at 1 m depth). Additionally, it is suggested that during the low tide period, the surf zone can experience increased values of ε.

Moreover, within this study the surf zone TKE values ranged from 10^{-4} m^2s^{-3} to 10^{-3} m^2s^{-3} and were lower than reported TKE values by Brinkkemper et al. (2017). The

dissimilarity between TKE values is likely due to the difference in beach slope between the two study sites, as both this study and Brinkkemper et al. (2017) experienced similar oceanographic forcing. However, TKE during the cold front events were similar to recorded turbulence measurements made by Feddersen and Williams (2007). Similar to ε findings, TKE values were found to be higher in shallower regions, where TKE values were found to be higher on the upper water column within the surf zone.Within the surf zone TKE values can reach up to 10^{-2} m^2s^{-2} (Huang et al., 2009). Therefore, TKE is enhanced with increasing wave height, but it is more affected with the relative depth of measurements. For example G3 stations encountered higher waves than G1 station, but still G1 station experienced higher turbulence.

Unlike the previous turbulent quantities (i.e. TKE, and ε), the temporal difference in τ was found to be relatively the same across all stations. The effect of cold front events on τ was minimal, where a 60% increase in τ values was experienced during the Gulf breeze events. This can be explained by comparing the wind direction and the coast orientation. During the cold front events, the surf zone is relatively sheltered by the island, resulting in less developed waves, and as a result τ was weaker. Modeled surf zone τ results from Tomás et al. (2012) suggest that during intense onshore wind τ, can range from 2 Nm^2 to 50 Nm^2, while Dufois et al. (2008) recorded a maximum of 10 Nm^2, and is in agreement with this study's τ observations.

4.5.3 Beach morphology and variation in suspended sediment flux

Post beach profile of CE#1, suggests that cold front results in erosion within areas that are characterized by a large fluctuation in bed elevation with lower depth (i.e. beach berm and sandbars). This is likely due to the increase in ε and τ over the sandbars and the beach berm, as previously suggested that turbulent quantities increase with decreasing depth. Additionally, the induced longshore currents from the local generated waves in

addition to the increase in cross-shore currents with the enhanced suspended sediment flux, may contribute to the erosion. Meanwhile, deposition of 0.14 m and 0.16 m of sediment occurred between sandbars and on the beach face (1–8 m), respectively. However, due to the lack of more profile observations, it is difficult to conclude that all offshore cold fronts will provide similar observations. Nevertheless, the post-CE#1 beach profile is in agreement with what was previously seen in Dingler and Reiss (1990). Dingler and Reiss (1990) observed a deposition of sediment onshore and between the sandbars, while erosion took place on the foreshore region. Additionally, Dingler and Reiss (1990) study experienced an onshore sandbar migration, whereas within this study there were no records indicating sandbar migration occurring during the cold front passage. The changes seen in the beach morphology is likely due to bed-load transport, which was not measured during the field experiment. However, according to Keen et al. (2003) during intense wind events the suspended sediment transport rate can be greater than the bed-load transport rate, which might be the case in this study.

The SSC levels within the surf zone demonstrated almost continuous suspensions, and whilst the SSC level never exceeded a 3 fold increase, still the suspended sediment flux was high during the field experiment. The peaks in SSC levels were correlated with observed peaks in energy levels from Figure 4.9. The phase shift in the tidal cycle is also believed to attribute to the observed peaks in SSC levels, but they were more effective during high tides associated with spring tidal cycle. Overall, the cross-shore suspended sediment flux ranged between -1.2 $kgm^{-2}s^{-1}$ and 0.78 $kgm^{-2}s^{-1}$, while the longshore suspended sediment flux ranged between -1.5 $kgm^{-2}s^{-1}$ to 0.8 $kgm^{-2}s^{-1}$. Generally, the recorded cross-shore suspended sediment flux during the Gulf breeze events demonstrated a similar behavior to those experienced during a sea breeze cycle, specifically during GE#3. For example, Masselink and Pattiaratchi (1998) observed an increase of 0.9 $kgm^{-2}s^{-1}$ during the onset of the sea breeze cycle. However, the longshore suspended sediment flux recorded within

this study was found to be lower than observations made by Masselink and Pattiaratchi (1998), as their study experienced significantly higher SSC levels (up to 21 gl^{-1}).

Unfortunately, there were no studies found within the literature that recorded suspended sediment fluxes within the surf zone during the passage of offshore-directed cold front to compare this study's findings to. However, comparing the resultant fluxes between the different events, it is suggested that Gulf breeze events induces both cross-shore and longshore suspended sediment flux. Meanwhile, cold front events demonstrated lower cross-shore suspended sediment flux compared to those observed during the Gulf breeze events. The difference was mainly due to the wave conditions experienced during both the cold fronts and the Gulf breeze events. Unlike energy conditions observed during the cold fronts, the Gulf breeze events had a higher τ that might resulted in more suspended sediment along with the increase in TKE and ε aid in sustaining the suspension for a longer period. As a result, the cross-shore and longshore suspended sediment flux values were higher during the Gulf breeze events by approximately 250% and 98%, respectively, compared to cold fronts values. Surely, these spatial observations are limited to one location and might not reflect the actual suspended sediment flux for the entire surf zone, but are sufficient to provide a comparison of changing magnitudes during both wind events.

A comparison of the total suspended sediment transport of all Gulf breeze and cold front events is presented in Figure 4.12. Figure 4.12 demonstrates a significant cross-shore transport of sediment during the Gulf breeze periods, when compared to cold front cross-shore loss results, with almost 5900% difference (Figure 4.12a). This suggests that the resulting total suspended sediment cross-shore transport during the early fall and early winter within the upper Texas coast is mainly affected by the Gulf breeze winds. Nonetheless, the magnitude of the longshore sediment transport during the Gulf breeze event was 70% higher than observations made during the cold front events, whereas the direction was eastward during the cold front events and westward during the Gulf breeze events

(Figure 4.12b). However, data of SSC during CE#3 were filtered out leading to significant data gap, and certainly has affected the outcome for the statistical analysis of computed suspended sediment transport. Nevertheless, according to the observations made for both currents and SSC levels, Gulf breeze events will still be significantly higher in terms of total cross-shore suspended transport.

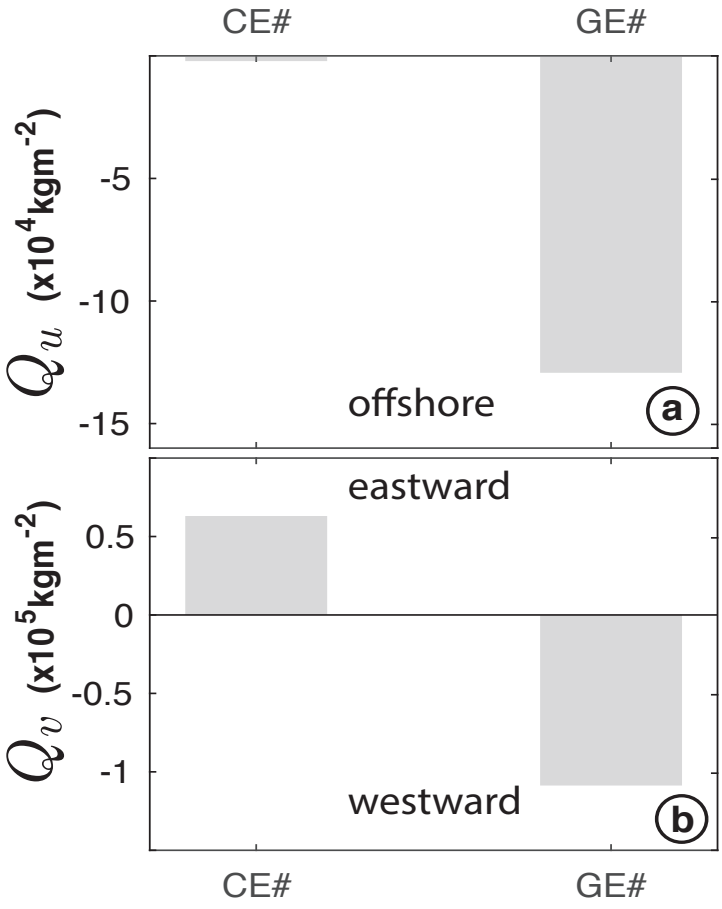

Figure 4.12. Total longshore and cross-shore suspended sediment transport computed using Eq.4.12 and Eq.4.13, respectively. The vertical axis represents total suspended sediment transport (kgm^{-2}, gray shaded columns), while the horizontal axis display compares CE#1–3 events combined to GE#1–3 combined. Values have been estimated from measurements at G2 station and are shown separately for cross-shore (panel a) and longshore (panel b) components.

Unfortunately, this field experiment is short lived and does not have an annual record to demonstrate the impact of cold front events on the nearshore suspended sediment flux compared to the onshore wind periods. However, assuming that on average 30 cold fronts passes the upper Texas coast yearly, that have the same characteristics as CE#1 (i.e. has the same wind and duration), and the entire surf zone experienced the same mean SSC levels and currents recorded at G2. Using these assumptions provided here, approximately 39,900 m^3 will be transported onshore, and 61,000 m^3 eastward, over a year period. Therefore, despite the weak cross-shore suspended sediment flux, overall cold fronts are capable of mobilizing large amount of suspended sediment within the surf zone.

4.6 Conclusions

Surf zone hydrodynamics and sediment dynamic processes within the upper Texas coast have been evaluated during three offshore cold front events and three onshore Gulf breeze events. The summarized findings regarding the resultant hydrodynamics and sediment dynamics for each type of wind forcing conditions are presented in the following:

[1] Hydrodynamics: The passage of cold fronts resulted in approximately 35% weaker cross-shore currents than the currents prevailing during the Gulf breeze events. Additionally, waves were less energetic during the cold fronts resulting in onshore flow, whereas higher broken waves during the Gulf breeze events resulted in offshore-directed currents (i.e. undertow currents). However, the longshore currents were approximately 18% higher during the Gulf breeze events compared to longshore currents recorded during the cold fronts. Additionally, the Gulf breeze events resulted in a westward flow, meanwhile waves arriving SE-S resulted in eastward flow during the cold fronts. Estimated turbulence quantities (i.e. TKE and ε) illustrated higher values within stations located in shallower depths and were overall 1.5 magnitude higher during the Gulf breeze events compared to cold fronts. Additionally,

estimated turbulence quantities can increase substantially during the spring tidal cycle (i.e. GE#3). Nevertheless, high turbulence quantities during the passage of cold fronts can occur, when wind shear stress exceeds 0.12 Nm^{-2}. In comparison, τ levels were approximately 60% higher during the Gulf breeze events due to the substantial increase in significant wave heights.

[2] Sediment dynamics: The most morphological response of the cross-shore beach profile during the passage of the cold front was the erosion of sandbars, while deposition of sediment took place on the foreshore and the trough region. Due to the elevated wave height during the Gulf breeze periods, energy levels increase within the surf zone leading to approximately 15% higher SSC levels than cold fronts. Additionally, the high turbulence experienced during the Gulf breeze events helped in maintaining high SSC levels for a longer period, as observed from GE#3. This was reflected on the cross-shore suspended sediment flux as it was more enhanced during the Gulf breeze events, leading to flushing the suspended sediment seaward out of the surf zone. However, the cold fronts impact within this study was considered to be positive in terms of suspended sediment transport, where the mean suspended sediment flux was onshore-directed.

Due to the enhanced eastward suspended sediment flux observed following the passage of cold fronts, it is highly likely that during late fall season and early spring season erosion of sediment will occur east of Galveston Island, while accretion of sediment on the west side of the Galveston Island. Clearly, the nearshore region long-term morphological and sediment dynamic response as a result of cold fronts and Gulf breeze events is crucial. Therefore, hydrodynamics, sediment dynamics, and additional spatial measurements is recommended to provide a better understanding of the long-term climatological evaluation of these wind forcing conditions and their impact on the nearshore region.

5. COMPARING SECTIONS 2, 3, AND 4 FINDINGS

The present work has demonstrated the impact of different wind forcing conditions and their complex coupling effects between wind-driven waves, currents, and the resulting sediment transport and morphodynamic processes. This Section is going to discuss the differences each wind system has on the nearshore region hydrodynamics, sediment dynamics, and the primary findings of Sections 2–4. However, due to the differences in the number of spatial sampling between Section 2, and Sections 3–4, the locations were limited to the surf zone and the inner-shelf region.

5.1 Hydrodynamic forcing in response to different wind systems

5.1.1 Waves and currents comparison

Overall, the prevailing significant wave height within the inner-surf and surf zone during the passage of Norte was approximately 40% higher than CE#1-3. As the cold front passes the northern GoM, it has more distance to cover until it reaches the Yucatán peninsula, where wind has less disturbance. Therefore, onshore-directed cold front winds has the ability to develop larger waves than offshore-directed cold fronts. On the other hand, during the Gulf breeze events the mean significant wave height recorded between the sandbars were 50% higher than those recorded during the sea breeze cycles. However, during the beginning of the Gulf breeze events, the difference between G2 and W4 were slightly different with 10% higher at G2. Later, during the end of the Gulf breeze event a 70% growth in wave height was observed. This increase is due to the difference in the wind event duration, as the sea breeze events had a mean duration of 9 hours, while the Gulf breeze events had a mean duration of 39 hours. Thus, during the Gulf breeze events high wind shear stress is sustained for longer periods, which leads to gradually increasing the wave height. Moreover, comparing the onshore and offshore-directed cold front tidal

observations, it is suggested that onshore-directed cold front results in increasing the water level, whereas the offshore-directed cold fronts result in suppressing the water level. Meanwhile, comparing Gulf breeze events and sea breeze cycles water level observations, it is suggested that both of these wind forcing results in increasing the water level.

The nearshore currents were found to be more enhanced during the passage of onshore-directed cold fronts, as the Norte event resulted in a mean cross-shore current of 0.2 ms^{-1}, while offshore-directed cold fronts had a mean of 0.13 ms^{-1}. The most noticeable difference in the cross-shore current was the direction of the flow, as the onshore-directed cold fronts resulted in offshore-directed flow, while onshore-directed currents were observed during the offshore-directed cold fronts. This is due to the difference in the nearshore energy levels, with higher waves breaking during the Norte, leading to undertow currents. On the other hand, the longshore currents magnitude during both the onshore and offshore-directed cold fronts were relatively the same, with approximately 15% higher during the Norte event. Similarly, the spatial current intensities in both studies were similar. For example, it was found that currents were induced in regions that are located before and after the sandbars. The maximum cross-shore currents recorded during the Gulf breeze events were 0.05 ms^{-1} higher than the maximum recorded cross-shore currents recorded during the sea breeze cycles. Furthermore, during both the Gulf breeze events and the sea breeze cycles, the currents were observed to be offshore-directed across the surf zone region.

Section 3 suggests that the inner-shelf circulation within the upper Texas coast during the passage of offshore-directed cold fronts was mainly driven by the LATEX shelf current and wind. This is similar to Torres-Freyermuth et al. (2017) observations, as during the onshore-directed cold front periods (i.e. Norte) the inner-shelf current of the Yucatán peninsula was mainly controlled by the Yucatán current and the wind. Meanwhile, based on the observations made in Section 3 and Torres-Freyermuth et al. (2017), during the period of onshore-directed cold fronts, the surf zone current circulation was mainly con-

trolled by the wind and wave breaking. However, during the period of offshore-directed cold fronts, the surf zone current circulation was mainly controlled by tides and waves breaking. Alternatively, unlike Torres-Freyermuth et al. (2017) observations in regards to current circulation during the sea breeze cycle, the Gulf breeze events showed a similar result to onshore-directed fronts. Therefore, waves and tides were the main driving mechanisms controlling the surf zone current circulation.

5.1.2 Turbulent quantities comparison

Turbulent quantities presented in Section 2 and 4 were within the range of previous study observations. However, during the offshore-directed cold fronts the mean recorded ε was 1.3×10^{-4} m^{2}s^{-3}, while during the onshore-directed cold front it was approximately 3×10^{-3} m^{2}s^{-3}. This increase in ε values during the onshore-directed cold front was due to the increase in the oceanographic forcing (i.e. wave heights and current intensity). On the other hand, the observed ε values during the Gulf breeze events were 4×10^{-3} m^{2}s^{-3} higher than values experienced during the sea breeze cycles.

TKE values during the offshore-directed cold fronts were found to be 5×10^{-3} m^{2}s^{-3} lower than the recorded TKE during the onshore-directed cold front. Meanwhile, the Gulf breeze events TKE values were approximately 30% higher than sea breeze TKE values observed within the trough region, while 60% higher within the inner-surf region. Estimated τ values within the surf zone during the onshore-directed cold fronts exceeded 20 Nm^{-2}. In comparison, the offshore-directed cold fronts had approximately 81% lower τ values than the observed τ during onshore-directed cold fronts. During the GE#1-2 and sea breeze cycles, the observed τ values were almost the same ranging between 2 Nm^{-2} and 11 Nm^{-2}. However, during the GE#3 τ values were 59% higher than observations made during the sea breeze events. This is primarily due to the substantial increase in oceanographic forcing observed during GE#3.

5.2 Sediment and morphodynamic processes in response to different wind systems

5.2.1 Morphodynamics comparison

Comparing the cross-shore beach profile results in Section 2 and 4 suggests that onshore-directed cold fronts have a greater impact on the nearshore region sediment loss when compared to onshore-directed cold fronts. During the period of offshore-directed cold front (CE#1), the beach profile experienced 0.24 m erosion of the beach berm and a mean of 0.15 m over the sandbars. Meanwhile, during the period of onshore-directed cold front the beach profile experienced similar erosion over the inner-sandbar (0.15 m) and higher erosion over the outer-sandbar (0.4 m). However, the offshore-directed cold fronts resulted in a total loss of the beach berm and erosion of sandbars, whereas the onshore-directed cold fronts resulted in significant erosion and was associated with offshore migration of the beach step and the outer sandbar.

Additionally, the results suggest that offshore-directed cold fronts leads to accumulation of sediment within the trough region and the transport is mainly landward. In contrast, onshore-directed cold fronts results in erosion of sediment across the whole beach profile including the trough region (up to 0.4 m) and deposition of sediment on the foreshore and the main transport direction was seaward. This high erosion during the onshore-directed cold front was due to the induced return flow (i.e. undertow currents), proven to be effective in eroding sediment (Thornton et al., 1996; Roelvink & Stive, 1989).

5.2.2 Suspended sediment fluxes comparison

In order to compare longshore and cross-shore suspended sediment flux between the studies, results from M4 during the 3rd sea breeze cycle and Norte event were selected from the Sisal experiment. Meanwhile, GE#3 and CE#1 events were selected from Galveston experiment. These events were selected based on their wind intensity and high wave energy conditions compared to their counterpart events.

The mean cross-shore suspended sediment flux during the offshore-directed cold front was 150% higher than the recorded mean cross-shore suspended sediment flux during the onshore-directed cold front (Figure 5.1a). Additionally, the mean longshore suspended sediment flux during the offshore-directed cold front was 130% higher than the recorded mean longshore suspended sediment flux during the onshore-directed cold front (Figure 5.1b). On the other hand, the mean cross-shore flux during GE#3 was approximately 0.4 $kgm^{-2}s^{-1}$ higher than sea breeze event mean cross-shore flux. However, the mean longshore suspended sediment flux during GE#3 was approximately 20% higher than mean value recorded during the 3rd sea breeze cycle.

The most significant differences between the onshore and offshore-directed cold fronts was the magnitude of sediment gain/loss during the events. The total cross-shore suspended transport results from Figure 5.1a suggest that onshore-directed cold front was approximately 500% higher in magnitude than the offshore-directed cold front. Additionally, the main total suspended transport was seaward during the onshore-directed cold front, while landward transport during the offshore-directed cold front. Similar observations can be seen from the total longshore suspended sediment transport, as the onshore-directed cold front shows 270% higher magnitude than the onshore-directed cold front (Figure 5.1b). Additionally, the difference between the 3rd sea breeze cycle and the Gulf breeze events was high, as GE#3 was 400% and 380% higher than the 3rd sea breeze cycle total cross-shore and longshore suspended transport, respectively. Comparing all events in terms of total suspended transport magnitude, the CE#1 and the 3rd sea breeze cycle were most similar, while the Norte event was similar to the Gulf breeze event.

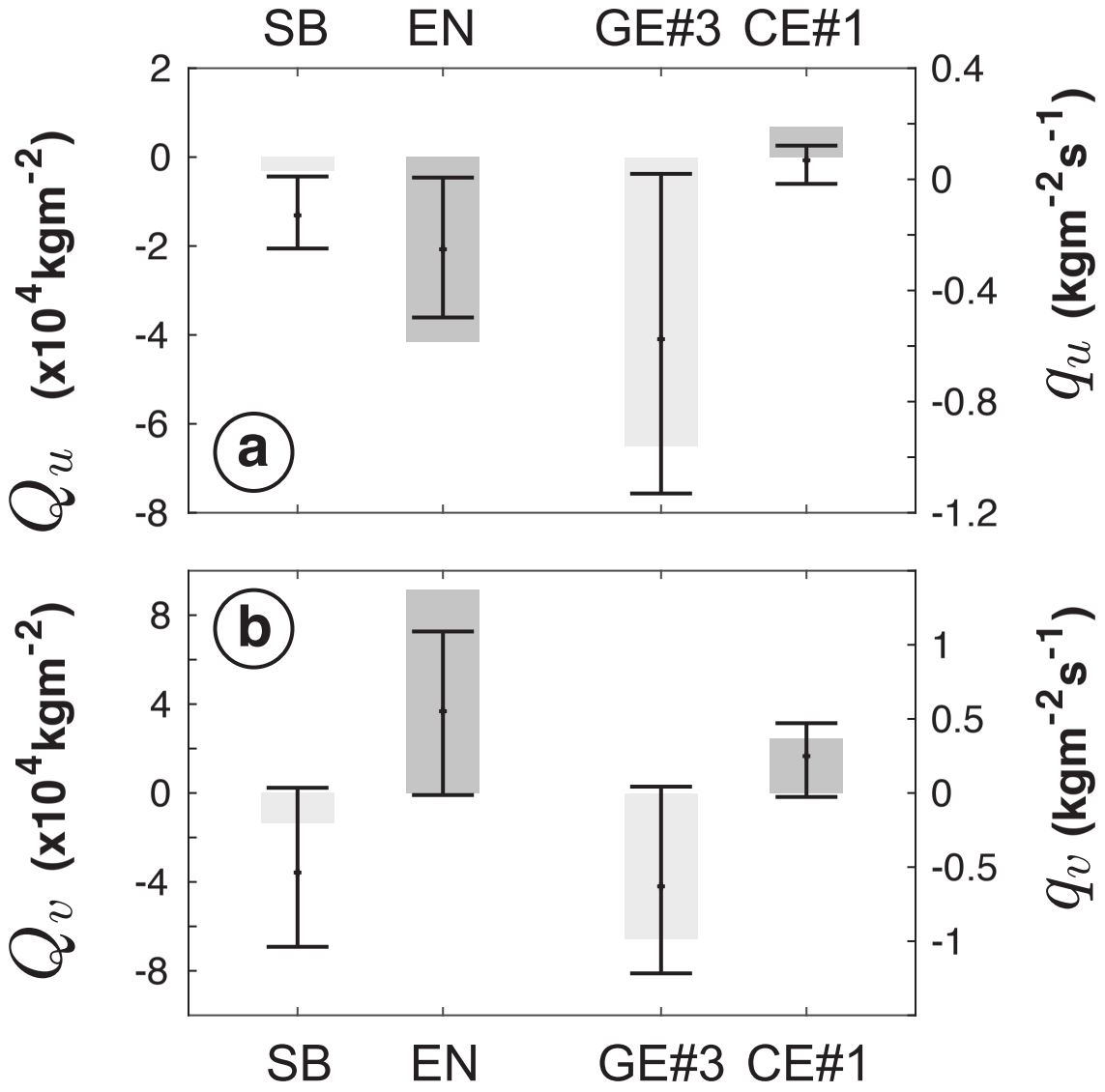

Figure 5.1. Overall sediment transport observations. The left vertical axis represents total suspended sediment transport (kgm^{-2}, gray shaded columns), while the right vertical axis display suspended sediment flux mean values with upper and lower 95% confidence intervals (kgm^{-2}s^{-1}, whisker plots) comparing the 3rd sea breeze cycle (SB), Norte (EN), Gulf breeze (GE#3), and onshore-directed cold front (CE#1). Panel (a) represent cross-shore and panel (b) alongshore components.

5.3 Conceptual models: surf zone currents and morphology in response to different wind systems

The major study findings in terms of the current response during the sea breeze cycles, Gulf breeze events, onshore and offshore-directed cold fronts are presented in Figure 5.2a-b. The figure shows a similar spatial cross-shore current intensity between the onshore and offshore-directed cold fronts. Meanwhile, during the onshore-directed cold fronts strong longshore currents were found on the sandbars (Figure 5.2a), while during the offshore-directed cold fronts they were weaker compared to stations located closer to the shore (Figure 5.2b).

Additionally, a comparison of both onshore and offshore-directed cold fronts impact on the surf zone morphology is displayed in Figure 5.3. The comparison suggests that onshore-directed cold fronts are characterized by intense energy conditions, resulting in a higher erosion rates and offshore sandbar migration. Meanwhile, the offshore-directed cold fronts are characterized by a milder energy conditions resulting in less erosion, and can result in accumulating sediment landward and in trough regions.

Nevertheless, these results do not reflect the total impact of cold fronts on the beach morphology, as different coasts will have different results, as the environmental conditions differ from one location to another. Additionally, the results provided only represent a short lived field based observations, which may not reflect the annual changes in these wind forcing conditions, and small data gaps has also effected the statistical analysis of this study. However, the results herein shed light on the response of a sandy microtidal beach to different wind systems, and the resultant hydrodynamic and sediment transport parameters.

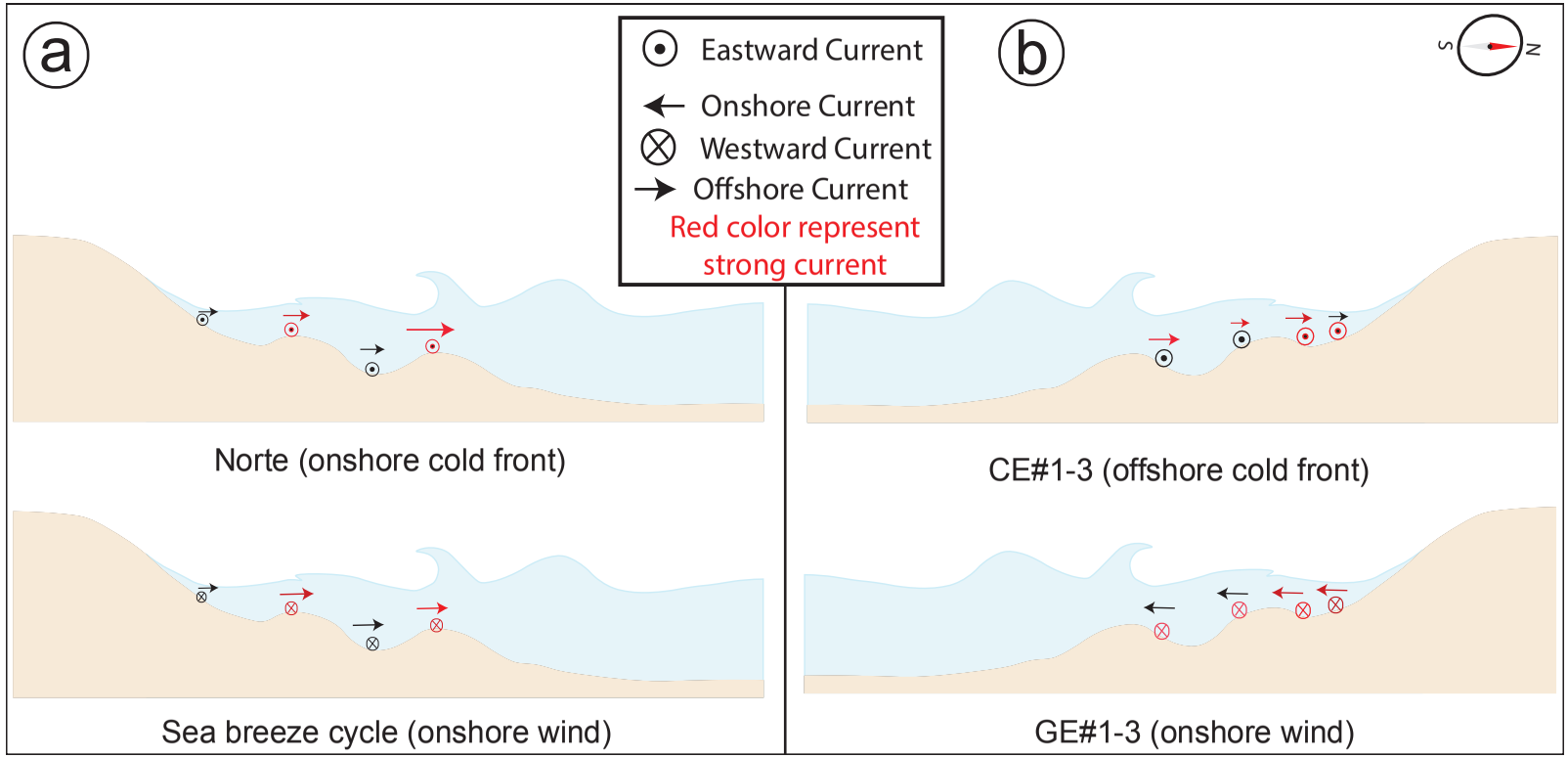

Figure 5.2. Concept model of current circulation from the field studies (a) cross-shore and longshore current during the Sisal field experiment, the upper sketch represent Norte currents, while the lower sketch represent the sea breeze currents, (b) cross-shore and longshore current during the Galveston field experiment, the upper sketch represent CE#1-3 currents, while the lower sketch represent GE#1-3 currents.

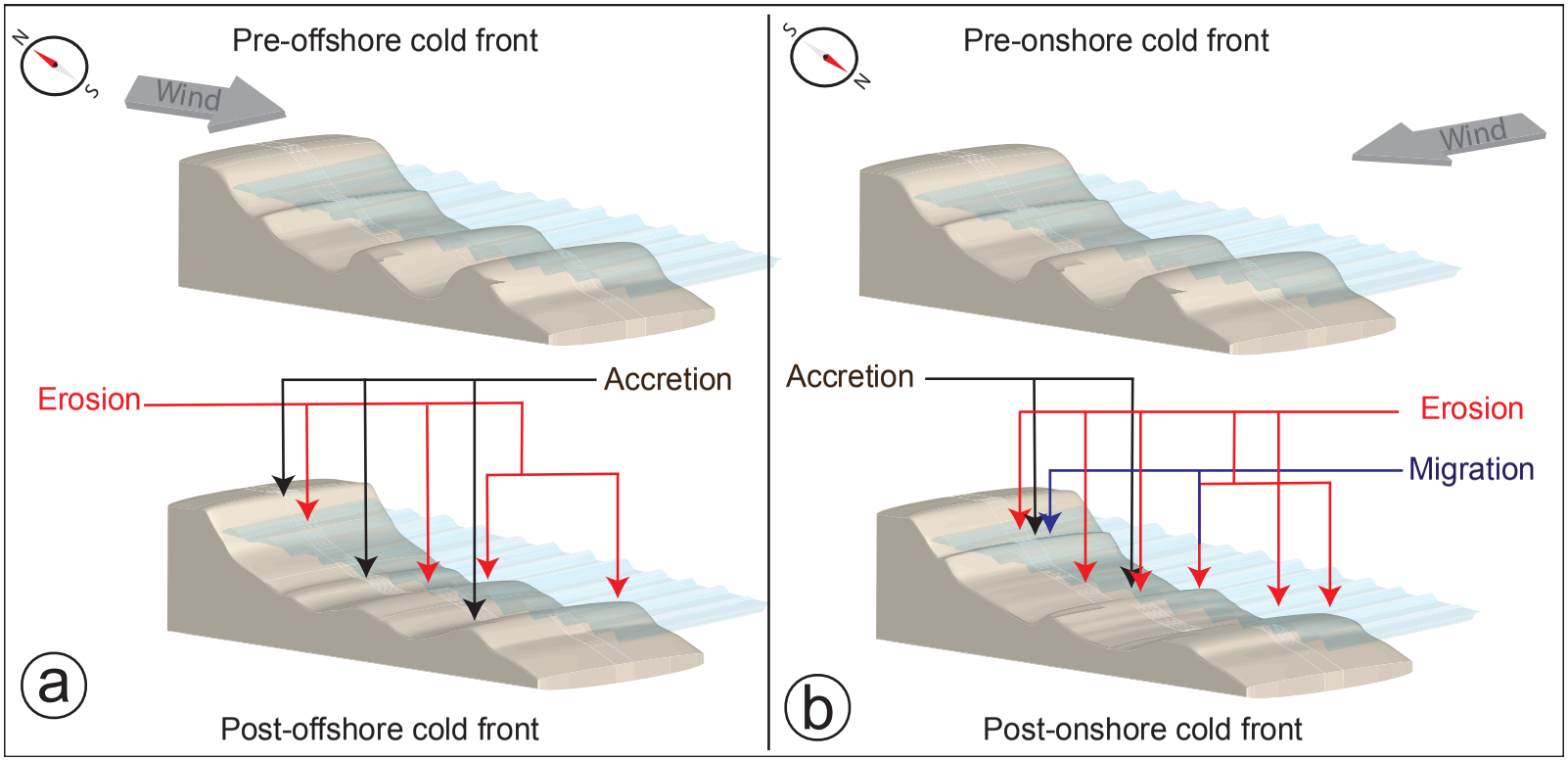

Figure 5.3. Concept model of beach morphology response to (a) offshore-directed cold fronts, the upper sketch represent the beach profile before the event, while the lower sketch represent the beach profile after the event (b) onshore-directed cold fronts, the upper sketch represent the beach profile before the event, while the lower sketch represent the beach profile after the event.

5.4 Study limitations and recommendations

The long-term understanding of the climatological evaluation of wind forcing, such as the onshore and offshore-directed cold fronts, the diurnal land and sea breeze cycles, and seasonal sustained onshore winds (i.e. Gulf breeze events) is crucial to better understand the complex nearshore region dynamics. Therefore, a short lived field experiment will not provide a full insight of the total impact of these winds on the nearshore region dynamics. However, this should shed light and provide a glance of nearshore dynamics response under short lived mild wind conditions. This problem can be solved by having a well organized long-term field experiment with a duration more than 2 years. The field experiment should also include a calibration between several organizations to help with maintaining the field experiment and provide more instrumentation to the site.

Nevertheless, in oceanography and coastal engineering studies the definition of cold fronts is blurred. For example, several studies have provided their own definition of cold fronts, that is based on some criteria such as temperature, wind, pressure. However, within this study cold fronts were defined using meteorological charts provided by NOAA national weather services, temperature, wind speed and direction, and pressure. Finally, the author's recommendations for future studies regarding investigating the nearshore region dynamics under different wind forcing events are as follows:

[1] Location: It is recommended to have two field experiment sites, one located at Galveston Island, Texas, and another at Sisal, Yucatán, México. These locations were chosen for several reasons, first, cold fronts usually enters GoM between Galveston Island and Corpus Christi (Henry, 1979), and can propagate all they way to Sisal (Torres-Freyermuth et al., 2017). This will allow a comparison of the following nearshore dynamics resulting from the passage of the cold fronts between the two sites. Second, this will help provide a long-term evaluation on the cumulative

effect of sea breeze cycles compared to cold fronts in terms of sediment transport, and also understand how fast the beach recovery phase during the land breeze cycles. Finally, this can contribute to our understanding of the seasonal variation in Gulf breeze events and also provide a better estimate of sediment transport within the upper Texas coast.

[2] Duration/time: Cold fronts orientation in reference to coast, such as CP fronts, varies seasonally, therefore to capture both fronts the field experiment has to cover both summer and winter season. In Section 2, sea and land breeze cycles were investigated during late spring. However, studies have suggested that sea breeze cycles are more intense during the summer season, due to the increase in temperature difference between the land and oceans (Federico et al., 2010; Masselink & Pattiaratchi, 1998; Hsu, 1988). Therefore, in order to investigate the full impact of the sea breeze cycle on the nearhsore dynamics, it is recommended have a summer field based experiment. Similarly, it would be interesting to compare the summer local wind cycle at Galveston Island compared to the Gulf breeze events discussed in Sections 3 and 4. Atmophseric parameters such as wind are significantly effected by El Niño-Southern Oscillation (ENSO) cycle. The changes that occurs between El Niño and La Niña will defiantly impact the frequency and intensity of cold fronts. Therefore, it is recommended to have at least one field experiment covering both of ENSO cycles, in order to understand how each phase will effect the wind-driven nearshore dynamics within the surf zone and the inner-shelf region.

[3] Measurement: This study has compared the suspended load during both onshore and offshore-directed cold fronts, but unfortunately there was no bed-load measurements. Therefore, it is recommended to have bed-load measurements during both wind events and compare it to the suspended load. Having multiple cross-shore pro-

files is time consuming and requires manpower, therefore it is recommended to limit the beach profile surveys for pre and post-events. Additionally, in Section 4 ADCPs were used in the surf zone using HR mode, but unfortunately could not drive SSC acoustically. Thus, it is recommended to at least have one ADCP within the surf zone to investigate the turbulence profile, the SSC profiles, their correlation within the water column. Atmospheric observations is going to be a key element in describing these wind forcing events. Therefore, it is recommended to have more spatial wind measurements and a higher sampling rate. This will allow to distinguish between MP and CP fronts. Once they are distinguish, the impact of each front type on nearshore region dynamics can be quantified separately and compare them to each other.

6. CONCLUSIONS

The presented work has described the influence of different wind forcing mechanisms including sea and land breeze cycles, onshore and offshore-directed cold fronts, and Gulf breeze winds on the nearshore hydrodynamics and morphodynmics. This was done to advance our understanding of the complex coupling effects between wind-driven waves, currents, and turbulence quantities, and the resulting flow circulation, sediment transport, and morphodynamic processes. This was achieved by conducting two field based studies using an array of sensors measuring water level, fluid velocity, and suspended sediment concentration distributed in a transect perpendicular to the coast, and covered the region from the inner-surf zone to the inner-shelf.

The first study (Section 2) investigated the effect of both mesoscale and synoptic scale meteorological wind systems on the surf zone currents, turbulent quantities, suspended sediment flux, and morphodynamic processes in the southern part of GoM. The second study (Section 3) was conducted on the upper Texas coast with a primary focus on understanding the governing forces that controls the nearshore circulation within the surf zone and the inner-shelf region, during the periods of offshore-directed cold fronts and onshore Gulf breeze winds. Finally, the third study (Section 4) investigated the impact of winter offshore-directed cold fronts compared to the Gulf breeze winds on suspended sediment concentration, current, suspended sediment flux, and beach morphology. The main findings and brief summary of Section 2–4 are presented in the following:

I. In-situ measurements from Section 2 suggests that intense currents and increase turbulence quantities occurred during the period of Norte and sea breeze cycles, leading to almost continuous sediment suspension and major erosion across the surf zone. Due to diminished wind prevailing during land breeze cycles, wave energy levels

were low and the combination of both weak currents and low SSC yield almost no sediment flux, allowing deposition of sediment. Nevertheless, when land breeze winds were sustained for longer periods than sea breeze, turbulence quantities were increased along with mild onshore currents, leading to significant sediment accretion across the surf zone. Overall, the estimated turbulence quantities, estimated wave heights, and suspended sediment fluxes were found to be substantially higher during the Norte event. However, the sea breeze cycle is a stable diurnal wind system, and the resultant cumulative impact of the sea breeze cycles will have a more significant influence on the nearshore sediment transport over time than the onshore-directed cold fronts.

II. Results from Section 3 shows that nearshore currents were intensified during both the passage of offshore-directed cold fronts and during the Gulf breeze events. During the periods of offshore-directed cold fronts, flow was mainly eastward directed within both the surf zone and the inner-shelf region. Additionally, the correlation between the selected forcing conditions (i.e. wind, wave, tide, and LATEX-shelf current) and current variability indicates that the surf zone currents were mainly controlled by tide and wave breaking, while wind and LATEX current controlled the inner-shelf current circulation. Meanwhile, during the Gulf breeze events, flow was mainly westward within the surf zone and varied between eastward and westward within the inner-shelf, except when wind shear stress exceeds 0.13 Nm^{-2} westward flow was sustained. The study suggests that during the Gulf breeze events the inner-shelf was controlled by wind and LATEX current, while tides and waves were suggested to be the main influence on the surf zone current circulation.

III. Section 4 observation indicates that during the passage offshore-directed cold front currents, suspended sediment flux, and turbulent quantities were mild. The cross-

shore suspended sediment flux was mainly onshore directed, while the longshore suspended sediment flux was mainly eastward. On the contrary, the Gulf breeze events increased currents and turbulent quantities leading to higher suspended sediment concentrations than values recorded during the cold front events. Therefore, the combination of both increased currents and suspended sediment enhanced both the cross-shore and the longshore suspended sediment flux. Additionally, the examined beach profile post cold front events suggest that offshore-directed cold fronts results in sandbar and beach berm erosion, while depositing sediment landwards on the foreshore and trough regions.

To this end, the different wind system discussed within this study displayed significant impact on the surf zone and the inner-shelf region by strengthening/weakening of either current circulation or sediment transport parameters. Nevertheless, our understanding on the complex nearshore sediment dynamics is not fully understood. However, it is anticipated that the outcomes from the present work will enhance our understanding on the impact of sea and land breeze cycles, onshore and offshore-directed cold fronts, and the Gulf breeze wind events have on nearshore hydrodynamics and sediment transport processes.

REFERENCES

Aagaard, T., & Greenwood, B. (1994). Suspended sediment transport and the role of infragravity waves in a barred surf zone. *Marine Geology*, *118*(1–2), 23–48. doi: https://10.1016/0025-3227(94)90111-2

Aagaard, T., Greenwood, B., & Nielsen, J. (1997). Mean currents and sediment transport in a rip channel. *Marine Geology*, *140*(1-2), 25–45. doi: https://doi.org/10.1016/S0025-3227(97)00025-X

Aagaard, T., & Hughes, M. G. (2010). Breaker turbulence and sediment suspension in the surf zone. *Marine Geology*, *271*(3-4), 250–259. doi: https://doi.org/10.1016/j.margeo.2010.02.019

Abbs, D., & Physick, W. L. (1992). Sea-breeze observations and modeling. *Australian Meteorological Magazine*, *41*, 7–19.

Al Senafi, F. (2015). Model aided observational study of physical processes in the northwestern Arabian/Persian Gulf in response to the Shamal wind event. *Texas A&M University*. doi: http://hdl.handle.net/1969.1/155338

Anderson, J. B. (2007). *The formation and future of the upper texas coast: A geologist answers questions about sand, storms, and living by the sea* (Vol. 11). College Station: Texas A&M University Press.

Appendini, C. M., Hernández-Lasheras, J., Meza-Padilla, R., & Kurczyn, J. A. (2018). Effect of climate change on wind waves generated by anticyclonic cold front intrusions in the Gulf of Mexico. *Climate Dynamics*, 1–17. doi: https://doi.org/10.1007/s00382-018-4108-4

Appendini, C. M., Salles, P., Mendoza, E. T., López, J., & Torres-Freyermuth, A. (2012). Longshore sediment transport on the northern coast of the Yucatan Peninsula. *Jour-*

nal of Coastal Research, *285*, 1404–1417. doi: https://10.2112/jcoastres-d-11-00162.1

Armbruster, C., Stone, G., & Xu, J. (1995). Episodic atmospheric forcing and bayside foreshore erosion: Santa Rosa Island, Florida. *Gulf Coast Association of Geological Societies Transactions*, *45*, 31–37.

Babaeyan-Koopaei, K., Ervine, D. A., Carling, P. A., & Cao, Z. (2002). Velocity and turbulence measurements for two overbank flow events in River Severn. *Journal of Hydraulic Engineering*, *128*(10), 891–900. doi: https://10.1061/(asce)0733-9429(2002)128:10(891)

Balsam, W. L., & Beeson, J. P. (2003). Sea-floor sediment distribution in the Gulf of Mexico. *Deep Sea Research Part I: Oceanographic Research Papers*, *50*(12), 1421–1444. doi: https://doi.org/10.1016/j.dsr.2003.06.001

Balseiro, C., Carracedo, P., Gómez, B., Leitao, P., Montero, P., Naranjo, L., … Pérez-Muñuzuri, V. (2003). Tracking the Prestige oil spill: An operational experience in simulation at MeteoGalicia. *Weather*, *58*(12), 452–458. doi: https://10.1002/wea.6080581204

Barber, N. (1963). *The directional resolving power of an array of wave detectors, Ocean Wave Spectra*. Prentice Hall Inc.

Bechle, A. J., & Wu, C. H. (2011). Virtual wave gauges based upon stereo imaging for measuring surface wave characteristics. *Coastal Engineering*, *58*(4), 305–316. doi: https://doi.org/10.1016/j.coastaleng.2010.11.003

Bever, A. J., McNinch, J. E., & Harris, C. K. (2011). Hydrodynamics and sediment-transport in the nearshore of Poverty Bay, New Zealand: Observations of nearshore sediment segregation and oceanic storms. *Continental Shelf Research*, *31*(6), 507–526. doi: https://doi.org/10.1016/j.csr.2010.12.007

Bianchi, T. S., DiMarco, S., Cowan, J., Hetland, R., Chapman, P., Day, J., & Al-

lison, M. (2010). The science of hypoxia in the northern Gulf of Mexico: A review. *Science of The Total Environment*, *408*(7), 1471–1484. doi: https://doi.org/10.1016/j.scitotenv.2009.11.047

Bird, E. C. F. (1985). *Coastline changes. A global review*. John Wiley and Sons Inc., New York, NY.

Biron, P. M., Robson, C., Lapointe, M. F., & Gaskin, S. J. (2004). Comparing different methods of bed shear stress estimates in simple and complex flow fields. *Earth Surface Processes and Landforms*, *29*(11), 1403–1415. doi: https://10.1002/esp.1111

Booth, J. G., Miller, R. L., McKee, B. A., & Leathers, R. A. (2000). Wind-induced bottom sediment resuspension in a microtidal coastal environment. *Continental Shelf Research*, *20*(7), 785–806. doi: https://10.1016/S0278-4343(00)00002-9

Brannstrom, C., Brown, H. L., Houser, C., Trimble, S., & Santos, A. (2015). "you can't see them from sitting here": Evaluating beach user understanding of a rip current warning sign. *Applied Geography*, *56*, 61–70. doi: https://doi.org/10.1016/j.apgeog.2014.10.011

Brannstrom, C., Trimble, S., Santos, A., Brown, H. L., & Houser, C. (2014). Perception of the rip current hazard on Galveston Island and north Padre Island, Texas, USA. *Natural Hazards*, *72*(2), 1123–1138. doi: https://doi.org/10.1007/s11069-014-1061-3

Brinkkemper, J., Christensen, D., Price, T., Naus, I., Hansen, A., van Bergeijk, V., ... Aagaard, T. (2017). Surf zone morphodynamics during low-moderate energetic condtions; The TASTI Field Experiment. In *Proceedings coastal dynamics 2017* (pp. 1038–1048). Helsingør, Denmark.

Brinkkemper, J., Freyermuth, T., Mendoza, E., Salles, P., & Ruessink, B. (2013). Parameterization of wave run-up on beaches in Yucatan, Mexico: a numerical study. *Coastal Dynamics*, *25*(225-233).

Buckley, R. L., & Kurzeja, R. J. (1997). An observational and numerical study of the nocturnal sea breeze. Part I: Structure and circulation. *Journal of Applied Meteorology*, *36*(12), 1577–1598. doi: https://doi.org/10.1175/1520-0450(1997)036<1577:AOANSO>2.0.CO;2

Butt, T., Russell, P., Puleo, J., Miles, J., & Masselink, G. (2004). The influence of bore turbulence on sediment transport in the swash and inner surf zones. *Continental Shelf Research*, *24*(7), 757–771. doi: https://doi.org/10.1016/j.csr.2004.02.002

Carlin, J. A., Lee, G.-h., Dellapenna, T. M., & Laverty, P. (2016a). Sediment resuspension by wind, waves, and currents during meteorological frontal passages in a micro-tidal lagoon. *Estuarine, Coastal and Shelf Science*, *172*, 24–33. doi: https://doi.org/10.1016/j.ecss.2016.01.029

Carlin, J. A., Lee, G.-h., Dellapenna, T. M., & Laverty, P. (2016b). Sediment resuspension by wind, waves, and currents during meteorological frontal passages in a micro-tidal lagoon. *Estuarine, Coastal and Shelf Science*, *172*, 24–33. doi: https://10.1016/j.ecss.2016.01.029

Chaney, P., & Stone, G. (1996). Soundside erosion of a nourished beach and implications for winter cold front forcing: West Ship Island, Mississippi. *Shore and Beach*, *64*, 27–33.

Chiba, O. (1993). The turbulent characteristics in the lowest part of the sea breeze front in the atmospheric surface layer. *Boundary-Layer Meteorology*, *65*(1-2), 181–195. doi: https://10.1007/BF00708823

Cho, K., Reid, R. O., & Nowlin, W. D. (1998). Objectively mapped stream function fields on the Texas-Louisiana shelf based on 32 months of moored current meter data. *Journal of Geophysical Research: Oceans*, *103*(C5), 10377–10390. doi: https://doi.org/10.1016/0302-3524(77)90098-6

Costanza, R. (1999). The ecological, economic, and social importance of the

oceans. *Ecological Economics*, *31*(2), 199–213. doi: https://doi.org/10.1016/S0921-8009(99)00079-8

Cuevas Jiménez, A., Euán Ávila, J. I., Villatoro Lacouture, M. M., & Silva Casarín, R. (2016). Classification of beach erosion vulnerability on the Yucatan coast. *Coastal Management*, *44*(4), 333–349. doi: https://doi.org/10.1080/08920753.2016.1155038

Culliton, T. J., Warren, M. A., Goodspeed, T. R., Remer, D. G., Blackwell, C. M., & McDonough, J. J. (1990). 50 years of population change along the nations coasts 1960-2010. *National Oceanic and Atmospheric Administration, Ocean Assessments Division Strategic Assessment Branch 1990 Apr, Rockville, MD*, 41.

Curtarelli, M., Alcântara, E., Rennó, C., & Stech, J. (2013). Effects of cold fronts on MODIS-derived sensible and latent heat fluxes in Itumbiara reservoir (Central Brazil). *Advances in Space Research*, *52*(9), 1668–1677. doi: https://10.1016/j.asr.2013.07.037

Darby, L. S. (2005). Cluster analysis of surface winds in Houston, Texas, and the impact of wind patterns on ozone. *Journal of Applied Meteorology*, *44*(12), 1788–1806. doi: https://doi.org/10.1175/JAM2320.1

Deines, K. L. (1999). Backscatter estimation using Broadband acoustic Doppler current profilers. In *Proceedings of the IEEE Sixth Working Conference on Current Measurement (Cat. No.99ch36331)* (pp. 249–253). Piscataway, N.J: IEEE Press. doi: https://10.1109/CCM.1999.755249

Dellapenna, T. M., Allison, M. A., Gill, G. A., Lehman, R. D., & Warnken, K. W. (2006). The impact of shrimp trawling and associated sediment resuspension in mud dominated, shallow estuaries. *Estuarine, Coastal and Shelf Science*, *69*(3), 519–530. doi: https://doi.org/10.1016/j.ecss.2006.04.024

Deser, C., & Blackmon, M. L. (1995). On the relationship between tropical and North

Pacific sea surface temperature variations. *Journal of Climate*, *8*(6), 1677–1680. doi: https://doi.org/10.1175/1520-0442(1995)008<1677:OTRBTA>2.0.CO;2

de Velasco, G. G., & Winant, C. D. (1996). Seasonal patterns of wind stress and wind stress curl over the Gulf of Mexico. *Journal of Geophysical Research: Oceans*, *101*(C8), 18127–18140. doi: https://10.1029/96JC01442

Dingler, J. R., & Reiss, T. E. (1990). Cold-front driven storm erosion and overwash in the central part of the Isles Dernieres, a Louisiana barrier-island arc. *Marine Geology*, *91*(3), 195–206. doi: https://10.1016/0025-3227(90)90036-j

Dingler, J. R., Reiss, T. E., & Plant, N. G. (1993). Erosional patterns of the Isles Dernieres, Louisiana, in relation to meteorological influences. *Journal of Coastal Research*, *9*(1), 112–125. doi: http://www.jstor.org/stable/4298073

Dufois, F., Garreau, P., Le Hir, P., & Forget, P. (2008). Wave-and current-induced bottom shear stress distribution in the Gulf of Lions. *Continental Shelf Research*, *28*(15), 1920–1934. doi: https://doi.org/10.1016/j.csr.2008.03.028

Edmiston, H. L., Fahrny, S. A., Lamb, M. S., Levi, L. K., Wanat, J. M., Avant, J. S., ... Selly, N. C. (2008). Tropical storm and hurricane impacts on a Gulf Coast estuary: Apalachicola Bay, Florida. *Journal of Coastal Research*, 38–49. doi: https://doi.org/10.2112/SI55-009.1

Elgar, S., Gallagher, E. L., & Guza, R. (2001). Nearshore sandbar migration. *Journal of Geophysical Research: Oceans*, *106*, 11623–11627. doi: https://10.1029/2000JC000389

Ellwood, B. B., Balsam, W. L., & Roberts, H. H. (2006). Gulf of Mexico sediment sources and sediment transport trends from magnetic susceptibility measurements of surface samples. *Marine Geology*, *230*(3), 237–248. doi: https://doi.org/10.1016/j.margeo.2006.05.008

Enriquez, C., Mariño-Tapia, I. J., & Herrera-Silveira, J. A. (2010). Dispersion in the

Yucatan coastal zone: Implications for red tide events. *Continental Shelf Research*, *30*(2), 127–137. doi: https://10.1016/j.csr.2009.10.005

Feagin, R. A., Sherman, D. J., & Grant, W. E. (2005). Coastal erosion, global sea-level rise, and the loss of sand dune plant babitats. *Frontiers in Ecology and the Environment*, *3*(7), 359–364. doi: https://10.1890/1540-9295(2005)003[0359:CEGSRA]2.0.CO;2

Feddersen, F. (2012). Observations of the surf-zone turbulent dissipation rate. *Journal of Physical Oceanography*, *42*(3), 386–399. doi: https://10.1175/jpo-d-11-082.1

Feddersen, F., Trowbridge, J. H., & Williams, A. J. (2007). Vertical structure of dissipation in the nearshore. *Journal of Physical Oceanography*, *37*(7), 1764–1777. doi: https://10.1175/jpo3098.1

Feddersen, F., & Williams, A. (2007). Direct estimation of the Reynolds stress vertical structure in the nearshore. *Journal of Atmospheric and Oceanic Technology*, *24*(1), 102–116. doi: https://doi.org/10.1175/JTECH1953.1

Fedele, F., Benetazzo, A., Gallego, G., Shih, P.-C., Yezzi, A., Barbariol, F., & Ardhuin, F. (2013). Space–time measurements of oceanic sea states. *Ocean Modelling*, *70*, 103–115. doi: https://doi.org/10.1016/j.ocemod.2013.01.001

Federico, S., Pasqualoni, L., Sempreviva, A. M., Leo, L. D., Avolio, E., Calidonna, C., & Bellecci, C. (2010). The seasonal characteristics of the breeze circulation at a coastal Mediterranean site in south Italy. *Advances in Science and Research*, *4*(1), 47–56. doi: https://doi.org/10.5194/asr-4-47-2010

Figueroa-Espinoza, B., Salles, P., & Zavala-Hidalgo, J. (2014). On the wind power potential in the northwest of the Yucatan Peninsula in Mexico. *Atmósfera*, *27*(1), 77–89. doi: https://10.1016/s0187-6236(14)71102-6

Fisher, A. W., Sanford, L. P., Scully, M. E., & Suttles, S. E. (2017). Surface wave effects on the translation of wind stress across the air-sea interface in a fetch-limited,

coastal embayment. *Journal of Physical Oceanography*(2017), 1921–1939. doi: https://doi.org/10.1175/JPO-D-16-0146.1

Flick, R. E., & George, R. A. (1991). Turbulence scales in the surf and swash. In *Proceedings of the 22nd international conference on coastal engineering* (pp. 557–569). Delft, The Netherlands: American Society of Civil Engineers. doi: https://doi.org/10.1061/9780872627765.045

Gallagher, E. L., Elgar, S., & Guza, R. (1998). Observations of sand bar evolution on a natural beach. *Journal of Geophysical Research: Oceans*, *103*(C2), 3203–3215. doi: https://10.1029/97JC02765

Gallop, S. L., Bosserelle, C., Pattiaratchi, C. B., & Eliot, I. (2011). Hydrodynamic and morphological response of a perched beach during sea breeze activity. *Journal of Coastal Research*, *SI 64*, 75–79.

Gallop, S. L., Bryan, K. R., Pitman, S. J., Ranasinghe, R., & Sandwell, D. (2016). Pulsations in surf zone currents on a high energy mesotidal beach in New Zealand. *Journal of coastal research*, *75*(sp1), 378–382. doi: https://doi.org/10.2112/SI75-076.1

Gallucci, F., & Netto, S. (2005). Effects of the passage of cold fronts over a coastal site: an ecosystem approach. *Marine Ecology-Progress Series*(281), 79–92. doi: https://10013/epic.25294

Gallucci, F., & Netto, S. A. (2004). Effects of the passage of cold fronts over a coastal site: an ecosystem approach. *Marine Ecology Progress Series*, *281*, 79–92. doi: https://10.3354/meps281079

Garreaud, R. (2000). Cold air incursions over subtropical South America: Mean structure and dynamics. *Monthly Weather Review*, *128*(7), 2544–2559. doi: https://10.1175/1520-0493(2000)128<2544:caioss>2.0.co;2

Gartner, J. W. (2004). Estimating suspended solids concentrations from backscatter inten-

sity measured by acoustic Doppler current profiler in San Francisco Bay, California. *Marine Geology*, *211*(3), 169–187. doi: https://10.1016/j.margeo.2004.07.001

George, R., Flick, R. E., & Guza, R. (1994). Observations of turbulence in the surf zone. *Journal of Geophysical Research: Oceans*, *99*(C1), 801–810. doi: https://10.1029/93JC02717

Gille, S. T., Llewellyn Smith, S. G., & Lee, S. M. (2003). Measuring the sea breeze from QuikSCAT Scatterometry. *Geophysical Research Letters*, *30*(3), 1114. doi: https://10.1029/2002GL016230

Gordon, L., & Lohrmann, A. (2001). Near-shore Doppler current meter wave spectra. In *Proceedings of the 4th international symposium on ocean wave measurement and analysis, waves2001* (pp. 33–43). San Francisco, CA: American Society of Civil Engineers. doi: https://doi.org/10.1061/40604(273)4

Gordon, L., Lohrmann, A., & Jonas, T. (1999). Internal wave generation in lakes with very slow flow. In *Proceedings of the IEEE Sixth Working Conference on Current Measurement* (pp. 212–215). San Diego, CA: IEEE Press. doi: https://10.1109/CCM.1999.755242

Grant, H., Stewart, R., & Moilliet, A. (1962). Turbulence spectra from a tidal channel. *Journal of Fluid Mechanics*, *12*(02), 241–268. doi: https://doi.org/10.1017/S002211206200018X

Grant, S. B., Kim, J. H., Jones, B. H., Jenkins, S. A., Wasyl, J., & Cudaback, C. (2005). Surf zone entrainment, along-shore transport, and human health implications of pollution from tidal outlets. *Journal of Geophysical Research: Oceans*, *110*(C10). doi: https://10.1029/2004JC002401

Grasso, F., Castelle, B., & Ruessink, B. (2012). Turbulence dissipation under breaking waves and bores in a natural surf zone. *Continental Shelf Research*, *43*, 133–141. doi: https://doi.org/10.1016/j.csr.2012.05.014

Ha, H. K., Maa, J. P. Y., Park, K., & Kim, Y. H. (2011). Estimation of high-resolution sediment concentration profiles in bottom boundary layer using pulse-coherent acoustic Doppler current profilers. *Marine Geology*, *279*(1), 199–209. doi: https://10.1016/j.margeo.2010.11.002

Hardy, J. W., & Henderson, K. G. (2003). Cold front variability in the Southern United States and the influence of atmospheric teleconnection patterns. *Physical Geography*, *24*(2), 120–137. doi: https://10.2747/0272-3646.24.2.120

Hendrickson, J., & MacMahan, J. (2009). Diurnal sea breeze effects on inner-shelf cross-shore exchange. *Continental Shelf Research*, *29*(18), 2195–2206. doi: https://doi.org/10.1016/j.csr.2009.08.011

Henry, W. (1979). Some aspects of the fate of cold fronts in the Gulf of Mexico. *Monthly Weather Review*, *107*(8), 1078–1082. doi: https://doi.org/10.1175/1520-0493(1979)107<1078:SAOTFO>2.0.CO;2

Hill, D. C., Jones, S. E., & Prandle, D. (2003). Derivation of sediment resuspension rates from acoustic backscatter time-series in tidal waters. *Continental Shelf Research*, *23*(1), 19–40. doi: https://10.1016/S0278-4343(02)00170-X

Hoitink, A. J. F., & Hoekstra, P. (2005). Observations of suspended sediment from ADCP and OBS measurements in a mud-dominated environment. *Coastal Engineering*, *52*(2), 103–118. doi: https://10.1016/j.coastaleng.2004.09.005

Houser, C., & Greenwood, B. (2007). Onshore migration of a swash bar during a storm. *Journal of Coastal Research*, *23*(1), 1–14. doi: https://doi.org/10.2112/03-0135.1

Hoyt, J. H., & Henry Jr, V. J. (1963). Rhomboid ripple mark, indicator of current direction and environment. *Journal of Sedimentary Research*, *33*(3), 604–608.

Hsu, S. (1988). *Coastal Meteorology* (1st ed.). New York: Academic Press.

Huang, Z.-C., Hsiao, S.-C., Hwung, H.-H., & Chang, K.-A. (2009). Turbulence and energy dissipations of surf-zone spilling breakers. *Coastal Engineering*, *56*(7), 733–746.

doi: https://doi.org/10.1016/j.coastaleng.2009.02.003

Huber, P. J. (1964). Robust estimation of a location parameter. *The Annals of Mathematical Statistics*, *35*(1), 73–101. doi: https://10.1214/aoms/1177703732

Huh, O. K., Walker, N. D., & Moeller, C. (2001). Sedimentation along the eastern Chenier Plain Coast: Down drift impact of a delta complex shift. *Journal of Coastal Research*, *17*(1), 72–81. doi: http://www.jstor.org/stable/4300150

Huh, O. K., Wiseman, W. J., & Rouse, L. J. (1978). Winter cycle of sea surface thermal patterns, northeastern Gulf of Mexico. *Journal of Geophysical Research: Oceans*, *83*(C9), 4523–4529. doi: https://10.1029/JC083iC09p04523

Inman, D. L., & Filloux, J. (1960). Beach cycles related to tide and local wind wave regime. *The Journal of Geology*, *68*(2), 225–231. doi: https://10.1086/626655

Jaffe, B., Sternberg, R., & Sallenger, A. (1984). The role of suspended sediment in shore-normal beach profile changes. In *Proceedings 19th International Coastal Engineering Conference* (pp. 1983–1996). New York, USA: American Society of Civil Engineers. doi: 10.1061/9780872624382.134

Jay, D. A., Orton, P., Kay, D. J., Fain, A., & Baptista, A. M. (1999). Acoustic determination of sediment concentrations, settling velocities, horizontal transports and vertical fluxes in estuaries. In *Proceedings of the IEEE Sixth Working Conference on Current Measurement (Cat. No.99ch36331)* (pp. 258–263). San Diego, California: IEEE Press. doi: https://10.1109/CCM.1999.755251

Jiménez, C., & Ávila, E. (2009). Morphodynamics of carbonate beaches in the Yucatán Peninsula. *Ciencias Marinas*, *35*, 307–320.

John, A., & Crompton, J. L. (1998). Developing and testing a tourism impact scale. *Journal of Travel Research*, *37*(2), 120–130.

Johnson, D. (2002). *Diwasp: DIrectional WAve SPectra Toolbox, version 1.1: User manual* (Tech. Rep.). Research Report No: WP 1601 DJ (V1. 4), Coastal Oceanography

Group Centre for Water Research, University of Western Australia, Perth.

Jolliffe, T., I. (2002). *Principal component analysis* (2nd ed.) [Book]. Springer. doi: https://10.1007/b98835

Kalnay, E., Kanamitsu, M., Kistler, R., Collins, W., Deaven, D., Gandin, L., ... others (1996). The NCEP/NCAR 40-year reanalysis project. *Bulletin of The American Meteorological Society*, *77*(3), 437–471. doi: https://doi.org/10.1175/1520-0477(1996)077<0437:TNYRP>2.0.CO;2

Keen, T. R. (2002). Waves and currents during a winter cold front in the Mississippi Bight, Gulf of Mexico: Implications for barrier island erosion. *Journal of Coastal Research*, *18*(4), 622–636. doi: http://www.jstor.org/stable/4299115

Keen, T. R., Stone, G., Kaihatu, J., & Hsu, Y. L. (2003). *Barrier island erosion during a winter cold front in Mississippi Sound* (Tech. Rep.). DTIC Document.

Keim, B. D. (1996). Spatial, synoptic, and seasonal patterns of heavy rainfall in the southeastern United States. *Physical Geography*, *17*(4), 313–328. doi: https://10.1080/02723646.1996.10642588

Kim, S. C., Friedrichs, C. T., Maa, J. P. Y., & Wright, L. D. (2000). Estimating bottom stress in tidal boundary layer from acoustic Doppler velocimeter data. *Journal of Hydraulic Engineering*, *126*(6), 399–406. doi: https://10.1061/(asce)0733-9429(2000)126:6(399)

Kineke, G., Higgins, E., Hart, K., & Velasco, D. (2006). Fine-sediment transport associated with cold-front passages on the shallow shelf, Gulf of Mexico. *Continental Shelf Research*, *26*(17), 2073–2091. doi: https://doi.org/10.1016/j.csr.2006.07.023

Kolmogorov, A. N. (1941). Dissipation of energy in the locally isotropic turbulence. *Proceedings of the Royal Society of London: Mathematical and Physical Sciences*, *434*(1890), 15–17. doi: https://10.1098/rspa.1991.0076

Lanckriet, T., & Puleo, J. A. (2013). Near-bed turbulence dissipation measurements in

the inner surf and swash zone. *Journal of Geophysical Research: Oceans*, *118*(12), 6634–6647. doi: https://10.1002/2013JC009251

Lee, T. H., & Hanes, D. M. (1995). Direct inversion method to measure the concentration profile of suspended particles using backscattered sound. *Journal of Geophysical Research: Oceans*, *100*(C2), 2649–2657. doi: https://10.1029/94JC03068

Lien, R.-C., & D'Asaro, E. A. (2006). Measurement of turbulent kinetic energy dissipation rate with a lagrangian float. *Journal of Atmospheric and Oceanic Technology*, *23*(7), 964–976. doi: https://doi.org/10.1175/JTECH1890.1

Lippmann, T., & Holman, R. (1990). The spatial and temporal variability of sand bar morphology. *Journal of Geophysical Research: Oceans*, *95*(C7), 11575–11590. doi: https://10.1029/JC095iC07p11575

Lippmann, T., Holman, R., & Hathaway, K. (1993). Episodic, nonstationary behavior of a double bar system at Duck, North Carolina, USA, 1986–1991. *Journal of Coastal Research*, *15*, 49–75. doi: http://www.jstor.org/stable/25735723

Madden, C. J., Day, J. W., & Randall, J. M. (1988). Freshwater and marine coupling in estuaries of the Mississippi River deltaic plain. *Limnology and Oceanography*, *33*(4part2), 982–1004. doi: https://10.4319/lo.1988.33.4part2.0982

Masselink, G., & Pattiaratchi, C. (1998). The effect of sea breeze on beach morphology, surf zone hydrodynamics and sediment resuspension. *Marine Geology*, *146*(1-4), 115–135. doi: https://10.1016/s0025-3227(97)00121-7

Matsunaga, N., Hashida, M., & Kawakami, H. (1997). Wind-induced waves and currents in a nearshore zone. In *Coastal engineering 1996* (pp. 3363–3377). doi: https://10.1061/9780784402429.260

Mendoza, E., Trejo-Rangel, M., Salles, P., Appendini, C., & Lopez-Gonzalez, J. (2013). Storm characterization and coastal hazards in the Yucatan Peninsula. *Journal of Coastal Research*(65), 790–795. doi: https://doi.org/10.2112/SI65-134.1

Meyer-Arendt, K. (1991). Tourism development on the north Yucatan coast: human response to shoreline erosion and hurricanes. *GeoJournal*, *23*(4), 327–336. doi: https://doi.org/10.1007/BF00193606

Meyer-Arendt, K. (1993). Shoreline changes along the north Yucatan coast. In *Proceedings of the 8th Symposium on Coastal and Ocean Management* (pp. 103–117). New Orleans: American Society of Civil Engineers.

Michel, J., Owens, E. H., Zengel, S., Graham, A., Nixon, Z., Allard, T., ... others (2013). Extent and degree of shoreline oiling: Deepwater Horizon oil spill, Gulf of Mexico, USA. *Plos One*, *8*(6), e65087. doi: https://doi.org/10.1371/journal.pone.0065087

Miller, S. T. K., Keim, B. D., Talbot, R. W., & Mao, H. (2003). Sea breeze: Structure, forecasting, and impacts. *Reviews of Geophysics*, *41*(3), 1011. doi: https://10.1029/2003RG000124

Moeller, C., Huh, O. K., Roberts, H. H., Gumley, L. E., & Menzel, W. P. (1993). Response of Louisiana coastal environments to a cold front passage. *Journal of Coastal Research*, 434–447. doi: http://www.jstor.org/stable/4298101

Morales-Vela, B., Saldivar, J., & Mignucci-Giannoni, A. A. (2003). Status of the manatee (trichechus manatus) along the northern and western coasts of the Yucatan Peninsula, Mexico. *Caribbean Journal of Science*, *39*(1), 42–49.

Morton, R. A. (1988). Interactions of storms, seawalls, and beaches of the Texas coast. *Journal of Coastal Research*, 113–134. doi: http://www.jstor.org/stable/25735355

Morton, R. A., Gibeaut, J. C., & Paine, J. G. (1995). Meso-scale transfer of sand during and after storms: implications for prediction of shoreline movement. *Marine Geology*, *126*(1), 161–179. doi: https://10.1016/0025-3227(95)00071-6

Morton, R. A., & McKenna, K. K. (1999). Analysis and projection of erosion hazard areas in Brazoria and Galveston counties, Texas. *Journal of Coastal Research*, 106–120. doi: http://www.jstor.org/stable/25736190

Mulligan, R. P., & Hanson, J. L. (2016). Alongshore momentum transfer to the nearshore zone from energetic ocean waves generated by passing hurricanes. *Journal of Geophysical Research: Oceans*, *121*(6), 4178–4193. doi: https://10.1002/2016JC011706

Nittrouer, C. A., & Wright, L. D. (1994). Transport of particles across continental shelves. *Reviews of Geophysics*, *32*(1), 85–113. doi: https://10.1029/93RG02603

Noda, E. K. (1974). Wave-induced nearshore circulation. *Journal of Geophysical Research*, *79*(27), 4097–4106. doi: https://10.1029/JC079i027p04097

Nowlin, W. D., Jochens, A., Reid, R., & DiMarco, S. (1998). Texas-Louisiana shelf circulation and transport processes study: Synthesis report. *Volume II: Appendices. US Dept. of the Interior, Minerals Management Service, Gulf of Mexico OCS Region, New Orleans, LA. OCS Study MMS*, 98–0036.

Nowlin, W. D., Jochens, A. E., DiMarco, S. F., Reid, R. O., & Howard, M. K. (2005). Low-frequency circulation over the Texas-Louisiana continental shelf. In W. Sturges & A. Lugo-Fernández (Eds.), *Circulation in the Gulf of Mexico: Observations and models* (pp. 219–240). American Geophysical Union. doi: 10.1029/161GM17

Ogawa, H., Kench, P., & Dickson, M. (2012). Field measurements of wave characteristics on a near-horizontal shore platform, Mahia Peninsula, north Island, New Zealand. *Geographical Research*, *50*(2), 179–192. doi: https://10.1111/j.1745-5871.2011.00715.x

Osborne, P. D., & Greenwood, B. (1993). Sediment suspension under waves and currents: time scales and vertical structure. *Sedimentology*, *40*(4), 599–622. doi: https://10.1111/j.1365-3091.1993.tb01352.x

Otvos, E. G. (2004). Beach aggradation following hurricane landfall: impact comparisons from two contrasting hurricanes, northern Gulf of Mexico. *Journal of Coastal Research*, 326–339. doi: https://10.2112/1551-5036(2004)20[326:BAFHLI]2.0.CO;2

Paine, J. G., Mathew, S., & Caudle, T. (2012). Historical shoreline change through 2007, Texas Gulf coast: Rates, contributing causes, and Holocene context. *Gulf Coast Association of Geological Societies*, *1*, 13–26.

Pattiaratchi, C., Hegge, B., Gould, J., & Eliot, I. (1997). Impact of sea-breeze activity on nearshore and foreshore processes in southwestern Australia. *Continental Shelf Research*, *17*(13), 1539–1560. doi: https://10.1016/s0278-4343(97)00016-2

Pattiaratchi, C., & Masselink, G. (1996). Sea breeze effects on nearshore coastal processes. In *Proceedings 25th international conference on coastal engineering* (pp. 4200–4213). Orlando, Florida, United States: American Society of Civil Engineers. doi: https://10.1061/9780784402429.325

Pawlowicz, R., Beardsley, B., & Lentz, S. (2002). Classical tidal harmonic analysis including error estimates in MATLAB using T_TIDE. *Computers & Geosciences*, *28*(8), 929–937. doi: https://doi.org/10.1016/S0098-3004(02)00013-4

Pepper, D. A., & Stone, G. W. (2004). Hydrodynamic and sedimentary responses to two contrasting winter storms on the inner shelf of the northern Gulf of Mexico. *Marine Geology*, *210*, 43–62. doi: https://10.1016/j.margeo.2004.05.004

Pepper, D. A., Stone, G. W., & Wang, P. (1999). Bottom boundary layer parameters and sediment transport on the Louisiana inner-shelf during cold front passages. *Gulf Coast Association of Geological Societies Transactions*, *49*, 432–439. doi: http://dx.doi.org/10.1306/2DC40C5B-0E47-11D7-8643000102C1865D

Pierson, W. J. (1954). An interpretation of the observable properties of 'sea' waves in terms of the energy spectrum of the Gaussian Record. *Transactions, American Geophysical Union*, *35*(5), 747. doi: https://10.1029/TR035i005p00747

Pope, N. D., Widdows, J., & Brinsley, M. D. (2006). Estimation of bed shear stress using the turbulent kinetic energy approach—A comparison of annular flume and field data. *Continental Shelf Research*, *26*(8), 959–970. doi:

https://10.1016/j.csr.2006.02.010

Prandle, D., & Matthews, J. (1990). The dynamics of nearshore surface currents generated by tides, wind and horizontal density gradients. *Continental Shelf Research*, *10*(7), 665–681. doi: https://doi.org/10.1016/0278-4343(90)90044-M

Pratt, T. C. (1990). *Near-bed optical backscatter sensor and vector-measuring velocity meter calibration* (Tech. Rep. No. Technical Report HL-90-10). U.S. Army Corps of Engineers.

Ravens, T. M., & Sitanggang, K. I. (2007). Numerical modeling and analysis of shoreline change on Galveston Island. *Journal of Coastal Research*, *23*(3), 699–710.

Reyes, P., Salles, P., López, J., & Casillas, E. (2015). Preview analysis to sand bypass system design in the port of Sisal, Yucatán. In *Proceedings of the coastal sediments 2015.* San Diego, CA: World Scientific. doi: https://doi.org/10.1142/9789814689977_0155

Roberts, H. H., Huh, O., Hsu, S., Rouse, L., & Rickman, D. (1987). Impact of cold-front passages on geomorphic evolution and sediment dynamics of the complex Louisiana coast. *American Society of Civil Engineers*, 1950–1963.

Roberts, H. H., Huh, O. K., Hsu, S., Rouse Jr, L. J., & Rickman, D. A. (1989). Winter storm impacts on the Chenier Plain coast of southwestern Louisiana. *Gulf Coast Association of Geological Societies Transactions*, *39*, 512–522.

Roelvink, J., & Stive, M. (1989). Bar-generating cross-shore flow mechanisms on a beach. *Journal of Geophysical Research: Oceans*, *94*(C4), 4785–4800. doi: https://10.1029/JC094iC04p04785

Rogers, A. L., & Ravens, T. M. (2008). Measurement of longshore sediment transport rates in the surf zone on Galveston Island, Texas. *Journal of Coastal Research*, *24*(2B), 62–73. doi: https://doi.org/10.2112/05-0564.1

Ruessink, B. (2010). Observations of turbulence within a natural surf

zone. *Journal of Physical Oceanography*, *40*(12), 2696–2712. doi: https://doi.org/10.1175/2010JPO4466.1

Rusello, P. (2009). *A practical primer for pulse coherent instruments (tn-027)* (Tech. Rep.). Nortek.

Russell, P. E. (1993). Mechanisms for beach erosion during storms. *Continental Shelf Research*, *13*, 1243–1265. doi: https://10.1016/0278-4343(93)90051-X

Salisbury, J. E., Campbell, J. W., Linder, E., Meeker, L. D., Müller-Karger, F. E., & Vörösmarty, C. J. (2004). On the seasonal correlation of surface particle fields with wind stress and Mississippi discharge in the northern Gulf of Mexico. *Deep Sea Research Part II: Topical Studies in Oceanography*, *51*(10), 1187–1203. doi: https://doi.org/10.1016/j.dsr2.2004.03.002

Salles, P., Souza, A., Torres-Freyermuth, A., López, J., Appendini, C., Menoza, E., & Meza-Padilla, R. (2013). Hydrodynamics over sand dunes in the northern Yucatan Peninsula coast. In *Proceedings of the coastal dynamics 2013* (pp. 1407–1416). France.

Sassi, M. G., Hoitink, A. J. F., & Vermeulen, B. (2012). Impact of sound attenuation by suspended sediment on ADCP backscatter calibrations. *Water Resources Research*, *48*(9), W09520. doi: https://10.1029/2012WR012008

Savitzky, A., & Golay, M. J. (1964). Smoothing and differentiation of data by simplified least squares procedures. *Analytical Chemistry*, *36*(8), 1627–1639. doi: https://10.1021/ac60319a045

Sebastian, A., Proft, J., Dietrich, J. C., Du, W., Bedient, P. B., & Dawson, C. N. (2014). Characterizing hurricane storm surge behavior in Galveston Bay using the SWAN + ADCIRC model. *Coastal Engineering*, *88*, 171–181. doi: https://10.1016/j.coastaleng.2014.03.002

Sen, L., & Mayfield, S. (2004). Accessible tourism: Transportation to and accessibility of

historic buildings and other recreational areas in the city of galveston, texas. *Public Works Management & Policy*, *8*(4), 223–234.

Smith, N. P. (1977). Meteorological and tidal exchanges between Corpus Christi Bay, Texas, and the northwestern Gulf of Mexico. *Estuarine and Coastal Marine Science*, *5*(4), 511–520. doi: https://10.1029/98JC00099

Smith, S. D. (1988). Coefficients for sea surface wind stress, heat flux, and wind profiles as a function of wind speed and temperature. *Journal of Geophysical Research*, *93*(C12), 15467. doi: https://10.1029/JC093iC12p15467

Sonu, C. J., Murray, S. P., Hsu, S. A., Suhayda, J. N., & Waddell, E. (1973). Sea breeze and coastal processes. *Eos, Transactions American Geophysical Union*, *54*(9), 820. doi: https://10.1029/EO054i009p00820

Stech, J. L., & Lorenzzetti, J. A. (1992). The response of the south Brazil Bight to the passage of wintertime cold fronts. *Journal of Geophysical Research*, *97*(C6), 9507. doi: https://10.1029/92jc00486

Stone, G., Liu, B., Pepper, D., & Wang, P. (2004). The importance of extratropical and tropical cyclones on the short-term evolution of barrier islands along the northern Gulf of Mexico, USA. *Marine Geology*, *210*(1), 63–78. doi: https://doi.org/10.1016/j.margeo.2004.05.021

Stone, G., & Wang, P. (1999). The importance of cyclogenesis on the short-term evolution of Gulf Coast barriers. *Transactions Gulf Coast Association of Geological Societies*, *49*, 47–48.

Svendsen, I. A. (1987). Analysis of surf zone turbulence. *Journal of Geophysical Research: Oceans*, *92*(C5), 5115–5124. doi: https://10.1029/JC092iC05p05115

Syvitski, J. P., Vörösmarty, C. J., Kettner, A. J., & Green, P. (2005). Impact of humans on the flux of terrestrial sediment to the global coastal ocean. *Science*, *308*(5720), 376–380. doi: https://10.1126/science.1109454

Tester, P. A., & Steidinger, K. A. (1997). Gymnodinium breve red tide blooms: Initiation, transport, and consequences of surface circulation. *Limnology and Oceanography*, *42*(5part2), 1039–1051. doi: https://10.4319/lo.1997.42.5_part_2.1039

Thomson, R. E., & Emery, W. J. (2014). *Data analysis methods in physical oceanography* (3rd ed.). Elsevier.

Thorne, P. D., Hardcastle, P. J., & Soulsby, R. L. (1993). Analysis of acoustic measurements of suspended sediments. *Journal of Geophysical Research: Oceans*, *98*(C1), 899–910. doi: https://10.1029/92JC01855

Thorne, P. D., Hurther, D., & Moate, B. D. (2011). Acoustic inversions for measuring boundary layer suspended sediment processes. *The Journal of the Acoustical Society of America*, *130*(3), 1188–1200. doi: https://10.1121/1.3618728

Thornton, E. B., Humiston, R. T., & Birkemeier, W. (1996). Bar/trough generation on a natural beach. *Journal of Geophysical Research: Oceans*, *101*(C5), 12097-12110. doi: https://10.1029/96jc00209

Thorpe, S. A. (2007). *An introduction to ocean turbulence*. Cambridge University Press.

Tomás, A., Méndez, F., & Losada, I. (2012). Bed shear stress during Sant Esteve's storm (26th December 2008) along the Catalonia's coast (NW Mediterranean) in : Assessment of the ecological impact of the extreme storm of Sant Esteves day (26 December 2008) on the littoral ecosystems of the north Mediterranean Spanish coasts. *Final Report (PIEC 200430E599). Centre de Estudis Avanats de Blanes (CEAB-CSIC), Blanes, Catalonia, Spain*, 45–54.

Torres, R., Barton, E., Miller, P., & Fanjul, E. (2003). Spatial patterns of wind and sea surface temperature in the Galician upwelling region. *Journal of Geophysical Research: Oceans*, *108*(C4). doi: https://10.1029/2002JC001361

Torres-Freyermuth, A., Puleo, J. A., DiCosmo, N., Allende-Arandía, M. E., Chardón-Maldonado, P., López, J., ... Candela, J. (2017). Nearshore circulation on a sea

breeze dominated beach during intense wind events. *Continental Shelf Research*, *151*, 40–52. doi: https://10.1016/j.csr.2017.10.008

Trembanis, A. C., & Pilkey, O. H. (1998). Summary of beach nourishment along the US Gulf of Mexico shoreline. *Journal of Coastal Research*, 407–417. doi: http://www.jstor.org/stable/4298795

Trowbridge, J., & Elgar, S. (2001). Turbulence measurements in the surf zone*. *Journal of Physical Oceanography*, *31*(8), 2403–2417. doi: https://10.1175/1520-0485(2001)031<2403:TMITSZ>2.0.CO;2

Vatvani, D., Zweers, N. C., van Ormondt, M., Smale, A. J., de Vries, H., & Makin, V. K. (2012). Storm surge and wave simulations in the Gulf of Mexico using a consistent drag relation for atmospheric and storm surge models. *Natural Hazards and Earth System Sciences*, *12*, 2399–2410. doi: 10.5194/nhess-12-2399-2012

Veron, F., & Melville, W. K. (1999). Pulse-to-pulse coherent Doppler measurements of waves and turbulence. *Journal of Atmospheric and Oceanic Technology*, *16*(11), 1580–1597. doi: https://doi.org/10.1175/1520-0426(1999)016<1580:PTPCDM>2.0.CO;2

Wallace, D. J., Anderson, J. B., & Fernández, R. A. (2010). Transgressive ravinement versus depth of closure: A geological perspective from the upper Texas coast. *Journal of Coastal Research*, 1057–1067. doi: https://10.2112/JCOASTRES-D-10-00034.1

Wang, P., & Oey, L. (2008). Hindcast of waves and currents in Hurricane Katrina. *Bulletin of the American Meteorological Society*, *89*(4), 487-496. doi: https://10.1175/bams-89-4-487

Wang, W., Nowlin, W. D., & Reid, R. O. (1998). Analyzed surface meteorological fields over the northwestern Gulf of Mexico for 1992–94: mean, seasonal, and monthly patterns. *Monthly Weather Review*, *126*(11), 2864–2883. doi: https://10.1002/2015JC011555

Welch, P. (1967). The use of fast fourier transform for the estimation of power spectra: a method based on time averaging over short, modified periodograms. *IEEE Transactions on Audio and Electroacoustics*, *15*(2), 70–73.

Wijnberg, K. M., & Kroon, A. (2002). Barred beaches. *Geomorphology*, *48*(1), 103–120. doi: https://doi.org/10.1016/S0169-555X(02)00177-0

Williams, J., Lee, G.-h., Shin, H.-J., & Dellapenna, T. (2015). Mechanism for sediment convergence in the anthropogenically altered microtidal Nakdong Estuary, South Korea. *Marine Geology*, *369*, 79–90. doi: https://10.1016/j.margeo.2015.08.004

Wright, L., & Short, A. D. (1984). Morphodynamic variability of surf zones and beaches: A synthesis. *Marine Geology*, *56*(1-4), 93–118. doi: https://doi.org/10.1016/0025-3227(84)90008-2

Zavala-Hidalgo, J., Gallegos-García, A., Martínez-López, B., Morey, S. L., & O Brien, J. J. (2006). Seasonal upwelling on the western and southern shelves of the Gulf of Mexico. *Ocean Dynamics*, *56*(3-4), 333–338. doi: https://doi.org/10.1007/s10236-006-0072-3

Zavala-Hidalgo, J., Morey, S. L., & O'Brien, J. J. (2003). Seasonal circulation on the western shelf of the Gulf of Mexico using a high-resolution numerical model. *Journal of Geophysical Research: Oceans*, *108*(C12). doi: https://10.1029/2003JC001879

Zavala-Hidalgo, J., Romero-Centeno, R., Mateos-Jasso, A., Morey, S. L., & Martínez-López, B. (2014). The response of the Gulf of Mexico to wind and heat flux forcing: What has been learned in recent years? *Atmósfera*, *27*(3), 317–334. doi: https://10.1016/S0187-6236(14)71119-1

Zhang, X., DiMarco, S. F., Smith IV, D. C., Howard, M. K., Jochens, A. E., & Hetland, R. D. (2009). Near-resonant ocean response to sea breeze on a stratified continental shelf. *Journal of Physical Oceanography*, *39*(9), 2137–2155. doi: https://doi.org/10.1175/2009JPO4054.1